Zeitschrift: IABSE reports = Rapports AIPC = IVBH Berichte
Band: 54 (1987)

Rubrik: Session 5: Cyclic and dynamic loading (applications)

SESSION 5

August 28, 1987 (morning)

Cyclic and Dynamic Loading (Applications)

Sollicitations cycliques et dynamiques (applications)

Zyklische und dynamische Belastung (Anwendungen)

Chairman: N. Ottosen, Sweden

Invited Lecturers: C. Meyer, USA
Analysis of Underwater Tunnel for Internal Gas Explosion

N. Inoue, Japan
Analysis of Reinforced Concrete Members Subjected to Cyclic Loads

Analysis of Underwater Tunnel for Internal Gas Explosion

Calcul d'un tunnel sous-marin dans le cas hypothétique d'une explosion interne de gaz

Berechnung eines durch Gasexplosion belasteten Unterwassertunnels

Christian MEYER
Assoc. Prof. of Civil Eng.
Columbia University
New York, N.Y., U.S.A.

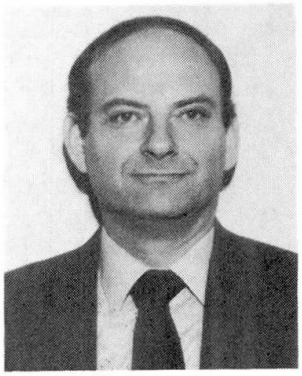

Christian Meyer received his M.S. and Ph.D. degree from the University of California at Berkeley and spent 8 years in the building and nuclear power industry before joining Columbia University. His research interests are in computer analysis of structures, earthquake engineering and analysis and design of concrete structures.

SUMMARY
Nonlinear finite element analysis of concrete structures is a new tool available for practitioners in situations where conventional simple methods of analysis may not be adequate. This paper illustrates the use of DIANA, a comprehensive state-of-the-art finite element program system, for the nonlinear dynamic analysis of an underwater tunnel subjected to a hypothetical internal gas explosion. Emphasis is placed on the care with which the engineer has to verify the correctness of the program, the model and the analysis results.

RÉSUMÉ
Le calcul statique de structures en béton à l'aide des méthodes aux éléments finis non linéaires est un nouveau moyen à disposition des praticiens dans les situations où les méthodes simples conventionnelles de calcul statique peuvent ne pas être satisfaisantes. La contribution illustre l'application de DIANA, un système global de programmes aux élémets finis pour le calcul dynamique non-linéaire d'un tunnel sous-marin sous la charge hypothétique d'une explosion de gaz à l'intérieur du tunnel. L'auteur souligne l'importance des précautions à prendre par l'ingénieur, afin de vérifier l'exactitude du programme, du modèle et des résultats d'analyse.

ZUSAMMENFASSUNG
Nichtlineare Finite Element Berechnungen von Betonkonstruktionen bieten dem Praktiker neue Möglichkeiten, wo die herkömmlichen vereinfachten Berechnungsmethoden nicht ausreichend sind. Dieser Aufsatz dient als Illustration einer Anwendung von DIANA, einem umfassenden Finite Element Programmsystem auf dem letzten Stand der Forschung. Als Beispiel dient die nichtlineare dynamische Berechnung eines durch Gasexplosion belasteten Unterwassertunnels. Besonders wird auf die Sorgfalt hingewiesen, mit welcher der Benutzer das Programm, das Rechenmodell und die Berechnungsergebnisse verifizieren muss.

1. INTRODUCTION

Designing reinforced concrete structures implies the capability to analyze such structures not only for the loads they are expected to carry during their design life, but also to determine the factor of safety against failure under overload. For most engineered structures, designers can rely on simple and proven analysis methods to do that. Behavior under service load is analyzed as a rule by linear elastic methods. These are routinely extrapolated for the determination of ultimate load capacities, whereby the structure's redistribution of loads is often accounted for in a more or less intuitive way. Designers are periodically confronted with unusual structures, for which their past experience is not sufficient for satisfactory treatment. Structures of this kind are generally surface structures such as plates, shells, deep beams, and often massive or thick-walled structures. To evaluate the performance of such structures, designers have the choice of further relying on their intuition, borne out of experience, or they may elect a novel analytical approach: nonlinear finite element analysis. Until only a few years ago they did not have this choice. Neither were the computational tools adequate for such tasks, nor were the properties known sufficiently well to allow the development of realistic mathematical models.

On both counts considerable progress has been made in recent years [1,2]. Nonlinear finite element solution techniques have matured to the extent that it is now possible to compute the highly nonlinear response of systems with thousands of degrees of freedom, effectively placing a new analysis tool at the disposal of engineering practitioners. Developments in hardware technology have made it possible to carry out such computations on VAX-size supermini computers. Yet, for all this progress, numerous pitfalls call for considerable caution. First, the advances in nonlinear computational mechanics were such that the realistic modeling of material properties has become the primary limitation of this analytical approach. Second, the finite element idealization of structures for nonlinear analysis requires considerable skills on the part of the analyst. Third, the vast amount of numerical computations involved are still taxing computer resources to such an extent, that full nonlinear finite element analyses will be restricted to unusual and special structures for some time to come.

In view of these concerns it is important that this new technology be introduced cautiously, lest it receive adverse publicitiy before having had a fair chance to prove itself in engineering practice. In the Netherland, two related developments are of interest in this regard. First, there is the continuing development of program DIANA [3], which contains state-of-the-art material models for reinforced concrete and efficient numerical solution algorithms. Second, the Netherlands Committee for Research, Codes and Standards for Concrete (CUR-VB) is funding an effort to demonstrate the capabilities of DIANA with an "Example-Book" [4], a publication containing a number of realistic examples taken from engineering practice. This author had the opportunity to participate in this effort while on Sabbatical leave in Delft, by analyzing an underwater tunnel for an internal gas explosion.

It is the purpose of this paper to use this example as an illustration both of the potential and the difficulties of nonlinear finite element analysis of concrete structures. The material models built

into programs like DIANA are discussed briefly, followed by some comments on practical nonlinear finite element analysis in general. The analysis example itself is presented here primarily as an illustration of how one should approach a problem of this kind in a practical setting.

2. MATHEMATICAL MODELS FOR REINFORCED CONCRETE

The first essential prerequisite for any realistic analysis is a thorough understanding of reinforced concrete behavior under load. This includes the following specific aspects:

1. plain concrete behavior under arbitrary stress states, i.e., constitutive behavior, cracking and crack propagation, and possible failure mechanisms in compression;
2. reinforcing steel behavior;
3. bond behavior at the steel-concrete interface;
4. shear transfer mechanisms across cracks;
5. long-term deformations due to creep and shrinkage;
6. dynamic strain rate effects in the case of impact and blast loads;
7. strength and stiffness degradation effects accompanying large inelastic cyclic loads.

New experimental techniques have made available a wealth of data that has improved our understanding of concrete behavior and is suitable to support the development of improved material models. These are based on a variety of different theories, such as nonlinear elasticity, plasticity, viscoplasticity, plastic-fracturing, and endochronic theories. References [1,2] give a broad overview of these theories and some of the models that have been used successfully in recent years to analyze realistic reinforced concrete structures. However, a word of caution is in order, because many of these models are still undergoing development and therefore should be used only with great care. It is appropriate to refer in this context to the international competition [5] which demonstrated that wide scatter of results is not limited to experimental investigations of concrete structures, but applies to analytical studies as well. For this reason it is inappropriate to place unrealistic expectations in the degree of accuracy with which these new models and theories can simulate concrete behavior as observed in the laboratory.

3. NONLINEAR FINITE ELEMENT ANALYSIS

The finite element method has invaded engineering practice in a relatively short time. Most engineering offices in the United States now have access to major finite element program systems [6]. Finite element analyses in engineering practice are generally limited to linear elastic response. Even then, the development of proper models requires a considerable amount of skill and experience on the part of the analyst. Possibly the most difficult part of this task is an independent verification of the correctness of the analysis results. All too often, analysts, for a number of reasons, fail to undertake this important step and therefore are bound to accept and use output results, even if these are completely wrong. In an effort to help analysts in proper techniques

of finite element idealization and output verification, a comprehensive guide for linear static and dynamic analysis has just been published [7].

In the case of nonlinear finite element analysis the difficulties are multiplied for a number of reasons. First, the material models are incomparably more complicated, requiring of the analyst an intimate knowledge of the material being modeled and of the details of the material model itself. In many cases the program user is offered a number of alternate material models, and he has to have the proper training and experience in order to make the right choices. Second, the powerful numerical angorithms now available in many nonlinear analysis programs, generally lack the "ruggedness" of linear analysis algorithms, i.e., they are much more vulnerable to improper use. As a rule, the user has to be intimately familiar with the algorithm's idiosyncrasies, its limitations and range of applicability. In linear analysis this is much less the case. A third complication is the greatly increased difficulty of interpreting and verifying the output results. For these reasons it is essential that the analyst, even if highly trained and expert in his field, proceeds very cautiously to verify step by step the correctness of the program, its algorithms and material models, then the finite element model of the structure to be analyzed, and finally the analysis results themselves. The need for this painstaking verification process is the main source of the high cost of nonlinear analysis of realistic structures, which limits the application of this sophisticated analysis tool to very unusual, important, or expensive structures. The example presented below shall serve as an illustration of what the author believes is a methodical procedure to solve a difficult problem.

4. DYNAMIC ANALYSIS OF UNDERWATER TUNNEL

4.1 General

Road tunnels that pass under waterways are very common in the Netherlands. They are normally designed to resist the loads associated with soil and water pressure. In the event of an internal gas explosion, the tunnel experiences a load reversal for which it may not be adequately reinforced. Thus, the question whether hazardous cargo should be permitted to pass through such tunnels is of some importance. The Dutch Public Works Department (Rijkswaterstaat) has developed standard tunnel cross sections that are widely used throughout the Netherlands. Figure 1 shows a typical cross section and material properties. The strength parameters listed in Fig. 1b are based on experimentally determined values and a 20% allowance for the strain-rate effect.

It was the objective of this analysis to predict the response of the tunnel to the pressure load associated with a hypothetical internal gas explosion. The solution of a problem of this nature requires a careful step-by-step approach, with continuous verification of the correctness of the program, the finite element model, and the results obtained. In order to achieve these goals, the following analyses were performed:

1. a linear elastic static frame analysis of the entire tunnel cross section;
2. a linear static finite element analysis of a segment of the tunnel roof;

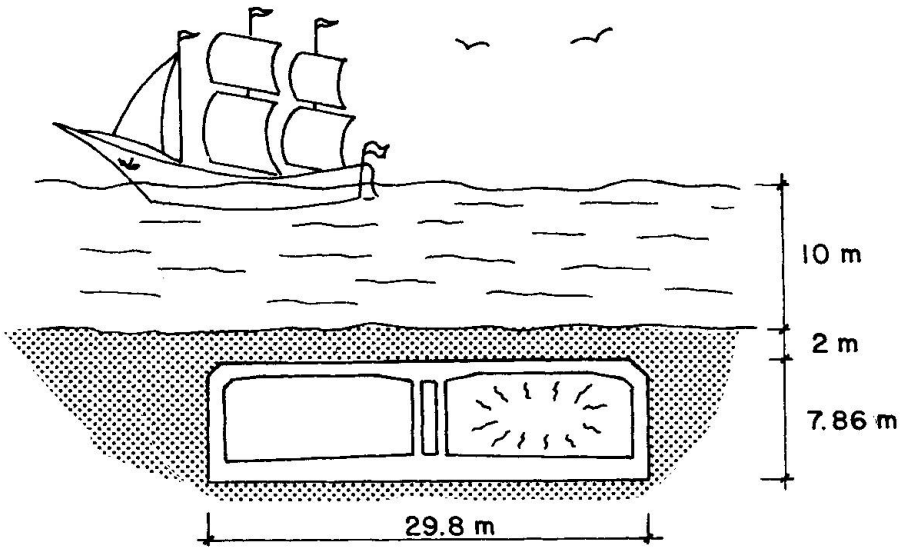

a) Typical Tunnel Section

Concrete

E_c = 22,000 N/mm^2

ν = 0.2

f'_t = 3.36 N/mm^2

f'_c = 30 N/mm^2

ε_{tu} = 0.001

Reinforcing Steel

E_s = 210,000 N/mm^2

f_y = 528 N/mm^2

b) Material Properties

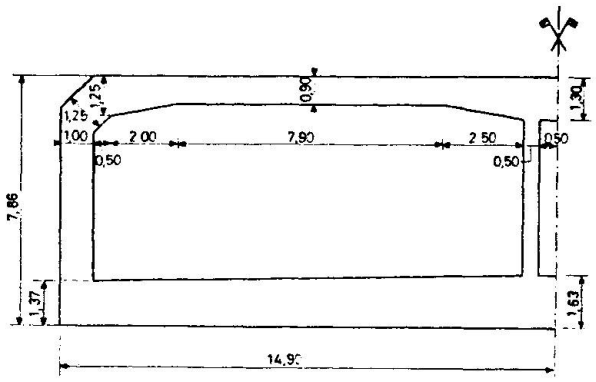

c) Dimensions

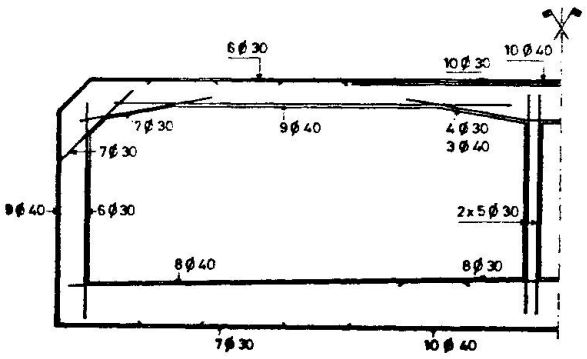

d) Reinforcement for 1.5m Wide Section

Fig.1 Typical Tunnel Section

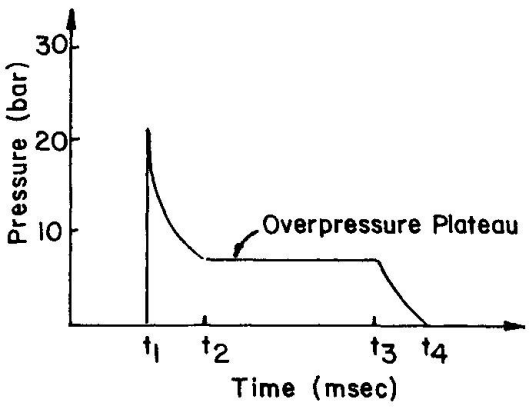

a) Generic Pressure Time History

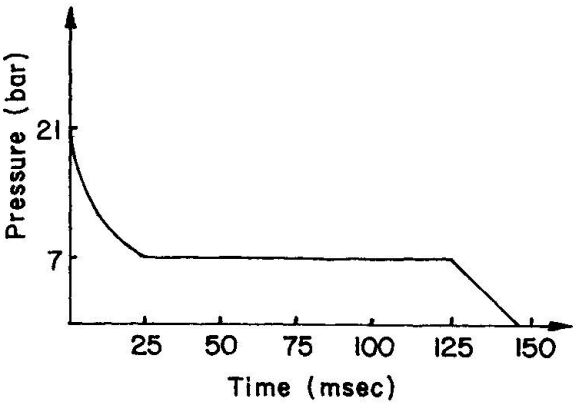

b) PressureTime History Used In This Analysis

Fig.2 Assumed Pressure Time History

3. a nonlinear static finite element analysis of the same tunnel roof segment;
4. an eigenvalue analysis of the finite element model;
5. a nonlinear dynamic time history analysis of a grossly simplified finite element model;
6. the final nonlinear dynamic time history analysis of the actual finite element model.

At each step measures were taken to verify that the analysis results were reasonable. For this purpose it was very helpful that a 1:5 scale model of a particular tunnel section had been tested at the TNO-IBBC Institute in 1976 [8]. The documentation of this work contains detailed information on dimensions, reinforcement, material properties and service loads on the prototype structure [8].

4.2 Loading

Little is known about the dynamic pressure loads generated by internal gas explosions. In a joint Dutch/Belgian effort, a series of tests have been conducted on an experimental tunnel of 1.8 m by 1.8 m cross section and 27 m length [9]. From these experiments it was possible to identify the following characteristics of a pressure time history; Fig. 2a,

1. The shock front is for all practical purposes vertical, i.e., the pressure increases instantaneously from ambient to a peak value of about 25 bar.
2. The peak pressure drops rapidly to an overpressure plateau, following approximately a parabolic shape.
3. The overpressure remains approximately constant at the value of 6 to 7 bar. This value can be computed from the gas-air mixture, considering the energy released during the chemical reaction. The length of the plateau is a function of the time needed to vent the overpressure.
4. Once the depressurization of the tunnel starts, the decrease of overpressure follows again an approximately parabolic shape.

The scaling of these experimental pressures for tunnels of different dimensions is not straightforward. Concerning the tunnel cross-sectional dimensions it can be argued that the energy released per unit volume is invariant, therefore both the peak pressure and the plateau pressure are approximately independent of the cross-sectional area, assuming the entire cross-section is filled with combustible gas. In contrast, the time of depressurization onset should be an approximately linear function of tunnel length, because the travel times of both the shock wave and its reflection are functions of tunnel length, again assuming the entire tunnel is filled with gas. Assuming further that detonation commences at the center of the 320 m long tunnel, and that the tunnel section to be analyzed is situated at the quarter point, i.e. 80 m from the tunnel exit, the pressure time history of Fig. 2b was arrived at. The shock wave velocity is about 2000 m/sec, and the velocity of the depressurization wave is about half that much, because depressurization is associated with fluid flow, a considerably slower process.

It is noteworthy that both the peak pressure of 25 bar (2.5 N/mm^2 or 362 psi) and the plateau pressure of 7 bar (0.7 N/mm^2 or 101 psi) applied for the duration of 0.1 sec represent a formidable

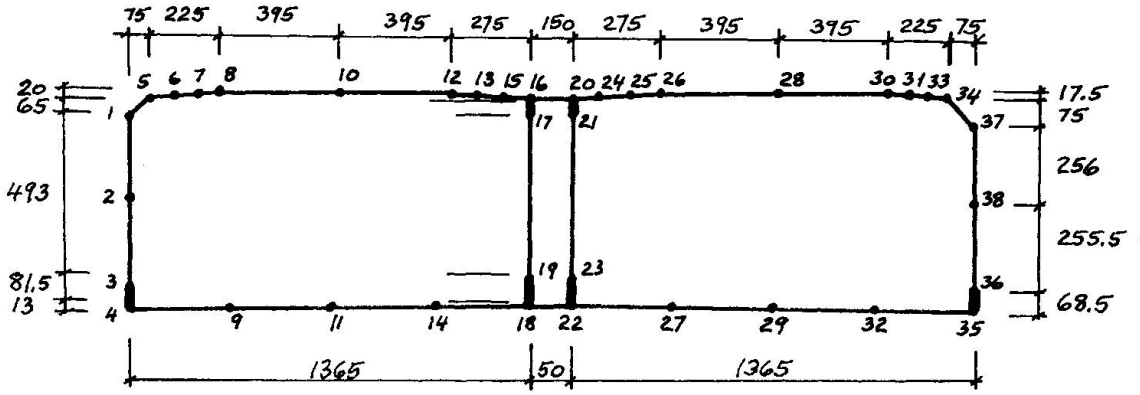

a) Frame Element Model (Dimensions in cm)

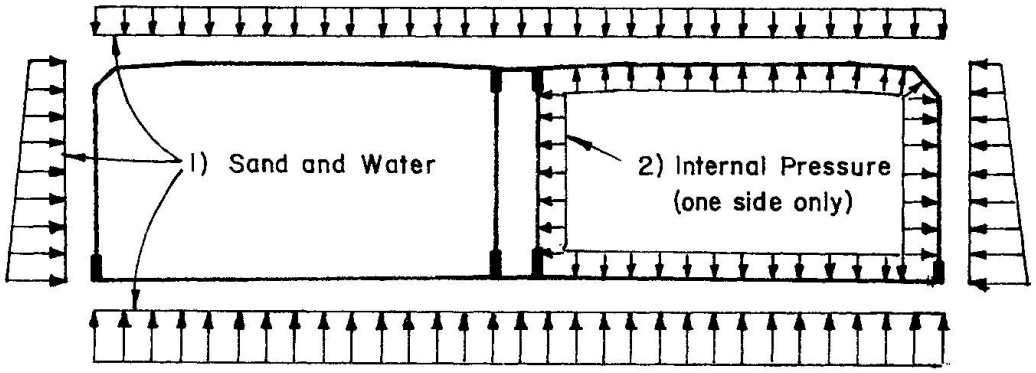

b) Load Cases

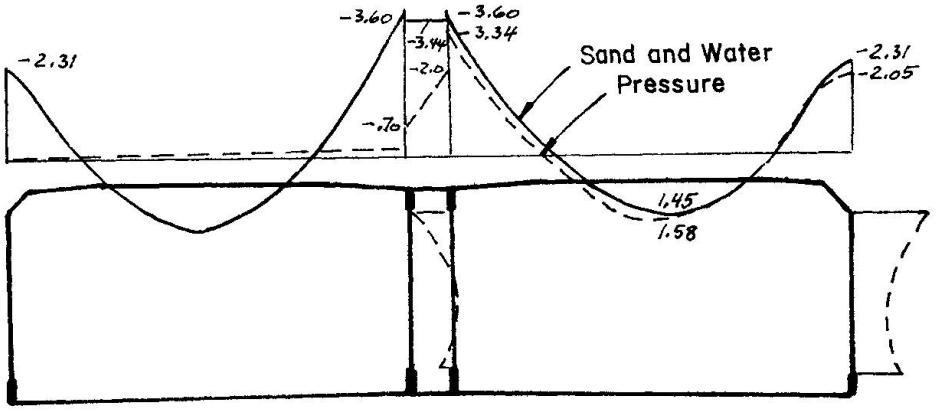

c) Roof Bending Moments

Fig.3 Linear Elastic Static Analysis of Frame Element Model

load which a conventionally reinforced structure is unlikely to survive without severe damage.

4.3 Modeling of Structure and Model Verification

The first analysis step was a linear static analysis of a simple frame model of the entire cross section, Fig. 3, for, 1) soil and water pressure and, 2) internal pressure. Because of the similarity of the moment distributions for the two load cases it could be justified to model only a quarter of the entire roof slab for the finite element analysis and to apply boundary conditions valid for both load cases.

In the finite element model, Fig. 4, 45 eight-noded plane stress elements CQ16M (in the final analysis, plane strain elements CQ16E) were used for the concrete, and the reinforcement was modeled by 34 bar elements as shown, resulting in a total of 172 nodes with 344 potential degrees of freedom. In order to compare the analysis results for the frame element and finite element models, it was necessary to account for the following modeling differences.

1. The right face of the finite element model was fixed against rotation, while the flexibility of the outside walls in the frame model shifted the point of maximum positive moment and zero rotation to the right. To correct the finite element model, the midspan rotation of the frame model was input as a specified rotation of the right face of the finite element model.
2. The axial deformations of the vertical walls were included in the frame element model but not in the finite element model.
3. The effect of steel reinforcement on the roof stiffness was explicitly accounted for in the finite element model, while in the frame element model only gross moments of inertia were used.
4. The representation of the haunched segment of the tunnel roof by a series of prismatic beams introduces a considerable error, which can be reduced by increasing the number of beam elements.

Once all of these factors were taken into consideration, both moments and displacements obtained by the two models agreed to within 15%.

As step three a nonlinear static analysis of the finite element model was performed, because experimental data were available for comparison and further model verification.

In the experiment, the applied loading simulated the service load distribution of Fig. 3b (load case 1) and was increased proportionally in stages, in multiples of the actual service load level. At each stage, the load was held constant for about 40 min to permit creep deformations to take place. Thereafter, the deformations were held constant for another 80 minutes for the taking of measurements. After this, the load was reduced by about 90% and increased again to the previous displacement level. 10,000 load cycles were thus applied, and the whole precedure repeated for the next load level. The five levels of 1.0, 1.2, 1.4, 1.6 and 1.7 service loads are illustrated in Fig. 5. Failure was initiated by large diagonal shear cracks and ended by crushing of concrete in the highly stressed corner where the roof joins the vertical wall.

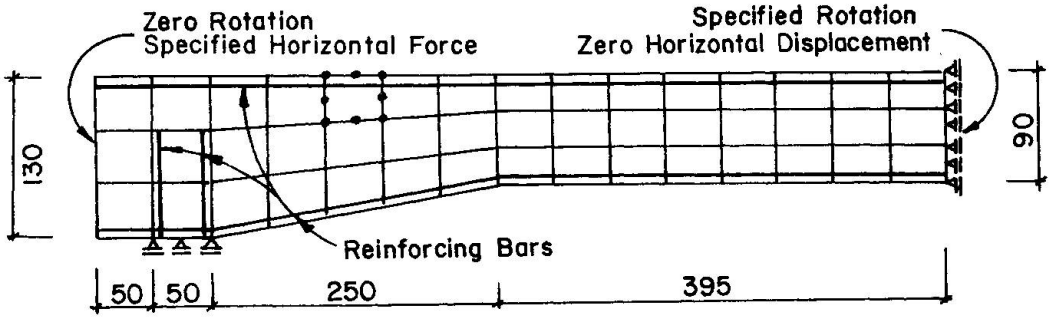

Fig.4 Finite Element Model of Tunnel Roof

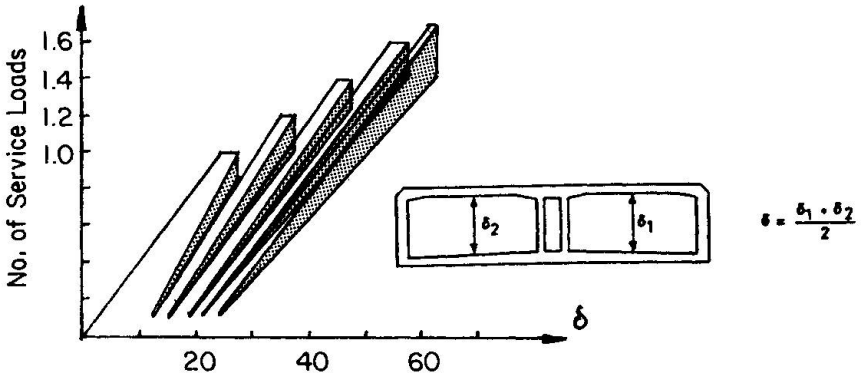

Fig.5 Load History for Scale Model Experiment

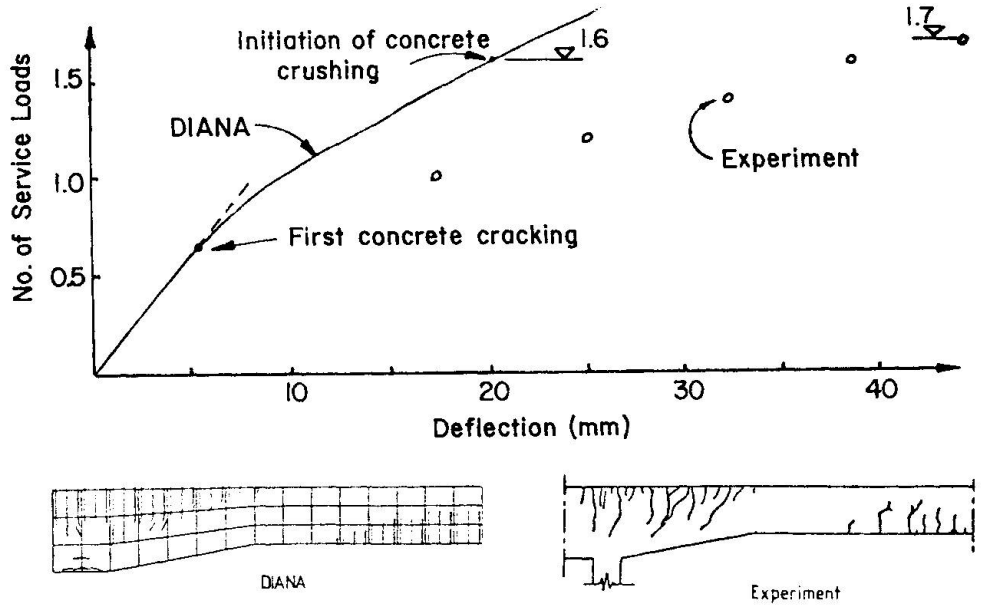

Fig.6 Experimental and Analytical Load-Deflection Information

The computed deflections did not agree particularly well with the experimental values, Fig. 6. But when comparing these results, the following factors have to be taken into consideration.

1. Experimental results were incompletely documented (see Fig. 5).
2. The large number of load cycles in the experiment resulted in cumulative damage which could not be simulated by the analysis for monotonic loading.
3. The analysis did not attempt to reproduce the creep deformations which took place in the experiment.
4. Concrete cracking can be expected to cause some moment redistribution and thus affect the boundary conditions for the finite element model, which were held constant throughout the analysis.
5. From the documentation of the experiment it was difficult to determine to what degree of accuracy all laws of similitude have been satisfied.

Even though the analysis tended to overestimate the stiffness of the structure, cracking patterns were reproduced rather accurately, and also the failure mode and failure load level agreed remarkably close, Fig. 6. It was primarily this encouraging agreement which gave rise to the confidence that it was possible to use DIANA to compute the tunnel response up to failure.

An eigenvalue analysis of the finite element model furnished mode shapes and frequencies which were in good agreement with an approximate beam solution, Fig. 7. For this and the subsequent analyses, the mass of the 2 m soil and 10 m of water was concentrated as lumped masses at the nodes along the upper boundary of the model. For the response of the structure to the primary shock load this approximation was felt to be permissible, and an involved fluid-structure interaction analysis was not justified.

The last preliminary analysis was a complete time history analysis of the grossly simplified finite element model of Fig. 8, which was very useful for familiarization with the program's dynamic analysis options and numerical algorithms, and for a first estimate of the structure's dynamic response. This analysis completed the confidence building preparation for the final analysis.

4.4 Final Nonlinear Dynamic Analysis

The final analysis consisted of 150 time steps of $\Delta t = 1.25$ msec. The adequacy of this choice of time step size was verified in a second run with 100 time steps of $\Delta t = .625$ msec which led to almost identical response results. The acceleration, velocity and displacement time histories of the roof midspan section are plotted in Fig. 9. These and the other output results permitted the following observations.

1. The first impact experienced by the structure was the axial load applied at the left boundary which is a result of the pressure on the vertical walls. This tensile impact wave propagated to the right at about 737 m/sec, causing large-scale concrete cracking in its wake and reaching the right boundary after only 7 time steps, long before the roof had any time to respond in bending to the upward pressure, Fig. 10.
2. The "concrete cracking wave" was followed by a somewhat slower

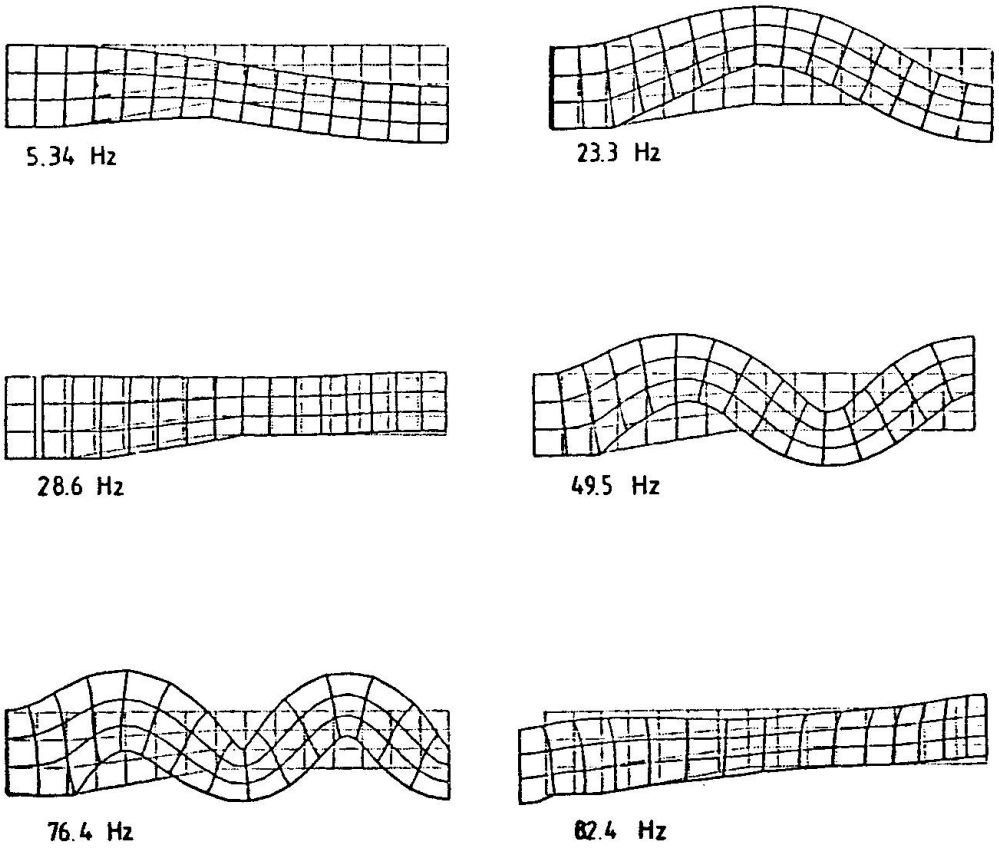

Fig.7 First Six Modes and Frequencies of Finite Element Model

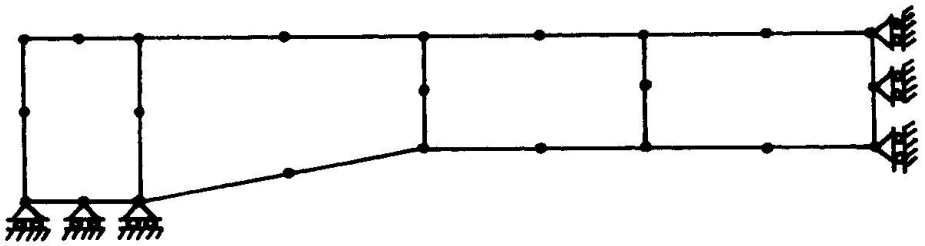

Fig.8 Grossly Simplified Finite Element Model

"steel yield wave," which caused the first steel bar to yield in the fourth time step and reached the midspan section after 22 time steps.

3. The steel stresses in the two vertical reinforcing bars, which tie the roof slab into the vertical walls, are plotted as functions of time in Fig. 11. Initially these two bars provide a fixed end moment, but as the vertical pressure tends to lift the roof off its supports, also the tensile stress in the left bar builds up.
4. Concrete stresses were not critical at any time of the analysis. The combination of flexure with axial tension forced the reinforcing steel to resist most of the load.
5. The results tend to point to the conclusion that the tunnel roof is not likely to survive a gas explosion of the kind stipulated in Fig. 2. The weakest detail appears to be the amount of vertical reinforcement which cannot prevent the vertical pressure from lifting the roof off its supports. Also, the large rotations in the plastic hinges above the support and at midspan, are associated with midspan deflections as large as 28.5 cm after 150 time steps (0.1875 sec), which can only be interpreted as failure.

5. CONCLUSIONS

Nonlinear finite element analysis of reinforced concrete structures is a new rational tool of analysis in situations where the more simplified methods are difficult or impossible to apply. In this paper, the potential of this tool has been illustrated by applying it to the dynamic analysis of an underwater tunnel subjected to an internal gas explosion. Emphasis was placed on the care with which the finite element model has to be verified and the analysis results checked for consistency and reasonableness. The time and effort required for such analyses are typically justified only for very unusual structures or situations.

Concerning the particular structure analyzed herein it was shown that both the failure mode and failure load level for service-type loads as recorded in a scale experiment were reprodued quite well. Moreover, it was possible to simulate failure under a highly dynamic blast load of a structure that was not designed for this kind of loading.

6. ACKNOWLEDGMENT

The analysis reported herein was performed during the author's Sabbatical stay at the TNO-IBBC Institute in Delft, The Netherlands. The author is indebted for the support of Prof. J. Blaauwendraad of the Delft Technical University and the DIANA development team, particularly G.M.A. Kusters and J.G. Rots.

REFERENCES

1. "Finite Element Analysis of Reinforced Concrete," Task Committee on Finite Element Analysis of Reinforced Concrete Structures, ASCE, New York, 1982.

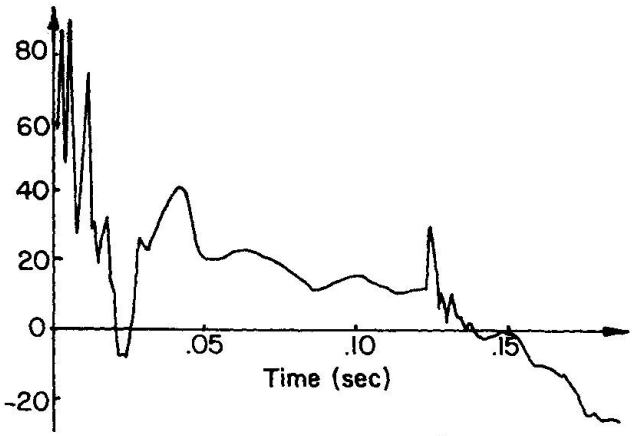

a) Acceleration (m/sec^2)

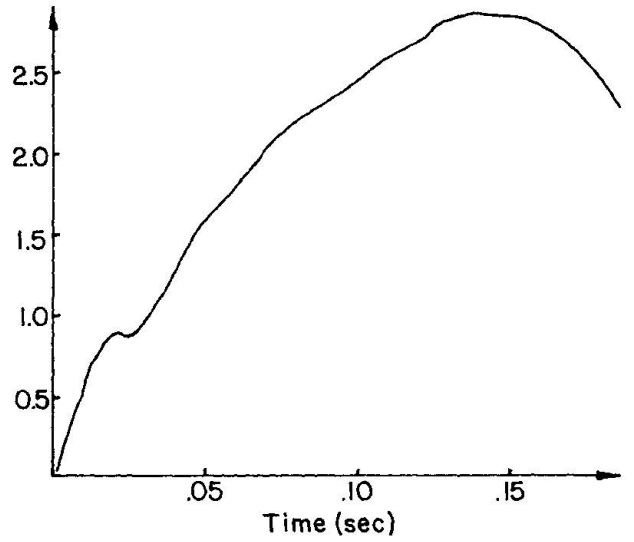

b) Velocity (m/sec)

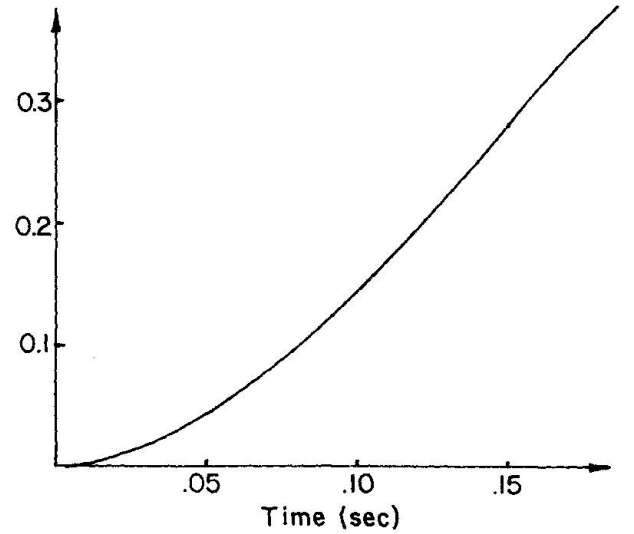

c) Displacement (m)

Fig.9 Time History Response of Tunnel Midspan Section

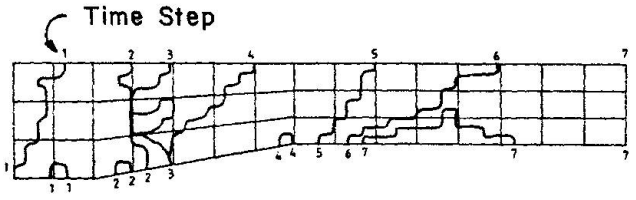

Fig.10 Propagation of Concrete Cracking Wave

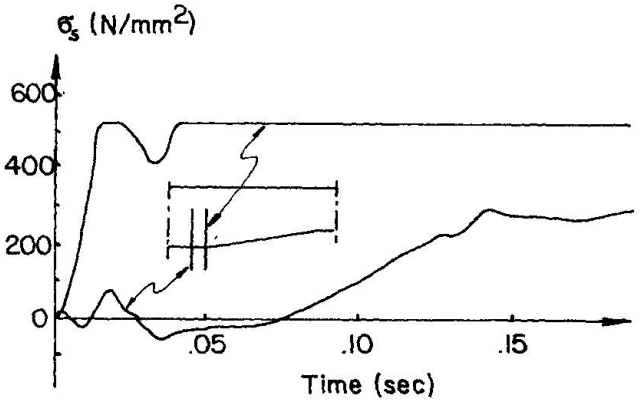

Fig.11 Time Histories of Stresses in Vertical Reinforcing Bars

2. MEYER, C. and OKAMURA, H., eds., "Finite Element Analysis of Reinforced Concrete Structures." Proceedings, U.S. - Japan Joint Seminar, Tokyo, ASCE, 1986.

3. BORST, R. DE et al., "DIANA - A Comprehensive but Flexible Finite Element System," Finite Element Systems Handbook, 3rd Edition, Springer Verlag, Berlin, Germany, 1983.

4. VAN MANEN, S.E. et al., "Example Calculations of Nonlinear Analysis for Reinforced Concrete Structures with DIANA," TNO-IBBC, Report No. BI-87-14/62.4.0000, TNO-IBBC, Delft, The Netherlands, 1987.

5. Collins, M.P., Vecchio, F.J. and Mehlhorn, G., "An International Competition to Predict the Response of Reinforced Concrete Panels," Canadian Journal of Civil Engineering (Ottawa), Vol. 12, No. 3, Sept. 1985, pp. 626-644.

6. MEYER, C., "Computer Analysis in Engineering Practice." Journal of the Boston Society of Civil Engineers Section ASCE, April 1983.

7. MEYER, C., ed., "Finite Element Idealization." ASCE, New York, 1987.

8. "Investigation of a Model of a Tunnel Section." TNO-IBBC, Report No. B-76-197/04.4.1080, TNO-IBBC, Delft, The Netherlands, 1976.

9. "Investigation of Transporting Dangerous Materials Through Tunnels," Rijkswaterstaat, Directie Sluizen en Stuwen, Utrecht, The Netherlands, 1982.

Analysis of Reinforced Concrete Members Subjected to Cyclic Loads

Analyse d'éléments en béton armé soumis à des charges cycliques

Berechnung von Stahlbetongliedern unter zyklischer Belastung

Norio INOUE
Dr. Eng.
Kajima Corporation
Tokyo, Japan

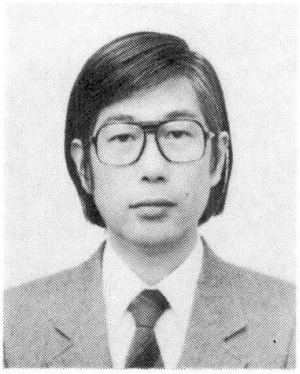

Norio Inoue, born 1947, got his Doctor of Engineering Degree from the University of Tokyo. For sixteen years he was involved in special dynamic and static problems of structures in Muto Institute of Structural Mechanics. Norio Inoue, now in Kajima Institute of Construction Technology, is specializing in nonlinear analysis of reinforced concrete structures by Finite Element Method.

SUMMARY

This study shows the analytical examples of reinforced concrete members subjected to cyclic loads like seismic forces. First,a shear wall and a panel were analyzed by macroscopic approaches based on the average stress-strain relationship. Next,columns were analyzed by a microscopic approach based on the characteristics of each element like concrete, reinforcement and bond. From these analytical studies, the applicability and future problems of cyclic analyses are described.

RÉSUMÉ

Cette étude montre des exemples analytiques d'éléments en béton armé soumis à des charges cycliques telles que les séismes. Une paroi de cisaillement et un panneau ont été analysés par approches macroscopiques basées sur la relation contrainte-déformation moyenne. Des colonnes ont été étudiées par une approche microscopique basée sur les caractéristiques de chaque élément, tel que béton, armature et adhérence. La valeur de ces analyses cycliques ainsi que les problèmes à étudier sont décrits.

ZUSAMMENFASSUNG

Diese Arbeit zeigt einige Berechnungsbeispiele für Stahlbetonbauteile unter wiederholter Belastung wie zum Beispiel Erdbeben. Zunächst werden eine Schubwand und eine Scheibe mit gemittelten Spannungs-Verformungsbeziehungen analysiert. Danach werden Stützen berechnet mit einem Mikromodell, das die charakteristischen Eigenschaften von Beton, Bewehrung und Verbund enthält. Nach diesen Beispielen werden die allgemeine Anwendbarkeit und zukünftige Probleme im Zusammenhang mit wiederholter Belastung beschrieben.

1. INTRODUCTION

Recently many researches have been performed concerning nonlinear analyses of reinforced concrete members and structures by using Finite Element Analysis [1] [2]. As to the loadings, several kinds of loads are considered in these studies. Among them the seismic forces are very important in the region like Japan where seismic intensity is very large.

Aseismic nonlinear behavior of structures is governed by the cyclic characteristics of members besides the monotonic ones. Such cyclic behaviors can be described generally by the envelope curve and the reversing loop of the load versus the displacement relationships. Therefore when the cyclic characteristics are investigated by static Finite Element Analysis, it is desirable to pursue the cyclic loops as they are. But the cyclic analyses are very complicated and need much computational time. So an alternative approach is often adopted in which reversing loops are assumed by referring to many experimental results and the envelope curve is obtained by analyses. In such a case it is necessary to make sure that the cyclic characteristics can be reflected to the assumed element properties and obtained results.

Concerning the analytical method itself there are two types of approaches, that is, a macroscopic one based on average stress vs. average strain relationship like Vecchio and Collins [3], and a microscopic one based on the characteristics of each element itself like concrete, reinforcement and bond.

In view of these circumstances, this study shows the applicability and future problems of cyclic analyses by presenting several analytical examples of both macroscopic and microscopic approaches.

First as an example to obtain envelope curves, a monotonic analysis is presented for a shear wall subjected to cyclic lateral forces by using a two-dimensional macroscopic approach. Next the cyclic analyses are shown for a reinforced concrete panel subjected to cyclic pure shear forces. In this case the same macroscopic method was applied with several additional cyclic rules. Finally the cyclic analyses are shown for a column subjected to one-dimensional cyclic lateral forces and a column subjected to two-dimensional lateral forces with circular displacements by using a three-dimensional microscopic approach.

2. MONOTONIC ANALYSIS OF SHEAR WALL

Monotonic analyses were performed for a shear wall subjected to cyclic lateral forces in order to investigate the envelope curve of hysteretic loops.

2.1 Analytical Method

The analytical method is based on the average stress vs. average strain relationship proposed by Vecchio and Collins [3] with some modification for being used with a Finite Element Method. This approach is very effectual for a shear wall in which many reinforcements are arranged uniformly. The detail was presented in the paper [4]. The main points and revisions are described below.

- The average strain of concrete is equal to that of reinforcement.

- The direction of principal stress for cracked concrete coincides with that of the principal strain.

- The compressive principal stress vs. strain relationship of the cracked concrete is represented by Eq. (1), (2) and Fig. 1.

- The tensile principal stress vs. strain relationship is represented by a third order function like Fig. 1 in which the stress becomes zero at 50 times of cracking strain ϵ_{cr}.

- A stiffness matrix is made by the principal stress strain relationship with addition of an adequate shear rigidity like Eq. (3). The solution is performed by an iteration method for total stress and strain.

$$fc_2 = fc_2 \max \left\{ 2\left(\frac{\epsilon_2}{\epsilon_c'}\right) - \left(\frac{\epsilon_2}{\epsilon_c'}\right)^2 \right\} \quad \cdots\cdots\cdots (1)$$

$$\frac{fc_2 \max}{fc'} = \frac{1}{0.8 - 0.34 \dfrac{\epsilon_1}{\epsilon_c'}} \leqq 1.0 \quad \cdots\cdots (2)$$

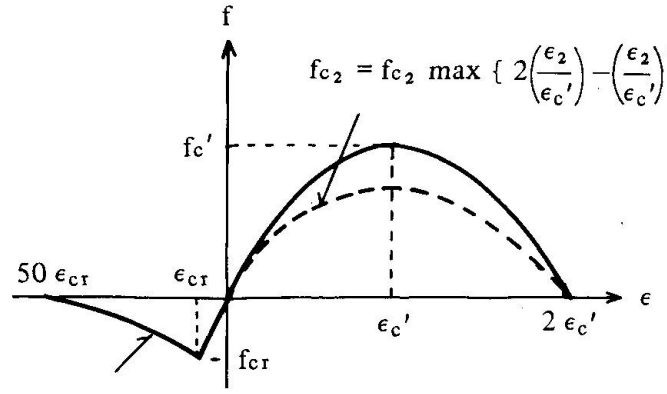

fc_1, fc_2 : Tensile and compressive principal stress
ϵ_1, ϵ_2 : Tensile and compressive principal strain
fcr, fc' : Uniaxial tensile and compressive strength
ϵ_{cr}, ϵ_c' : Strain at the tensile and compressive strength

Fig.1 Stress strain relationship of concrete

$$\begin{Bmatrix} fc_1 \\ fc_2 \\ \tau \end{Bmatrix} = \begin{bmatrix} E_1 & 0 & 0 \\ & E_2 & 0 \\ \text{sym} & & G \end{bmatrix} \begin{Bmatrix} \epsilon_1 \\ \epsilon_2 \\ \gamma \end{Bmatrix} \quad \cdots\cdots\cdots (3)$$

E_1 : Secant modulus in tension
E_2 : Secant modulus in compression
G : Shear modulus

2.2 Test Specimen and Analytical Model

The analyzed test specimen is a shear wall which was tested by Shiohara and Aoyama et al. shown in Fig. 2 [5]. The shear span-to-depth ratio is 0.5 and the lateral reinforcement ratio is 0.85%. Several cyclic lateral forces were loaded with a constant axial force. In this test relative displacements in three directions were measured at several portions by LVDTs. From these data the average strains in each zone could be calculated. The mesh layout used in this analysis is presented in Fig. 3.

2.3 Analytical Results

The obtained load vs. displacement relationship is shown in Fig. 4. The analysis could represent well the envelope curve of the observed one.

The Mohr's circles of average strains for three zones (A, B and C) are shown in Fig. 5. When paying attention to the diameter of the circles, the analytical results represented well the observed ones up to the ultimate stress. This

means that this monotonic analysis can predict well the shear strain and accordingly can represent well the load vs. displacement relationship. But as to the center of the circle the experimental results shifted to the tension side compared with the analytical ones. Considering that the center of a Mohr's circle means the dilatancy of a panel, it is thought that cyclic loading caused an additional dilatancy compared with monotonic loading. Therefore to investigate such a phenomenon the load vs. the sum of normal strains ($\varepsilon_x + \varepsilon_y$) in the zone B is presented in Fig. 6. It is noticed that the analytical strains have good agreement with the experimental ones up to the level of 980 kN before the first reversing step. But just after reversing the experimental strain is larger than analytical one. Such tendency was also observed for the second reversing step of 1560 kN. Then the residual strains were estimated by the test results and added to the analytical results. That is, between the load 980 kN and 1560 kN, the residual strain (0.70×10^{-3}) observed after the first cycle was added to the monotonic results at each step. Beyond the load 1560 kN the observed residual strain (2.35×10^{-3}) after the second cycle was added. This procedure caused a good agreement.

From these studies it is considered that the proposed monotonic analysis can predict the shear strain and the envelop curve of load vs. displacement relationship and that residual strains should be considered to estimate the normal strains and dilatancy.

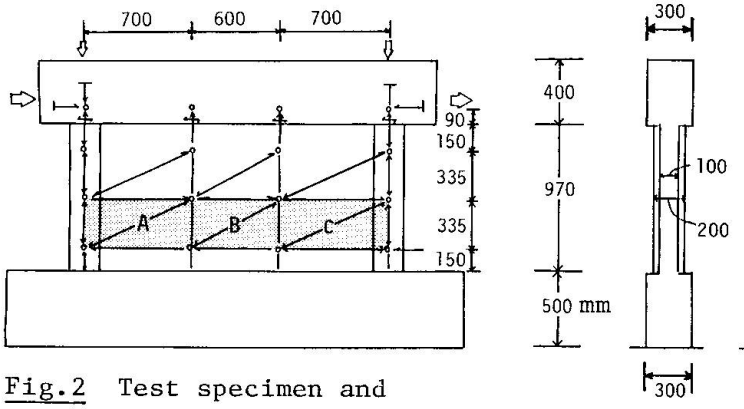

Fig.2 Test specimen and measuring points of displacement [5]

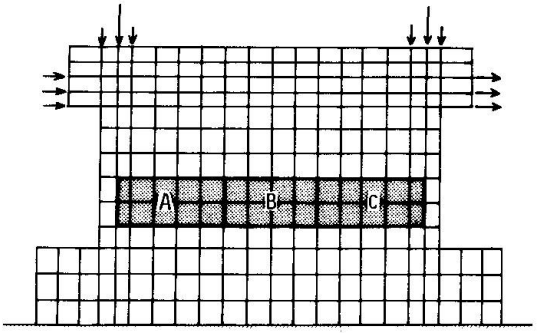

Fig.3 Mesh layout

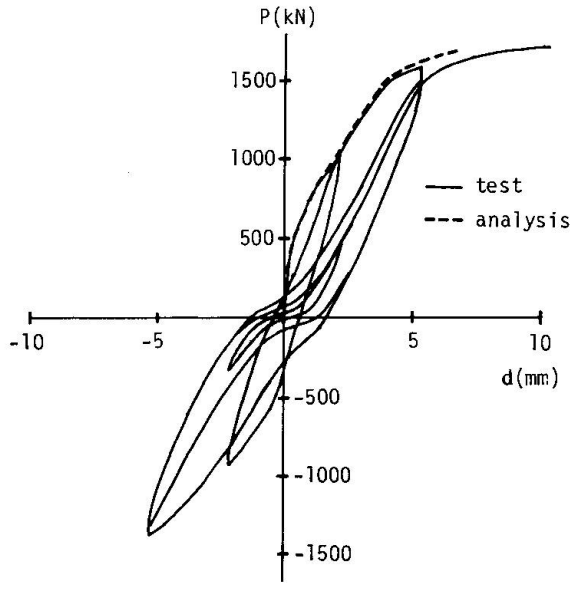

Fig.4 Load - displacement relationship

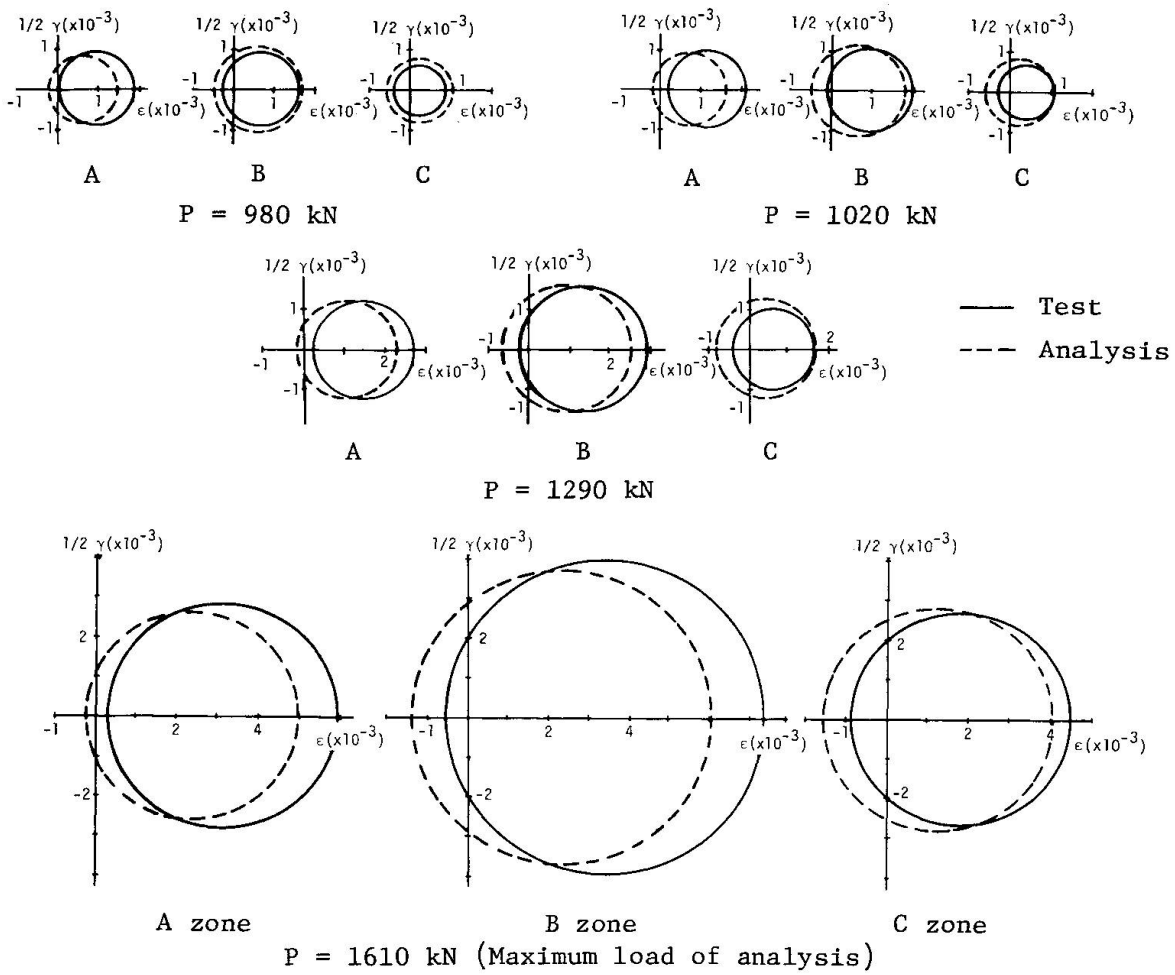

Fig.5 Mohr's circle of strain

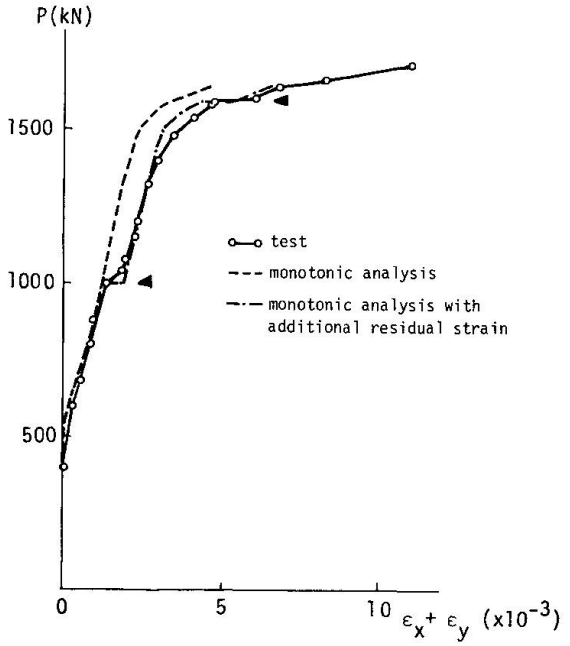

Fig.6 Load - sum of normal strains ($\varepsilon_x + \varepsilon_y$) relationship

3. CYCLIC ANALYSIS OF PANEL

Ohmori, Tsubota, Kurihara and the author et al. have been conducting a series of studies to clarify the characteristics of reinforced concrete panels subjected to in-plane forces at Kajima Institute of Construction Technology. An experimental and analytical study has already been presented concerning panels subjected to cyclic pure shear forces [6]. The study herein is aimed to propose a simple analytical method which can be applied in the design of actual complicated structures.

3.1 Panel Test

Several reinforced concrete panels have already been tested. The test specimens were 2,500 mm square and 140 mm thick and deformed rebars were arranged in two layers in two orthogonal directions as shown in Fig. 7. The percentage of reinforcing steel was varied from 0.8 to 2.0%, but always with the ratio of transverse reinforcement equal to that of longitudinal reinforcement.

The test panels were loaded by a newly developed testing facility as shown in Fig. 8. This facility can apply any combination of in-plane shear and normal forces to the test panels by automatically controlled 24 closed loop hydraulic actuators and a network of links. All tests presented in this paper were conducted in reversed cyclic in-plane pure shear.

The total average shear stress applied to the test panel was evaluated from measured data of 24 load cells attached to the hydraulic actuators. For evaluating the average strains of the test panel, 6 LVDTs were attached to the surface of the specimen.

The measured data from 6 LVDTs were reduced to average strains in the longitudinal, transverse and two diagonal directions. These strains were then used to define a Mohr's circle of average strains for each load stage and finally one optimum circle passing through all four measured points as close as possible was determined. Having defined the strain circle, the remaining strain parameters such as principal compressive strain, principal tensile strain and shear strain, could be determined.

Average stresses of reinforcement were determined from the measured strains in the longitudinal and transverse directions. Using these reinforcement stresses, the average concrete stresses in the longitudinal and transverse directions were calculated from equilibrium equations. By knowing the applied shear stress

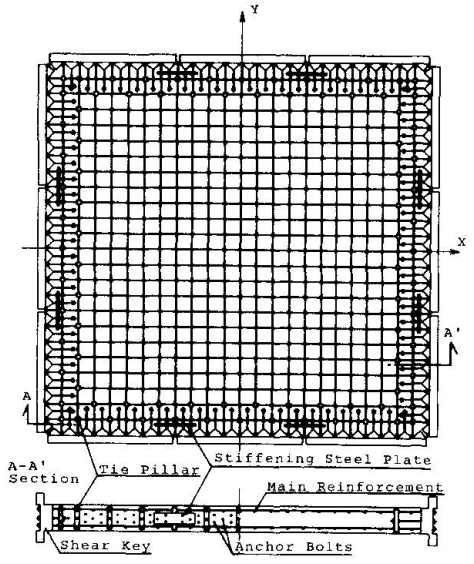

Fig.7 Test specimen

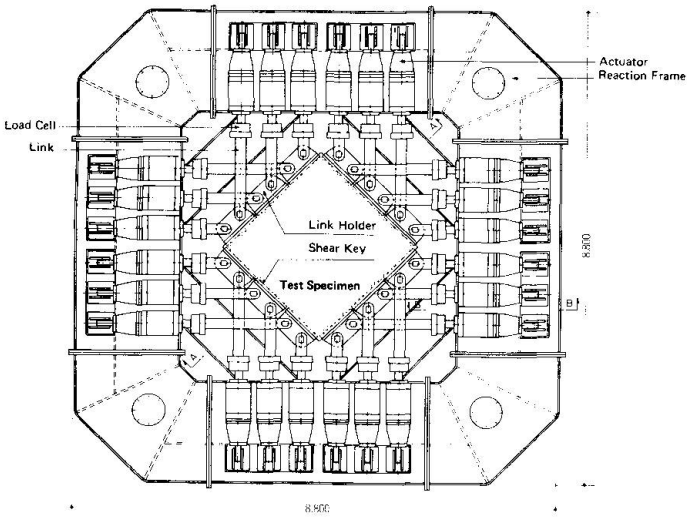

Fig.8 Testing facility

acting on the test panels the remaining concrete stress parameters could be determined. Thus, it was possible to determine concrete strain and stress circles at each load stage [3].

For example, the shear stress-strain relationship and the principal stress-strain relationship of concrete obtained from a typical panel (KP6) are shown in Fig. 13(a) and Fig. 14 (a) respectively. The reinforcement ratio of this specimen was 2.0% and its failure mode was a sliding shear failure of concrete prior to yielding of reinforcement. Among these test results, the principal stress-strain relationship of concrete is most important and from this relationship some significant characteristics of cracked concrete subjected to reversed cyclic in-plane shear stresses can be found. Namely, the decrease of stiffness during the unloading stage, the successive slip phenomena and the restoration of compressive stiffness at reloading stage are obvious.

In these figures, the predicted responses by Vecchio and Collins' model for monotonic loading are also indicated for reference. Here, the cracking strength of concrete was assumed to be the observed values.

3.2 Analytical Method

3.2.1 Principal Stress-Strain Relationship for Cracked Concrete

Fig. 9(a) shows a schematic hysteretic loop model of the principal stress-strain relationship of cracked concrete. The points C, F, I, L and Q correspond to the maximum applied shear stress stages in each loading cycle and the points A, D, G, J, M and R correspond to the loading step when applied shear stress is equal to zero.

The outlines of the proposed hysteretic loop model for cracked concrete are described below.

- At first, the residual stresses and strains of cracked concrete are defined as the stresses and strains when the applied shear stress is equal to zero (D, G, J, M, and R in Fig. 9(a)). This consideration is the main point of the analysis as the importance of residual strains has been presented in the aforementioned monotonic analysis of a shear wall. The magnitude of the residual strain is considered to depend on the maximum strain at the start of unloading. In Fig. 10 relationships between the measured residual strains and measured maximum strains are shown. From these data, an approximate function to define the magnitude of the residual strain used in the proposed analytical model was assumed as the curve indicated in Fig. 10. Since the residual stress and strain are known, the unloading path (CD, FG, IJ, LM and QR in Fig. 9(a))

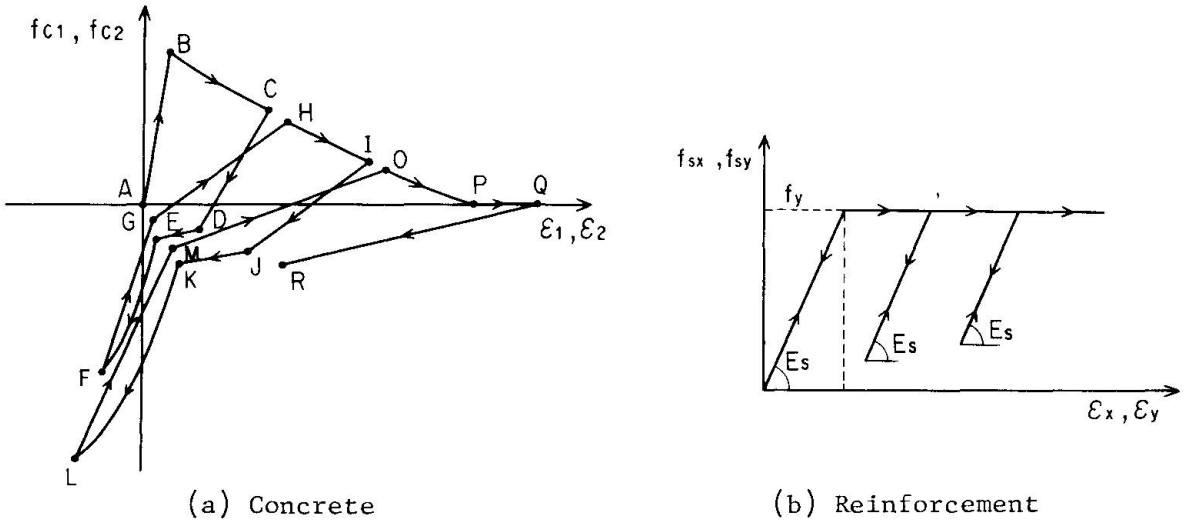

(a) Concrete (b) Reinforcement

Fig.9 Schematic hysteretic loop of principal stress - strain relationship

can be defined.

- Next, the stiffness of cracked concrete in the slip region must be defined. Fig. 11 shows the relationship between the decreasing ratio (β) of the slip stiffness to the elastic stiffness of concrete and the residual principal strain with an approximate function. Since the behaviour in this slip region is unstable, the measured data displays considerable dispersion.

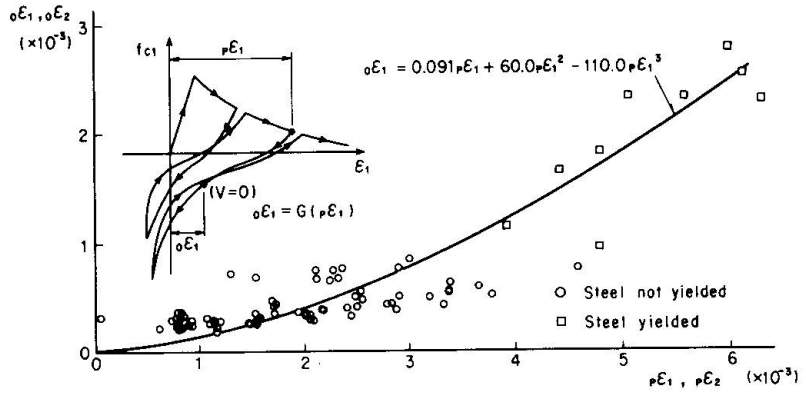

Fig.10 Residual principal strain - maximum principal strain relationship

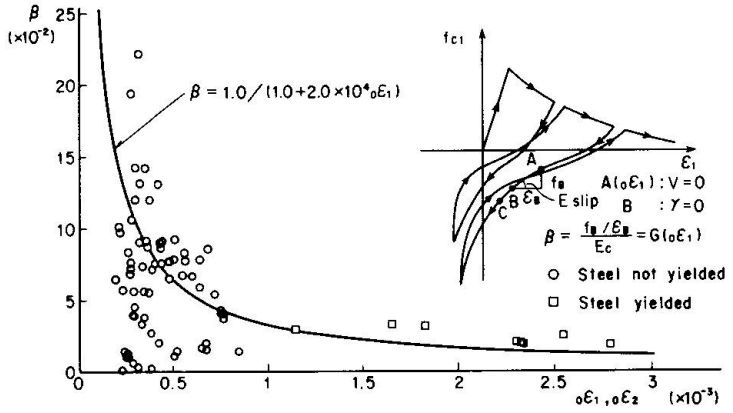

Fig.11 Slip stiffness ratio (β=Eslip/Ec) - residual principal strain relationship

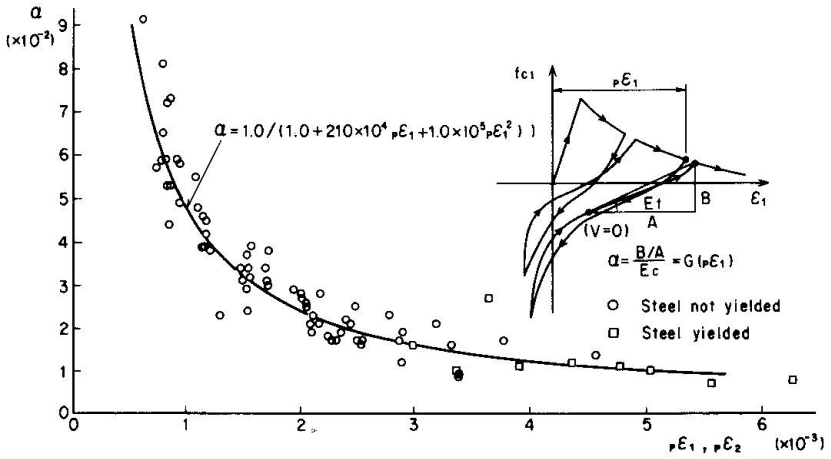

Fig.12 Restoring stiffness ratio (α=Et/Ec) - maximum principal strain relationship

- The restoring tensile stiffness (Et) of cracked concrete from the residual stress state to reloading tensile stress state is defined as a function of the maximum tensile strain experienced in the former loading cycle. Fig. 12 shows the relationship between the ratio (α) of restoring tensile stiffness to elastic stiffness and maximum tensile strain with an approximate function.

- The original principal compressive and tensile stress-strain relationships of cracked concrete proposed by Vecchio and Collins were adopted for evaluating the envelope stiffness of cracked concrete during the loading stage (EF and KL in compressive region and BC, HI and OPQ in tensile region shown in Fig. 9(a)). In the proposed analytical model, however, appropriate coordinate transformations of the original stress-strain relationships are performed in order to satisfy the continuous conditions of the hysteretic loop at the junction points (E and K in Fig. 9(a)).

3.2.2 Stress-Strain Relationship for Steel

As for the stress-strain relationship of reinforcing steel, the usual bilinear uni-axial stress-strain relationship was adopted as shown in Fig. 9(b) .

3.2.3 Numerical Solution Technique

By using the aforementioned stress-strain relationships of concrete and steel, equilibrium equations and compatibility requirements, nonlinear simultaneous equations of unknown average stress and strain parameters were derived. The Newton-Raphson iteration technique was adopted to solve these nonlinear equations. The solutions were continuously obtained step by step at each loading stage.

3.3 Analytical Results

The proposed analytical model was adopted to predict the response of the specimens tested in this investigation. Among the obtained analytical results, the shear stress-strain relationship for specimen KP6, is presented in Fig. 13 (b). As shown in this figure, the predicted envelope curve represents the observed behavior well. However, the predicted ultimate shear strength is larger than the observed one. Such a discrepancy is also found in the predicted result of monotonic loading as shown in Fig. 13 (a). This means that more precise studies are necessary to evaluate more accurate envelope curves under not only reversed cyclic loading but also monotonic loading.

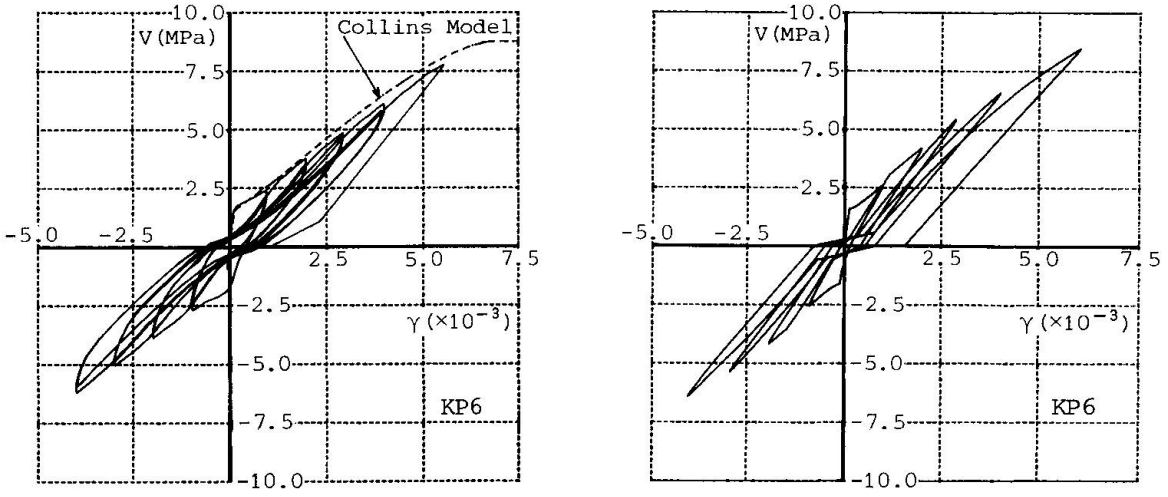

(a) Test (b) Analysis

Fig.13 Shear stress - shear strain relationship

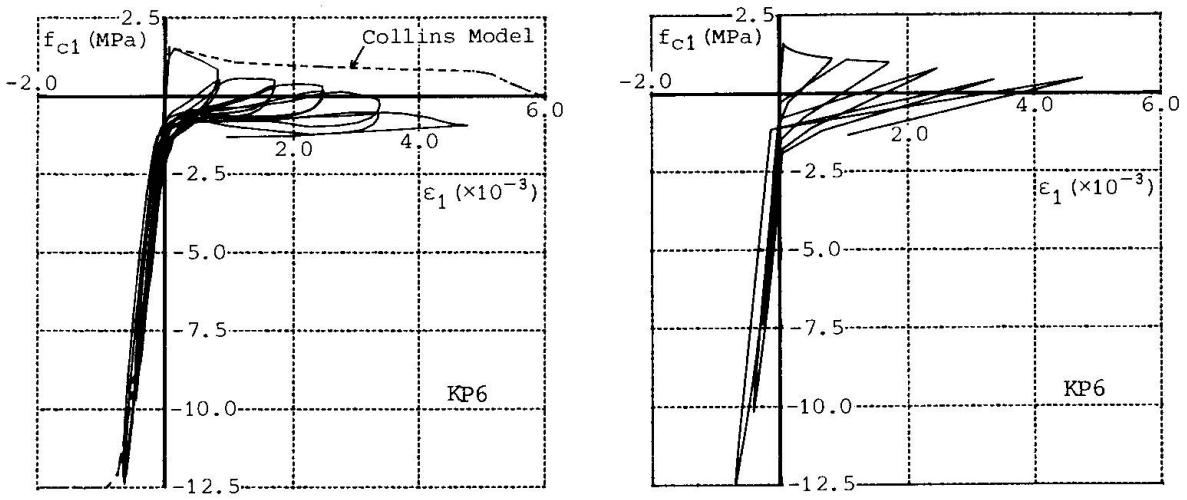

(a) Test (b) Analysis

Fig.14 Principal stress - strain relationship of concrete

As to the hysteretic loop of the shear stress-strain relationship, the following characteristic behaviors under reversed cyclic shear loading are well predicted by the proposed method such as, a) decrease of concrete stiffness at unloading stage, b) slip stiffness depending on residual strain and c) keeping a constant value of shear stress at shear strain equal to zero.

Next the predicted principal stress-strain relationship of concrete is presented in Fig. 14 (b). The analytical result well represents the dominant decrease of stiffness in the unloading stage from the tensile stress state, the successive slip phenomena and the restoration of compressive stiffness at the reloading stage.

4. CYCLIC ANALYSIS OF COLUMN

A column contains comparatively thick reinforcing bars which are arranged rather sparsely. From this specific feature a microscopic approach is effectual which can model the behaviors of reinforcements and bonds. As to the loading condition bi-directional lateral forces are very important. For such a case the three-dimensional approach is necessary.

4.1 Analytical Method

A reinforced concrete column is considered to be composed of core concrete, cover concrete, reinforcing bars and bonds. Nonlinear analyses are performed incrementally based on the nonlinear properties of each element. The approach is almost the same as indicated in the previous paper [7]. Hereunder only the main points are described below.

- Core concrete is represented by a hexahedral isoparametric element. The constitutive equation is defined by the plasticity theory based on the Drucker Prager's yield criterion like Eq. (4),(5). Here the parameter α is assumed by the simulation analysis of hooped columns subjected to axial forces. The hysteretic loop is defined as the tri-linear curve which is expressed under uniaxial force like Fig. 15.

$$f = \frac{3}{2}\alpha(\sigma_x + \sigma_y + \sigma_z) + f_0 = k \qquad \cdots\cdots\cdots\cdots (4)$$

$$f_0^2 = \frac{1}{2}\{(\sigma_y - \sigma_z)^2 + (\sigma_z - \sigma_x)^2 + (\sigma_x - \sigma_y)^2 + 6(\tau_{yz}^2 + \tau_{zx}^2 + \tau_{xy}^2)\} \cdots\cdots (5)$$

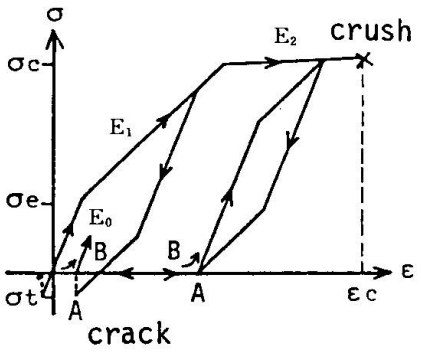

Fig.15 Hysteretic loop of core concrete

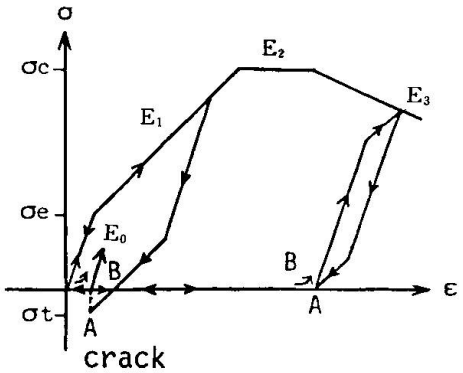

Fig.16 Hysteretic loop of cover concrete

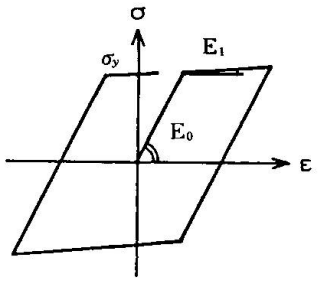

Fig.17 Hysteretic loop of reinforcement

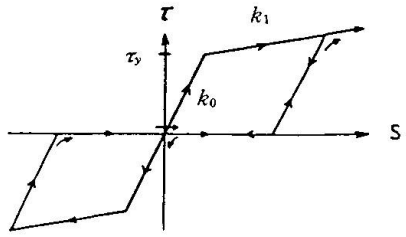

Fig.18 Hysteretic loop of bond

- Cover concrete is represented by a rod element or a *quasi*-three-dimensional element in which the displacements of each node are extrapolated from its adjoining core concrete. But the nonlinear characteristic is estimated from the axial stress only. This approach can make it simple to treat the negative property of cover concrete after peak stress like in Fig. 16.

- A reinforcing bar is represented by a rod element possessing only axial stiffness. The stress vs. strain relationship is assumed to be a bilinear loop as shown in Fig. 17.

- Bond is modeled as a set of link elements connecting reinforcing bars and concrete elements. For bond vs. relative diplacement in-between , a slip-type bilinear loop is assumed as shown in Fig. 18.

4.2 Column Subjected to One-dimensional Lateral Forces

4.2.1 Test Specimen and Analytical Model

The analyzed test specimen is a hooped column with the total longitudinal reinforcement ratio of 0.91% and the lateral reinforcement ratio of 0.36% [8]. The shear span-to-depth ratio is 2 and the compressive strength of concrete is 31.6 MPa. Many cyclic lateral forces were applied under rigid conditions at both ends with a constant axial force.

Analysis was performed for a quarter portion of the column like Fig. 19. The assumed mesh layout of core concrete is shown in Fig. 20. Here three cycles of loading were applied, that is, the first cycle up to 70% of the yielding load, the second cycle at yielding deflection δ_y and the third cycle at $2\delta_y$.

4.2.2 Analytical Results

An obtained deflection is shown in Fig. 21. As to the envelope curve the experimental results were well predicted. But the analyzed area surrounded by

the hysteretic loop was smaller comparatively. To solve this problem it is necessary to estimate well the restoration of stiffness of cracked concrete considering the residual strain after cracking and to represent a more detailed hysteretic rule of bond slip behavior [9]. Such problems can be investigated adequately by two-dimensional approaches.

The strains of longitudinal reinforcement at the critical section are shown in Fig. 22. Analytical results represented well the observed behavior in tension and compression bars. Reversing loops were also well predicted.

The strains of lateral reinforcement parallel to the loading direction are shown in Fig. 23 (a) and (b). The remarkable phenomena were well predicted that under positive loading the strain suddenly increased after shear cracking of core concrete and shear forces were carried directly by the lateral reinforcement, and that under the reversing and sequent negative loading the strains were reduced rapidly at the first stage and then some residual strains remained.

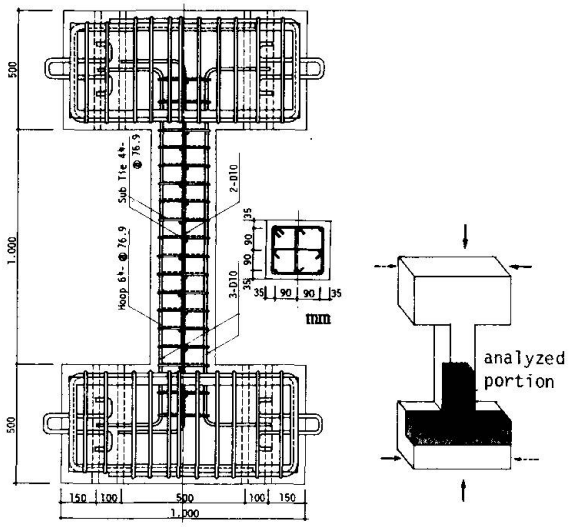

Fig.19 Test specimen

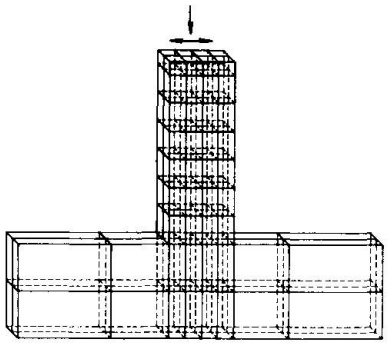

Fig.20 Mesh layout of core concrete

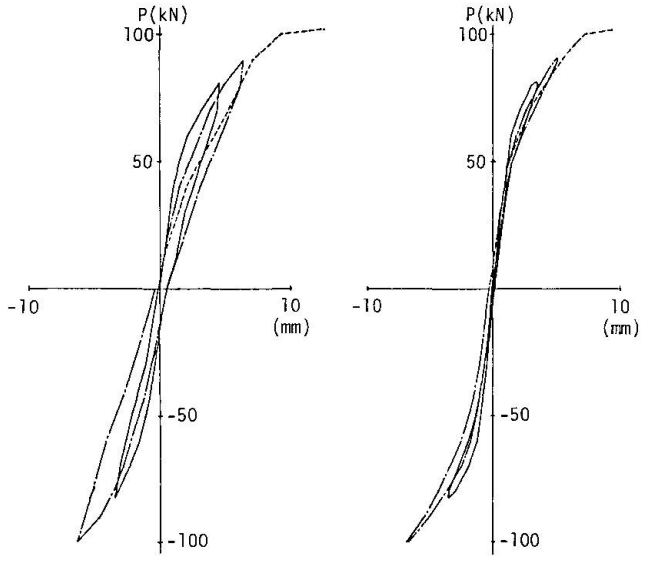

Test Analysis

Fig.21 Load - story deflection relationship

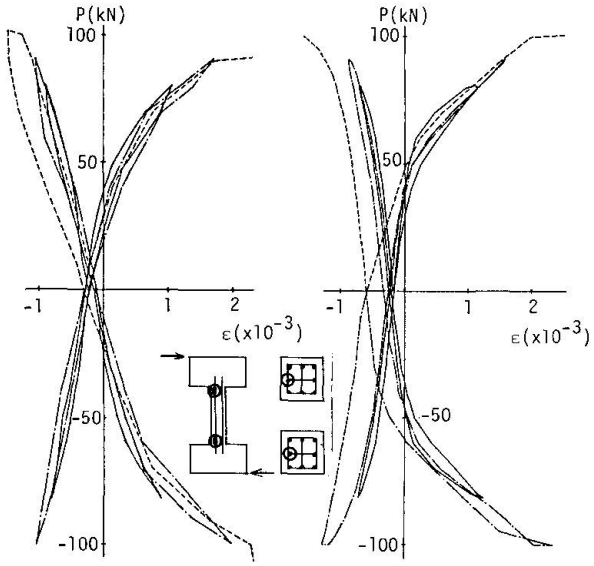

Test Analysis

Fig.22 Load - strain of longitudinal reinforcement relationship

The strains of lateral reinforcement perpendicular to the loading direction are shown in Fig. 23 (c). Under positive loading the strains increased gradually and under reversing they recovered the same curve. Under negative loading the strains decreased at first and then increased after shear cracking. Such behavior can be investigated only by a three-dimensional analysis.

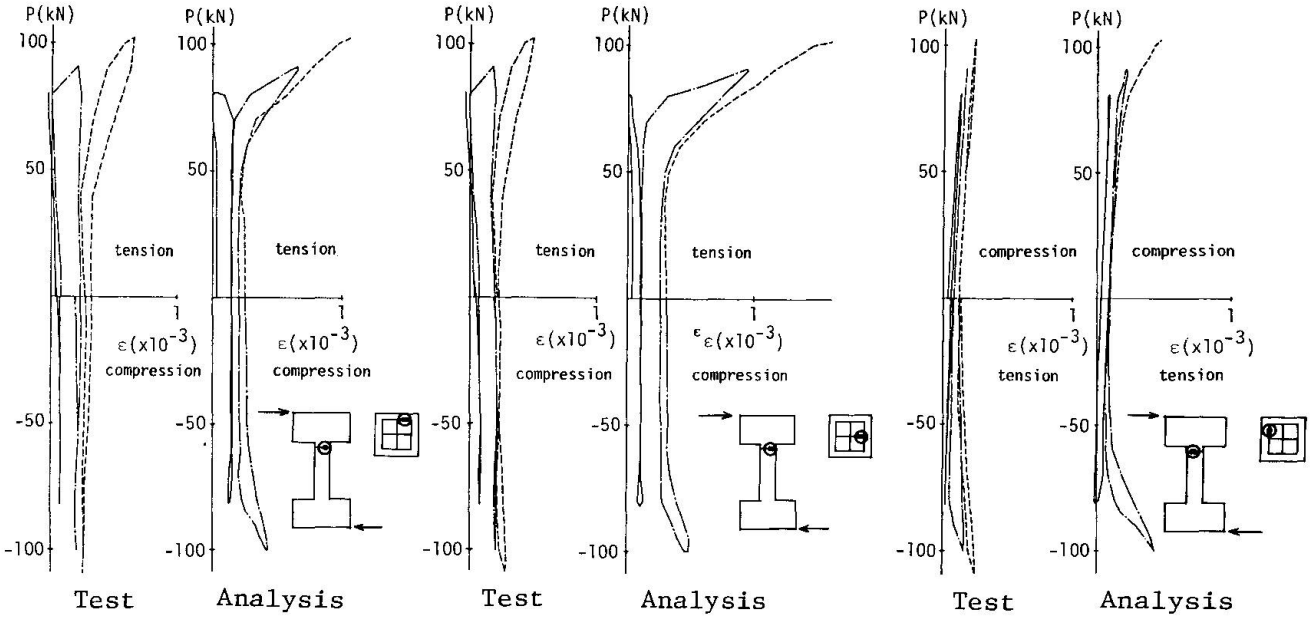

(a) Hoop parallel to loading direction (b) Tie parallel to loading direction (c) Hoop perpendicular to loading direction

Fig.23 Load - strain of lateral reinforcement relationship

4.3 Column Subjected to Two-dimensional Lateral Forces with Circular Displacement

4.3.1 Test Specimen and Analytical Model

The analyzed test specimen is a cantilever column with the total longitudinal reinforcement ratio of 1.42% and the lateral reinforcement ratio of 0.64% as

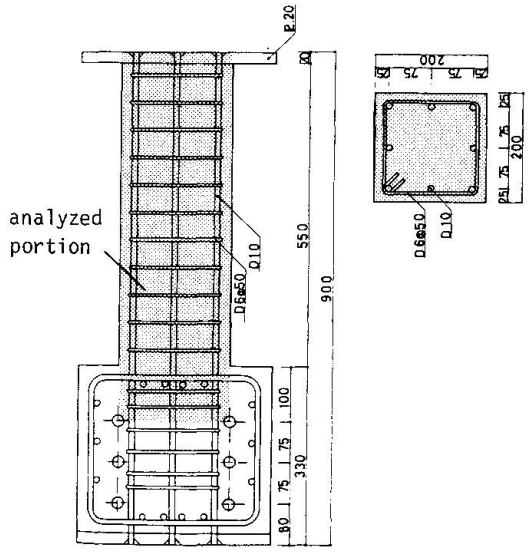

Fig.24 Test specimen and analyzed portion

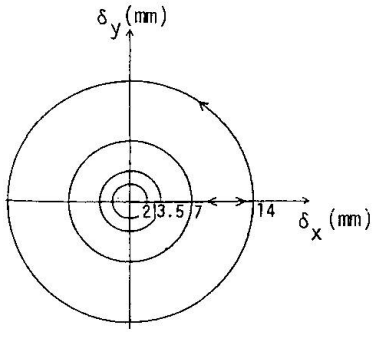

Fig.25 Hysteresis of displacement at top of column

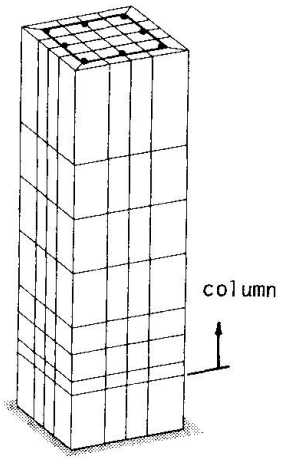

Fig.26 Mesh layout of concrete

shown in Fig. 24[10]. The shear span-to-depth ratio is 3 and the compressive strength of concrete is 15.7 MPa. Two-dimensional lateral forces were applied at the top of the column with circular displacements. The hysteretic displacement is shown in Fig. 25. That is, at first it became deformed in the X-direction from the center and then several circles were traced at a constant displacement.

The analyzed portion and mesh layout are shown in Fig. 24 and Fig. 26 respectively. The basement was modeled as elastic elements in which the anchorage of longitudinal bars could be considered. Axial loads were introduced at the first step and after the second steps the lateral displacements were given. Here one-dimensional diplacement was introduced up to 2.5 mm and after that two cycles were analyzed at a constant displacement of 2.5 mm.

This application is considerably complicated in comparison with the one-dimensional cyclic loading because the stress direction changes every moment in accordance with the looped hysteresis.

4.3.2 Analytical Results

The hysteresis of shear forces in two directions is shown in Fig. 27. The test results showed that they became stable with almost circular shapes, excluding the first cycle of increasing displacements and that the direction of two-dimensional forces preceded the direction of two-dimensional displacements at about 15 degrees. Here the shear forces at the initial stage were not zero because the eccentric loads were added by the actuator weights.

In the analytical results the locus of shear forces showed almost circles from the zero point because of neglecting the initial eccentric loads. This locus predicted well the experimental results. As to the phase lag the angle of forces preceded at 7.5 degree to that of displacements. This tendency was observed in tests. But this value was nearly one half of the observed one. The discrepancy means that the area surrounded by the hysteretic loop of load vs. displacement curve was smaller than observations because the shear forces were smaller at the displacements zero. This problem has already been discussed in the previous one-dimensional study.

The analyzed strains of longitudinal bars and lateral bars are presented in Fig. 28 and Fig. 29 respectively. Here the loads in the X-direction were adopted. The results of longitudinal bars show that the hysteresis converged to certain constant loops excluding the first step with each different shape, inclination and rotating direction. From the results of lateral bars it was shown that the shapes of loops were different in accordance with their locations and that the

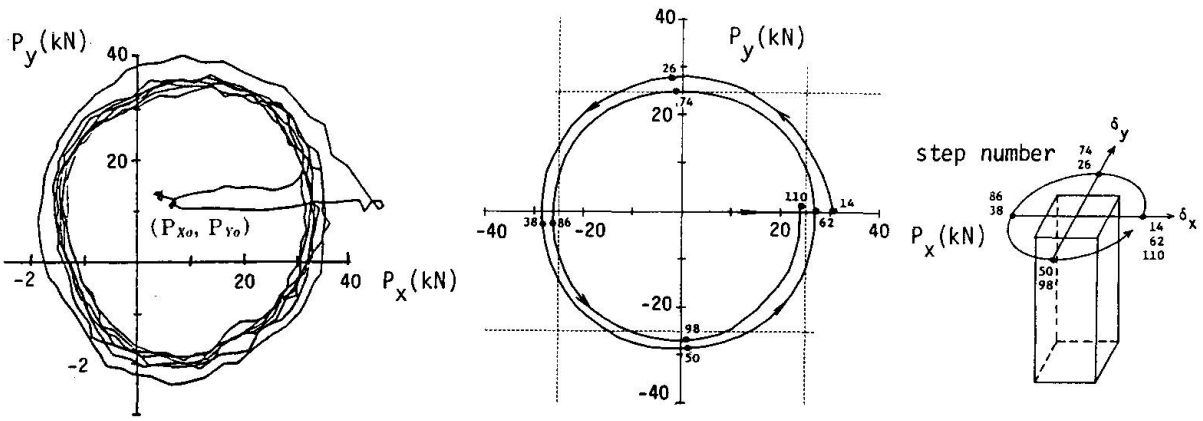

(a) Test (b) Analysis

Fig.27 Cyclic shear forces in two horizontal directions

strains were accumulated while cyclic loading. The latter means that the damage of the column progressed while loading cyclically. This accumulation was verified in the previous study of one-dimensional loaded column.

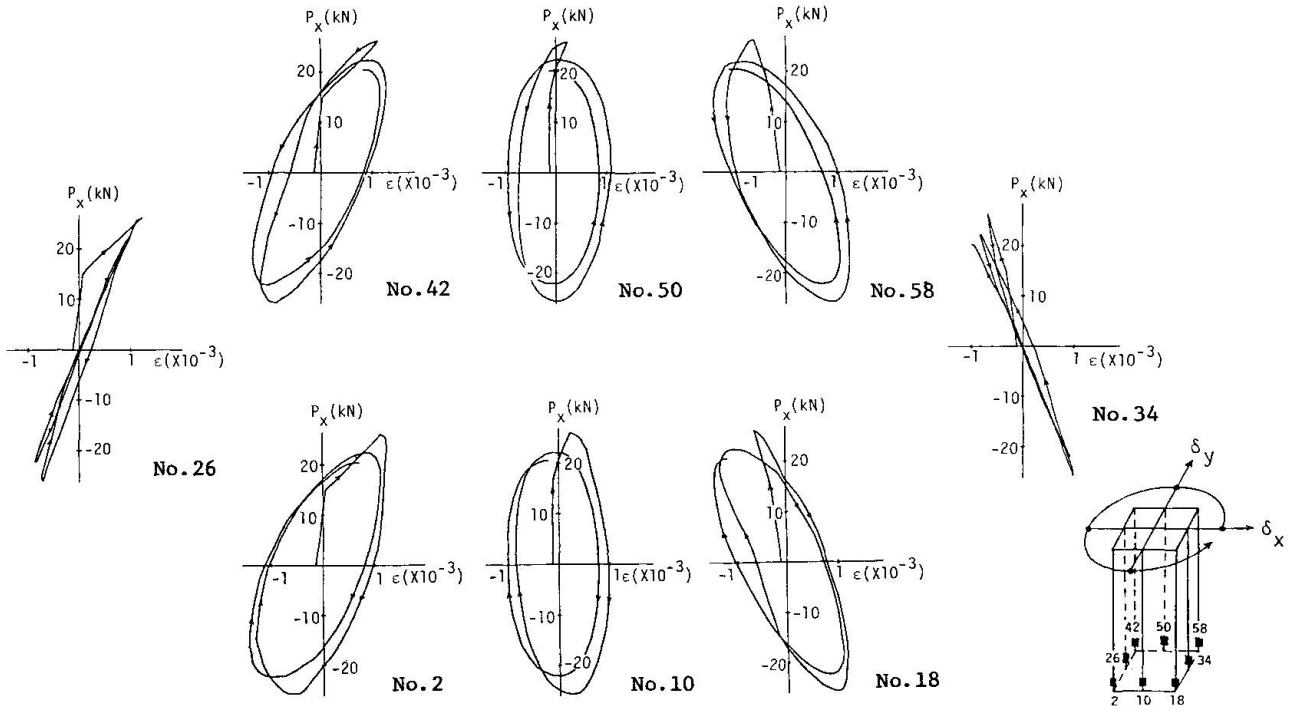

Fig.28 Load in X-direction - strain of longitudinal reinforcement relationship

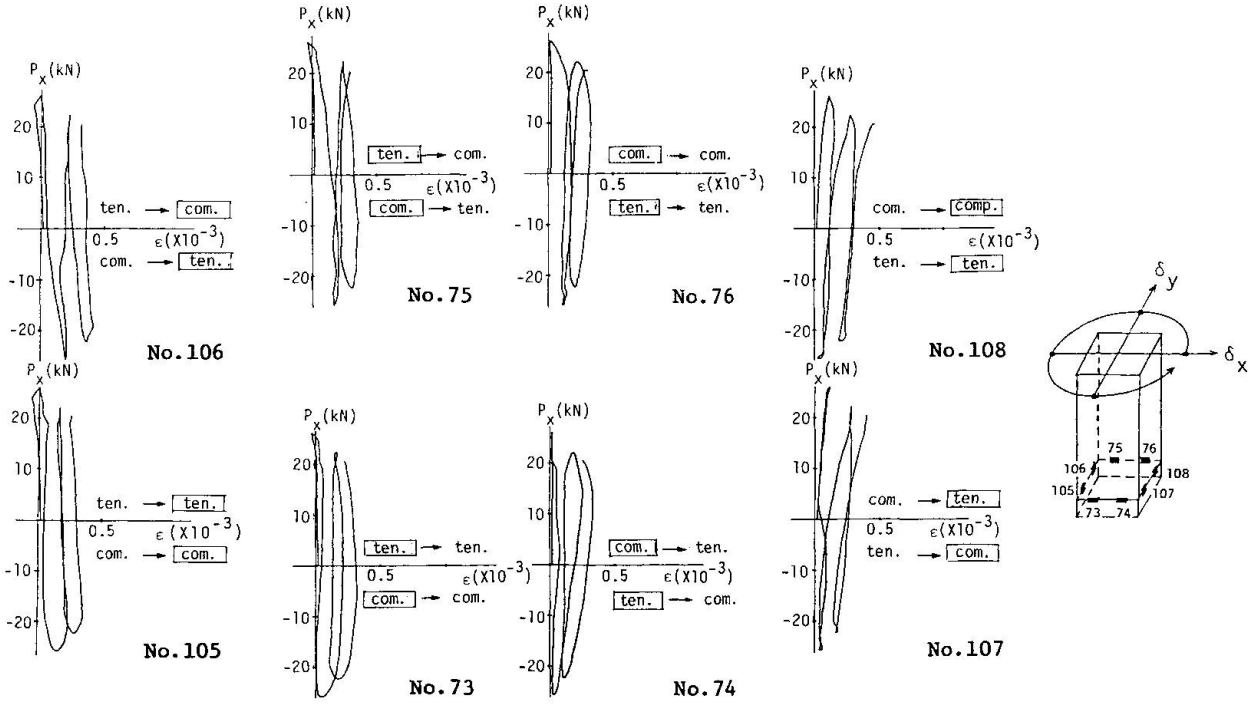

Fig.29 Load in X-direction - strain of lateral reinforcement relationship

5. CONCLUSION

A macroscopic approach based on the average stress strain relationship was effectual for a shear wall in which many reinforcements were arranged uniformly. A microscopic approach considering reinforcement and bond was effectural for a column with thick rebars which were arranged rather sparsely.

In the monotonic analysis of a shear wall subjected to cyclic lateral forces, it was found that the proposed method could predict the shear strain and the envelope curve of load vs. displacement relationship and that the residual strains should be considered to estimate the normal strains and dilatancy.

In the analysis of a panel subjected to cyclic pure shear forces, the cyclic behavior including the reversing loops could be well represented by modeling of residual strains, slip stiffness and restoring stiffness of concrete derived from experimental data.

In the analysis of columns subjected to cyclic one-dimensional or two-dimensional lateral forces, the proposed three-dimensional approach could represent well the envelope of load vs. displacement curve and the cyclic behaviors of reinforcements, especially the strain accumulation of the lateral reinforcements by modeling the three-dimensional characteristics of concrete and the slip behavior of bonds. But it is necessary to model more precisely the cyclic rules of each element in order to predict well the loop area surrounded by the load vs. displacement curve.

REFERENCES

1. INOUE N. and NOGUCHI H., Finite Element Analysis of Reinforced Concrete in Japan. Proceedings of the Seminar "Finite Element Analysis of Reinforced Concrete Structures", ASCE, May 1985, pp. 25-47.
2. NOGUCHI H. and INOUE N., Analytical Techniques of Shear in Reinforced Concrete Structures by Finite Element Method. Proc. of JCI Colloquium on Shear Analysis of RC Structures, JCI, Sep. 1983, pp. 57-92.
3. VECCHIO F.J. and COLLINS M.P., The Modified Compression - Field Theory for Reinforced Concrete Elements Subjected to Shear. ACI Journal, March - April 1986, pp. 219-231
4. INOUE N., KOSHIKA N. and SUZUKI N., Analysis of Shear Wall based on Collins Panel Test. Proceedings of the Seminar "Finite Element Analysis of Reinforced Concrete Structures", ASCE, May 1985, pp. 288-299
5. SHIOHARA H., HOSOKAWA Y., YAMAMOTO T. and AOYAMA H., Shear Distribution in Earthquake Strengthening Post-Cast Shear Wall. Proceeding of JCI 7th Conference, 1985, pp. 389-392 (in Japanese).
6. OHMORI N., TSUBOTA H., INOUE N., WATANABE S. and KURIHARA K., Reinforced Concrete Membrane Elements Subjected to Reversed Cyclic In-plane Shear Stresses. 9th SMIRT, 1987.
7. MUTO K., SUGANO T., MIYASHITA T. and INOUE N., 3-Dimensional Nonlinear Analysis of Reinforced Concrete Columns. Reports of the Working Commissions, IABSE Colloquium Delft 1981, pp. 381-396.
8. OHMORI N., TAKAHASHI T., ISHII K. and WATANABE S., Study on Prevention of Collapse of Reinforced Concrete Short Column (Part 13). Proceeding of Annual Conv., AIJ, Oct. 1974 (in Japanese).
9. NOGUCHI H., Analytical Models for Cyclic Loading of RC Members. Proceedings of the Seminar "Finite Element Analysis of Reinforced Concrete Structures", ASCE, May 1985, pp.486-506.
10. SUZUKI N. and AOYAMA H., Restoring Force Characteristics of Reinforced Concrete Columns Subjected to Bi-directional Forces (Part 1 Test Results). Proceeding of Kanto District Symposium, AIJ, 1978 (in Japanese).

Unified Approach in the Application of the Finite Element Method

Approche unifiée dans l'application de la méthode des éléments finis

Vereinheitlichter Ansatz bei der Anwendung der Methode der Finiten Elemente

Yasumitsu WATANABE
Shimizu Constr. Co.
Tokyo, Japan

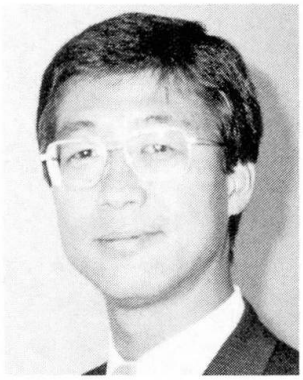

Yasumitsu Watanabe, born 1948, received his civil eng. degree at Waseda Univ., Tokyo. Involved in the design of prestressed concrete structures and in onsite quality control management for ten years.

Hideo ONO
Taisei Corp.
Tokyo, Japan

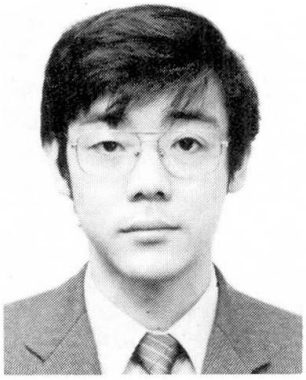

Hideo Ono, born 1955, graduated from Science Univ. of Tokyo. He is now a structural engineer in the nuclear facilities engineering department.

Tatsumi ENDO
Res. Inst. Electric Power Ind.
Tokyo, Japan

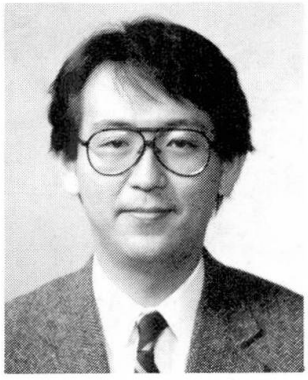

Tatsumi Endo, born 1957, received his civil engineering degree at the Tokyo Institute of Technology. He has been engaged mainly in research in the non-linear analysis of RC structures in electric power facilities.

Kazuhiro NAGANUMA
Obhayashi Corp.
Tokyo, Japan

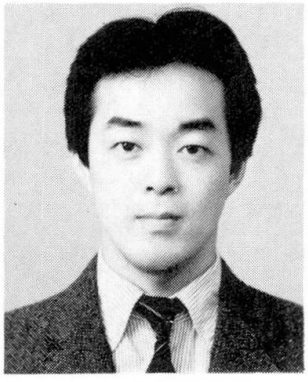

Kazuhiro Naganuma, born 1957, graduated from Chiba Univ. He is a research engineer at the Technical Research Institute. His research interests include non-linear FEM analysis of RC structures.

SUMMARY
The authors investigate problems concerning the application of the finite element method to the design of reinforced concrete structures in Japan, and describe approaches for modeling methodology and evaluating results.

RÉSUMÉ
Les auteurs étudient les problèmes relatifs à l'application d'une méthode des éléments finis pour le projet de structures en béton armé au Japon. Ils décrivent la méthodologie proposée pour l'étude par modèle et commentent les résultats.

ZUSAMMENFASSUNG
Die Autoren untersuchen Probleme der Anwendung der FE-Methode beim Entwurf von Stahlbetonkonstruktionen in Japan, beschreiben Möglichkeiten der Modellmethodologie und werten Resultate aus.

1.INTRODUCTION

Recently, the increase in large-scale and complex structures coupled with the improvement of the availability and popularization of computer technology have created opportunities for the direct and indirect use of the finite element method (FEM) as a tool for designing concrete structures. FEM analysis has proven to be an extremely effective means of obtaining section forces and stress distributions that could not be obtained by frame analysis. In actual applications, however, there are as yet no generally standardized guidelines for the analytical method, modeling methodology, or interpretation of results. In practice, these matters are left up to the individual designer.

Accordingly, the Committee on Finite Element Analysis of Reinforced Concrete (RC) structures (chairman Hiroshi NOGUCHI) organized by the Japan Institute, had commenced its activities in order to establish guidelines for the application of FEM analysis to the actual design of RC structures. At the beginning, the committee made inquiries about application examples of FEM analysis to design and problems encountered in these applications, to structural designers and researchers that are almost members of the committee. This report summarizes the responses and briefly describes current practices in modeling techniques incorporating treatment of nonlinearity through the evaluation of results in Japan.

Forty-four specific applications were reported. As indicated in Table 1, FEM is being employed in work ranging from large-scale structures such as nuclear reactor plants and underground tanks to localized analysis of the structural components.

Table 1 Examples of FEM Design Applications Cited in Response to Questionnaire

Examples of Design Applications	Number of response
Foundation slabs, abutments, underground walls, etc.	8
Tanks for liquefied natural gas, liquefied propane gas	8
Floor slab ,etc	7
joint, opening, etc.	4
Nuclear reactor plants	4
Bridges	3
Tunnels	2
Other structures (dams, towers, etc.)	8
TOTAL	44

2. TREATMENT OF NONLINEARITY

In most design applications, the FEM analysis is conducted with linear rather than nonlinear conditions, partly because of computational cost restrictions, partly because it is considered that linear analysis generally shows safe results, partly because of difficulties in evaluating results, and because of the unreliability of nonlinear analysis. Of the 44 applications described in response to the questionnaire, only 8 used nonlinear analysis, and the proportion would probably have been even smaller if the survey had been limited to designs that were actually executed. Several engineers pointed that nonlinear analysis or treatment of nonlinearity was appropriate for the following.

[1]Designs involving problems of cracking or deformation
[2]When a more economical design could be achieved by considering the cracking behavior through excessive resisting stress
[3]Design of structures such as nuclear reactor plants that must be made fail-safe.

At present, the nonlinearity of concrete is reflected in several ways in which thermal stress causes cracking on a scale extensive enough to have a large effect on stress distribution and rigidity. As indicated in Table 2, nonlinearity was frequently taken into direct or indirect consideration in this problem.

Table 2 Consideration of Nonlinearity in Thermal Stress Analysis

Treatment of Nonlinearity	Number of responses
[1] Nonlinearity Considered	13
<items>	
Nonlinear analysis	2
Pseudo elasto-plastic analysis	5
Using a uniform decreasing rate of rigidity	5
Using empirical formula of rigidity	1
[2] Nonlinearity ignored	2

3.MODELING

3.1 Analysis Area and Boundary Conditions

When the scale of the structure is too big to permit analysis of the whole structure, FEM analysis may be carried out for part rather than the whole. The problems in this case are to determine the area of analysis and the boundary conditions.

At present, the following two methods are generally used;
[1]The analysis is carried out over an area large enough that the effect of boundary conditions can be ignored.
[2]A rough analysis is made for the entire structure, and the results are used to set the boundary conditions .

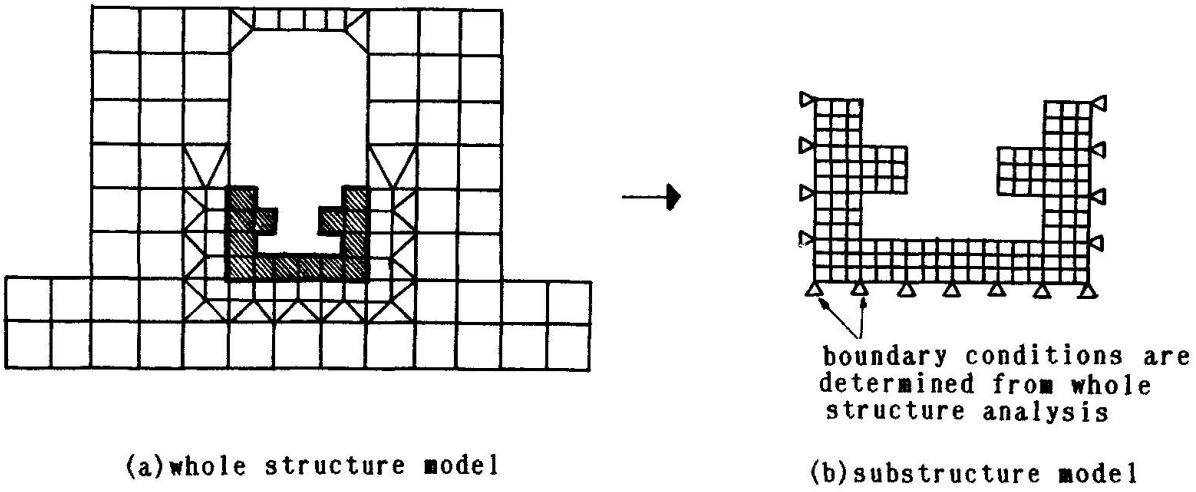

(a)whole structure model (b)substructure model

Fig. 1 An example of substructure model

In case of method[1], some of the respondents calculated the displacement and stress distributions of rough whole model, while others used a model for which the size is 3 to 7 times of the area acted on by the load.

For method [2], the boundary conditions were in general set according to an overall analysis of a rough model to have on equal displacement in the boundary area.

3.2 Element types

When FEM analysis is applied to the design of an RC structure consisting of slabs and walls, the section forces are required directly, so shell elements or axial-symmetric shell elements is usually used.

On the other hand, 2-dimensional plane elements and 3-dimensional solid elements are not frequently used for the purpose of estimating section forces that are applied to the actual design, because the section force cannot be obtained easily. In many cases, these elements were used for obtaining the properties of deformation, those of stress distribution, those of cracking, and that of failure.

For the 3-dimensional analysis in the design applications, the use of shell elements predominated as shown in Table 3. Solid elements tended to be used only for massive parts such as foundation slabs.

Table 3 Applications Classified by Types of Elements

Type of element used	Number of responses
shell elements	18
shell+solid elements	5
2-dimensional plane elements	10
3-dimensional solid elements	9
multi-layered element	2
TOTAL	44

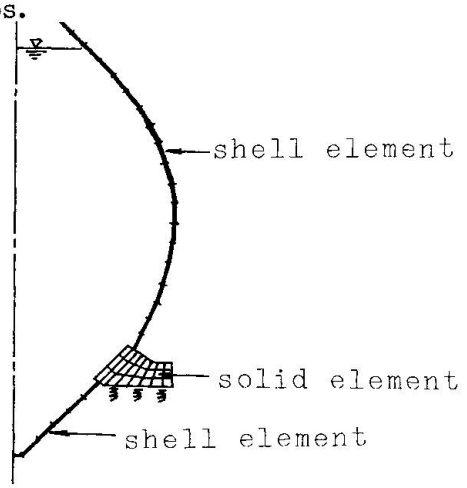

Fig. 2 An example of a model with shell elements and solid elements (egg-shaped tank)

3.3 Element Discretization Techniques

It is generally recognized that a fine mesh raises the accuracy of the analysis but also raises its cost. In this trade-off between accuracy and cost, the guideline generally followed has been to employ a fine mesh in [1] area of particular interest, [2] area of stress concentration, [3] areas acted on by loads, and [4] the vicinity of joints between different types of materials, and to employ a coarse mesh wherever this will not significantly affect the accuracy of the analysis.

All the respondents recognized that the ideal length-to-width ratio of rectangular elements is 1:1, but most designers allow length-to-width ratios up to 1:5 where necessary.

It is advisable to avoid joining isoparametric elements in high-order interpolation functions to triangular elements and elements with low-order interpolation functions. The concentration of stress in the low-order elements in this

type of mesh has a deleterious effect on the results.

3.4 Modeling with Shell Elements

Though using shell elements instead of 2-dimensional plane elements or 3-dimensional solid elements enable section forces to be obtained directly, the use of thin-plate theory to treat objects having a finite thickness requires decisions concerning the following modeling problems:

(1) Treatment of the rigid zone
In only a few cases were joints between walls and floors or between two walls modeled by setting a rigid zone. When a rigid zone was used, the reported practice was to set the area of the rigid zone in accordance with the specifications of RC structures and performed the analysis by increasing the flexural rigidity of this portion, or to use the thickness of the orthogonally joined members as a rigid zone.

Many designers reported that they did not use the results of the analysis near the regions of joints.

(2) Scope of shell elements application
Recently most commomly-used FEM software is able to treat out-of-plane shearing deformation of shell elements. This function enables the limits of the applicability of shell elements to be greatly widened.

Some respondents, however, reported difficulty in determining the location of external forces on foundation slabs etc. unless the element does not have a thickness ,for which reason solid elements were used. Solid elements were also used when gradients of thickness variations could not be represented with shell elements.

(3)Treatment of abrupt change in thickness
A problem in the use of shell elements with axial-symmetry is the unreliability of analysis results in regions with abrupt changes in thickness. Most designers took steps in their models to deal with this problem, such as subdividing the cross-section at the massive end of such regions with solid elements and using the principle of 'plane section remains plane' regarding the joints between the solid and shell elements, or by creating a separate and more detailed model for these regions.

(4) Modeling joins between beams and plates
When a section like Fig. 3 is modeled using a beam element and shell element, three types of models can be considered: Model (a) gives the true cross-sectional area; model (b) gives a better evaluation of flexural rigidity than model (a) and is easier to apply to ordinary sectional design; model (c) ignores the flexural rigidity of the plate and incorporates it into the effective width of the beam. Model (b) is the one of most commonly used.

4. EVALUATION OF ANALYSIS RESULTS

It is considered that it is important for designers to establish guidelines for evaluating the results of FEM analysis rather than to solve the problem in the techniques in applying FEM analysis itself. Several problems and current practices for them concerning evaluation of results are described below.

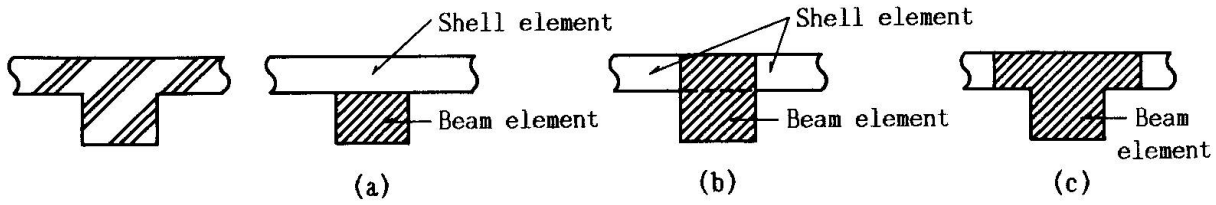

Fig. 3 Modeling of beam and shell elements

4.1 Evaluation of Shell Analysis Result

(1) Treatment of section forces on elements

In the responses to the questionnaire there were many cases in which the section forces at the center of the element were employed as a result. Section forces at nodal points were employed when the reliability of the figures justified their use, because they sometimes give unreasonable value.

The bending moment at intermediate points was generally calculated from the value at the element center points by linear interpolation. For axial forces and shearing force, the general practice was to assume a constant value within the element.

Sectional design is usually performed on an element-by-element basis, but for local stress concentrations it is common to extend the sectional design to include the surrounding elements. It is important that guidelines be given concerning how far to extend the section and what degree of stress concentration can be ignored. In the near future guidelines must be developed and specified.

(2) Treatment of shearing force in plane and torsional moment

There are two general methods of treating shearing force in plane and torsional moment .

[1]They can be treated as equivalent section forces, combining shearing force with axial force or torsional moment with bending moment.

[2]The design formula can be applied to each component individually.

In most cases in which method [2] was reported, torsional moment was ignored. If the magnitude of torsional moment cannot be neglected, some effective treatment must be carried out.

4.2 Evaluation of Results of Plane Stress Analysis and 3-Dimensional Stress Analysis

Since plane stress analysis or 3-dimensional stress analysis give stress itself , these results can be reflected in designs in two ways:

[1]Stress values to be converted to section force values.

[2]The quantity and position of reinforcing bars to be calculated directly from the stress values.

In method [1], the section forces are found by integrating the nodal force or element stress at the center of gravity of the element or at Gaussian integral-point around the axis at the center of gravity.

In method [2], the quantity of steel bars is determined as the quantity needed to deal with the total tensile force or the tensile force exceeding the allowable stress. The bars are either positioned to match the stress distribution or placed in the vicinity of the tension line. It is required that the appropriate method should be specified according to the type of structure and type of load.

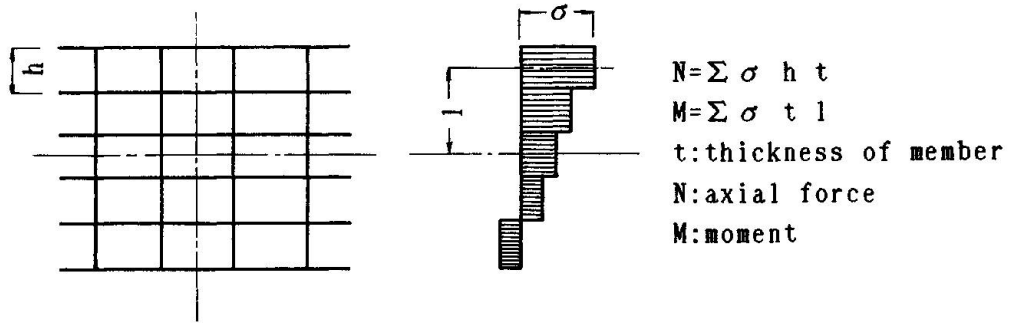

(a)element discretization (b)stress distribution

Fig. 4 An example of a conversion to section force in plane stress analysis

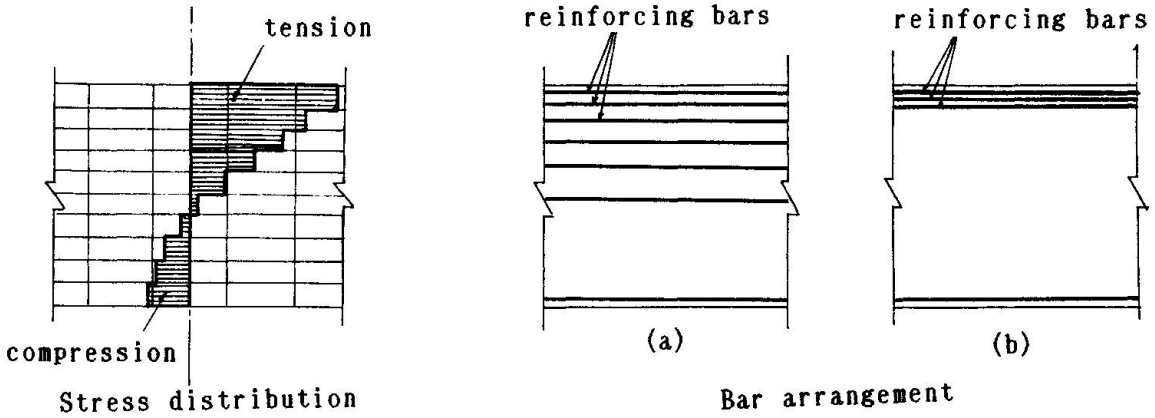

Fig. 5 Reinforcing bar arrangement example according to plane stress analysis

4.3 Evaluation of Dynamic Analysis

When the dynamic response of a structure including ground behavior is studied, it is inappropriate to apply the resulting peak values directly to the design in some cases ,depending on the magnitude of the input seismic oscillations, the scale of the structures, and the importance of the structure. The survey indicated a variety of ways in which results are being applied:

[1]The peak value is used directly
[2]The r.m.s.(root-mean-square) value for the principal oscillation is used
[3]Since the r.m.s. value is normally 60% to 70% of the peak value, 70% of the peak value is added statically to the model.

The following practices were reported concerning the comparison of results of static and dynamic analysis:

[1]The base shear coefficient is made to match the seismic coefficient.
[2]The response acceleration at the center of gravity of the structure is made to match the static seismic coefficient.
[3]Priority is given to the static analysis.
[4]Sectional calculation is made from static analysis, then tested against dynamic analysis, and this procedure is iterated .
[5]Use of large value of static calculation results and dynamic one

It is pointed out that there is at present few commonly accepted procedures for applying the analysis results to design while rapid progress is being made in techniques of dynamic analysis.

5.CONCLUSION

A survey of the actual FEM design applications has found that FEM analysis is a widely employed, but that much is left to the individual designer's judgment in the process of modeling, setting the analysis conditions, and evaluating the results.

This report is intended as an initial step toward setting guidelines for the application of FEM analysis to the design of an RC structure. It has briefly presented some problems, principally in linear FEM analysis which is the most generally employed method at present, and summarized the solutions to these problems that are currently employed in Japan. In the future it will be essential to prepare a wider and more detailed set of guidelines, including those for nonlinear analysis. We hope that this report, by summarizing current practice regarding the application of FEM analysis to design, will help in the attainment of more efficient and reliable designs.

Shear Resistance Mechanisms of Beam-Column Joints under Reversed Cyclic Loading

Résistance au cisaillement d'assemblages poutre-colonne sous l'effet de charges cycliques inversées

Der Schubwiderstand von Stahlbetonknoten unter Wechsellast

Hiroshi NOGUCHI
Assoc. Professor
Chiba University
Chiba, Japan

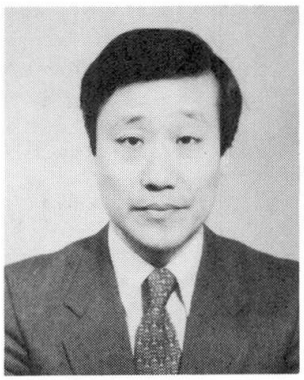

Hiroshi Noguchi, born 1946, received his doctor of engineering degree at the University of Tokyo in 1976. Since then he has been responsible for research in the application of FEM to reinforced concrete structures. He has been involved in the seismic design of reinforced concrete structures.

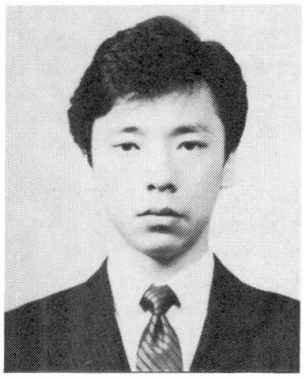

Kazuhiro Watanabe, born 1964, received his engineering bachelor's degree at Chiba Institute of Technology in 1986. Since then he has been involved in the application of FEM to reinforced concrete beam-column joints in the master course of Chiba University.

Kazuhiro WATANABE
Graduate Student
Chiba University
Chiba, Japan

SUMMARY

The nonlinear behaviour of RC beam-column joints under reversed cyclic loading was analyzed by the FEM with the emphasis on the shear resistance mechanisms of a joint. Shear forces contributed by concrete and shear reinforcing bars were calculated from the FEM analytical data. Shear forces contributed by the corresponding components of the previous macro model: the strut mechanism and truss mechanism were also calculated from the corresponding FEM analytical data. The applicability of the macro model was discussed by comparing with the shear distribution model and beam shear model.

RÉSUMÉ

Le comportement non-linéaire d'assemblages poutre-colonne en béton armé sous l'effet de charges cycliques inversées est étudié à l'aide de la méthode des éléments finis en insistant sur les mécanismes de résistance au cisaillement de l'assemblage. Les efforts tranchants dans le béton et dans l'armature sont calculés à partir de données analytiques fournies par la méthode des éléments finis. Les comportements d'étais et de fermes ont également été calculés à l'aide de la méthode des éléments finis. L'application du macro-modèle est étudiée par comparaison avec le modèle de distribution des efforts tranchants et le modèle de la poutre.

ZUSAMMENFASSUNG

Das nichtlineare Verhalten von Stahlbetonknoten zwischen Stützen und Balken unter Wechselbelastung wurde mit FE berechnet mit besonderer Berücksichtigung der Schubtragfähigkeit. Der Beitrag der Schubkräfte von Beton und Stahl wurde aus den FE-Ergebnissen berechnet. Bei den Berechnungen wurden das Streben- und das Fachwerkmodell gegenübergestellt. Die Anwendbarkeit des vorgestellten Macromodells wird diskutiert.

1. INTRODUCTION

In Japan , the Architectural Institute of Japan (AIJ) Standard for Structural Calculation of Reinforced Concrete (RC) Structures [1] does not specify a method to design a beam-column joint against shear nor bond deterioration under seismic loading mainly because most Japanese buildings are in low-rise or medium-rise range and contain large columns and earthquake damage was rarely observed in the beam-column joint [2]. Therefore, the joint is normally reinforced laterally in a manner similar to the middle part of a column. However, with the rationalization in the design, use of higher-strength materials, large-sized deformed bars and the application of the weak-beam design concept has become popular. Application to high-rise buildings has been also discussed and translated into practice. Under these present situation, the development of a rational design method for beam-column joints has become a matter of great concern.

In the ACI Building Code [3] and New Zealand RC Code [4], the provisions for beam-column joints were recently made, but they have very different view of the shear resistance mechanisms of a joint. Therefore, it is of urgent necessity to clarify the shear resistance mechanisms for the development of a rational design method for beam-column joints.

There have been many active experimental studies for beam-column joints, but it is necessary to investigate the nonlinear behaviour of beam-column joints analytically in order to clarify the shear resistance mechanisms. The number of previous analytical studies on beam-column joints is small, and the loading history in the analysis is limited to monotonic loading [5]. Therefore, in this study, the nonlinear behaviour of beam-column joints under reversed cyclic loading was analyzed by the FEM with the emphasis on the shear resistance mechanisms of a joint [6], [7], [8]. An investigating approach in this study is shown in Fig. 1. Reflecting on that previous finite element analyses have been used rather complementally for the investigation of test results, the change of stress flow in joint concrete and the progress of bond deterioration of beam longitudinal bars after beam flexural yielding are investigated from FEM analytical data in detail [9]. It is one of the most distinctive points in the FEM analysis that internal stress flow is visible, and it is rather difficult to measure the internal stress flow in the experiment. Shear forces contributed by concrete and shear reinforcing bars are calculated from the FEM analytical data. Shear forces contributed by the corresponding components of the previous macro model: the strut mechanism and truss mechanism are also calculated from the corresponding FEM analytical data, and they are compared with those which are calculated by shear distribution model and beam shear model.

2. ANALYTICAL MODELS

2.1 General

In this study, the subject of analysis was limited to the joint without lateral beams or eccentric beams, and the plane stress was assumed. In this FEM model, the rotation of principal axes and the stress-strain curves of concrete under cyclic stresses, the criterion for opening and closing of a crack and the bond stress-slip curves under cyclic stresses were considered. These analytical models are especially important in the FEM analysis of shear and bond behaviour of R/C members under reversed cyclic loading. The development process for the analytical models was written in Refs. [8].

2.2 Concrete

The linearly varying strain triangular element was used for concrete. The nonlinear constitutive law of concrete under biaxial stresses was based on the modified Darwin's orthotropic model [10] and the Kupfer's failure criteria [11]. Darwin's model was modified substantially for the rotation of the principal stress axis, because it is very important for the analysis under reversed cyclic loading. The post-crushing behaviour of concrete, the strain-softening portion of the stress-strain curve, was represented by the step-by-step releasing method of the residual stress.

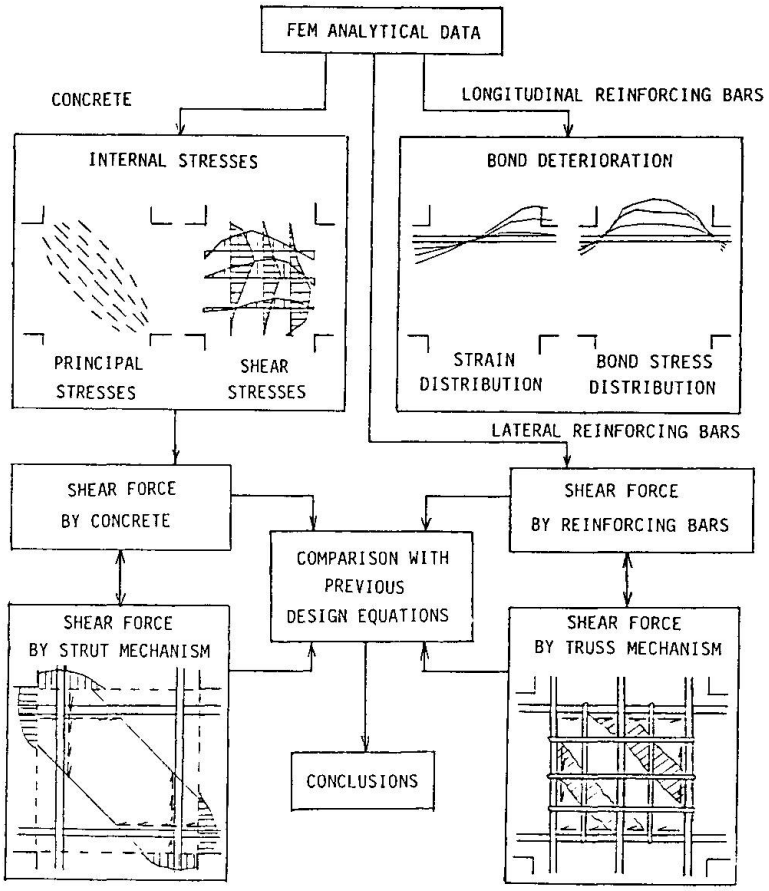

Fig. 1 Investigating Approach

2.3 Reinforcing Bars

The longitudinal bar, the stirrup and tie were represented by the bar elements. A simple bi-linear model was used for the stress-strain curve.

2.4 Bond Slip under Reversed Cyclic Loading

Bond slip was modelled by the bond-link element. Slip characteristics parallel to the bar axis were obtained from the modified bond stress-slip curves under reversed cyclic loading, which were originally proposed by Morita and Kaku [12]. As a modified point for Morita's model, when the bond stress yielded, half of the bond stress was released and the bond stiffness was set to zero. The bond deterioration near the crack was also considered in the proposed model.

2.5 Opening and Closing of a Crack

The discrete crack model was adopted. The crack-link element was inserted between two nodes on both surfaces of a crack along the crack path which was predicted from the test results. When the principal stress at a crack nodal point exceeded the modulus of rupture, the crack is initiated by setting the spring stiffnesses both normal and parallel to the crack surface from the initial large value to zero, and the nodal forces released by the crack are applied.

When a crack was closed, the value of the spring stiffness increased gradually. The proposed model represented the following effect of the local contact of

crack surfaces; as the slip parallel to the crack surface got larger, the recovery of the spring stiffness got earlier and the local contact effect came to be larger. The reopening of a crack was judged on both accumulative spring forces and principal stresses at the nodes of the crack surfaces.

2.6 Nonlinear Analytical Method

The load incremental method using the tangent modulus was adopted for the nonlinear analysis. The releasing nodal forces caused by the cracking, crushing in concrete and bond failure were applied at the next loading stage. The frontal method was used for the solution of the simultaneous, linear algebraic equations.

3. SPECIMENS FOR SUBJECTS OF ANALYSIS

Four half-scaled cross-type specimens, J - 1, J - 1', J - 2 , J - 3, were selected for the subject of analysis as shown in Table 1. The corresponding previous test results were available for the three specimens, J - 1, J - 2, J - 3. Specimen J - 1 was tested by Kamimura and Hamada [13], and specimens J - 2 and J - 3 were tested by Tada and Takeda [14]. Each specimen had its own failure mode: joint failure and bond deterioration of beam longitudinal bars (J - 1), joint failure with good bond for beam longitudinal bars (J - 1'), bond deterioration of beam bars after beam flexural yielding (J - 2), and beam flexural yielding (J - 3). It is necessary to investigate the variable failure modes affected by shear and bond derterioration for clarifying the shear resistance mechanisms in a joint. The middle longitudinal reinforcing bars were set up only in the column of J - 1' to study the role of the column middle reinforcing bars in the shear resistance of a joint with good bond for beam longitudinal bars.

The detail and the finite element idealization of interior beam-column joint specimens are shown in Figs. 2 - 3, respectively. Only half of the whole specimen was analyzed due to the symmetry of the shape and loading condition around a point. The crack pattern was set up using link elements in general accord with the test results under reversed cyclic loading. In the analysis, the specimen was loaded to the positive loading of the third cycle for J - 1, J - 2, J - 3, and to the negative peak load of the second cycle for J - 1'.

4. RESTORING FORCE CHARACTERISTICS

Table 1 Specimens for Subjects of Analysis

Specimen	J-1	J-1'	J-2	J-3
Failure Mode	Joint Failure Bond Deterio-ration	Joint Failure	Bond Deterio-ration after Beam Yielding	Beam Yielding
Bond of Beam Longitudinal Bars	Poor	Good	Poor	Perfect
Middle Longi-tudinal Bars of Column (SD35)	——	D-22	——	——

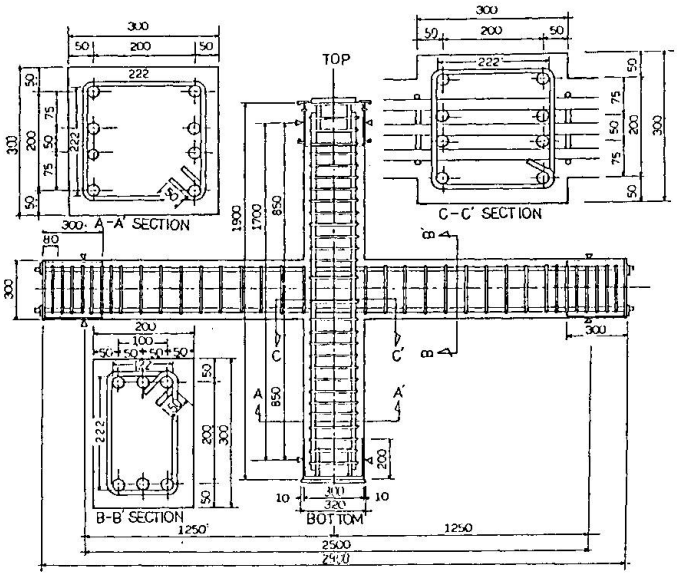

Fig. 2 Detail of Specimen

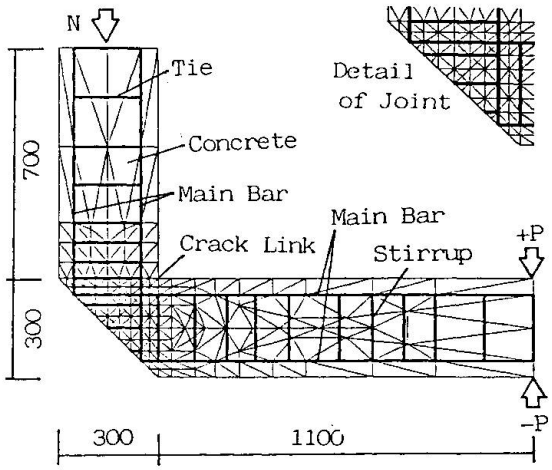

Fig. 3 Finite Element Idealization

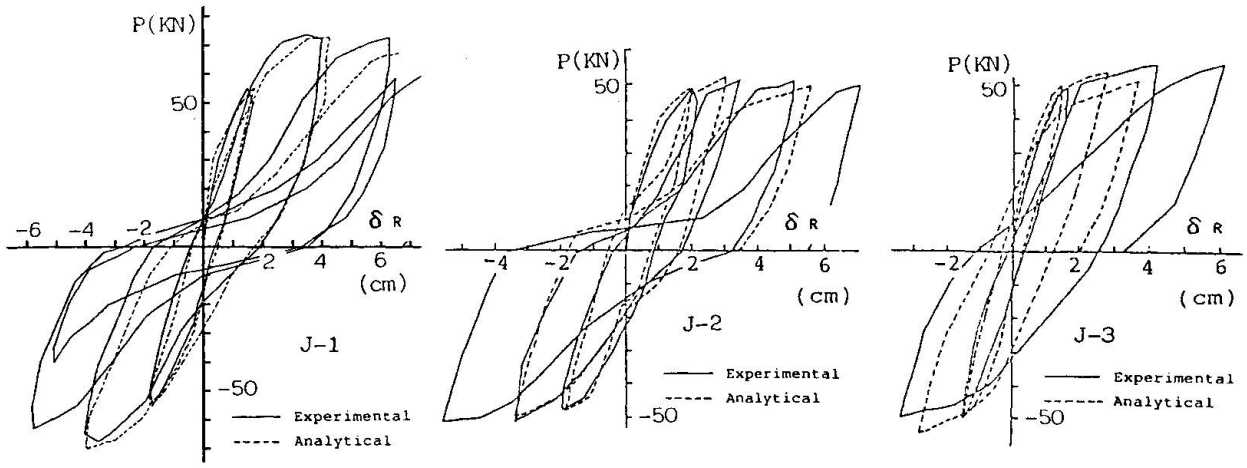

Fig. 4 Load-Story Displacement Relationships

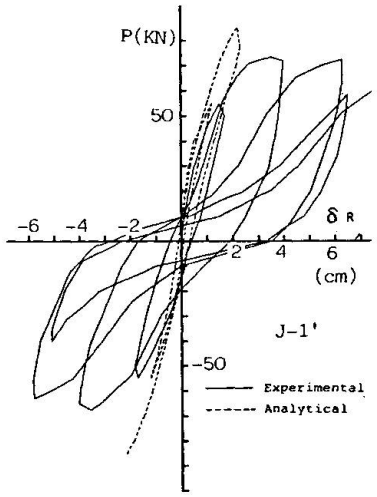

The analytical load-story displacement relationships are compared with the test results in Fig. 4. For J - 1 and J - 2, the analytical results gave good agreement with the experimental results for the shape of hysteresis loops. The analytical restoring force characteristics adopted the contra-S-shape with poor energy dissipation capacity, as cracking and bond deterioration of beam longitudinal bars in the joint progressed under the subsequent cyclic loading. This tendency was more pronounced for J - 2 in which bond deterioration became significant after yielding of beam longitudinal bars. For specimen J - 3, the analytical restoring force characteristics maintained the stable spindle-shape hysteresis loops and almost the same tendency as the test results. For specimen

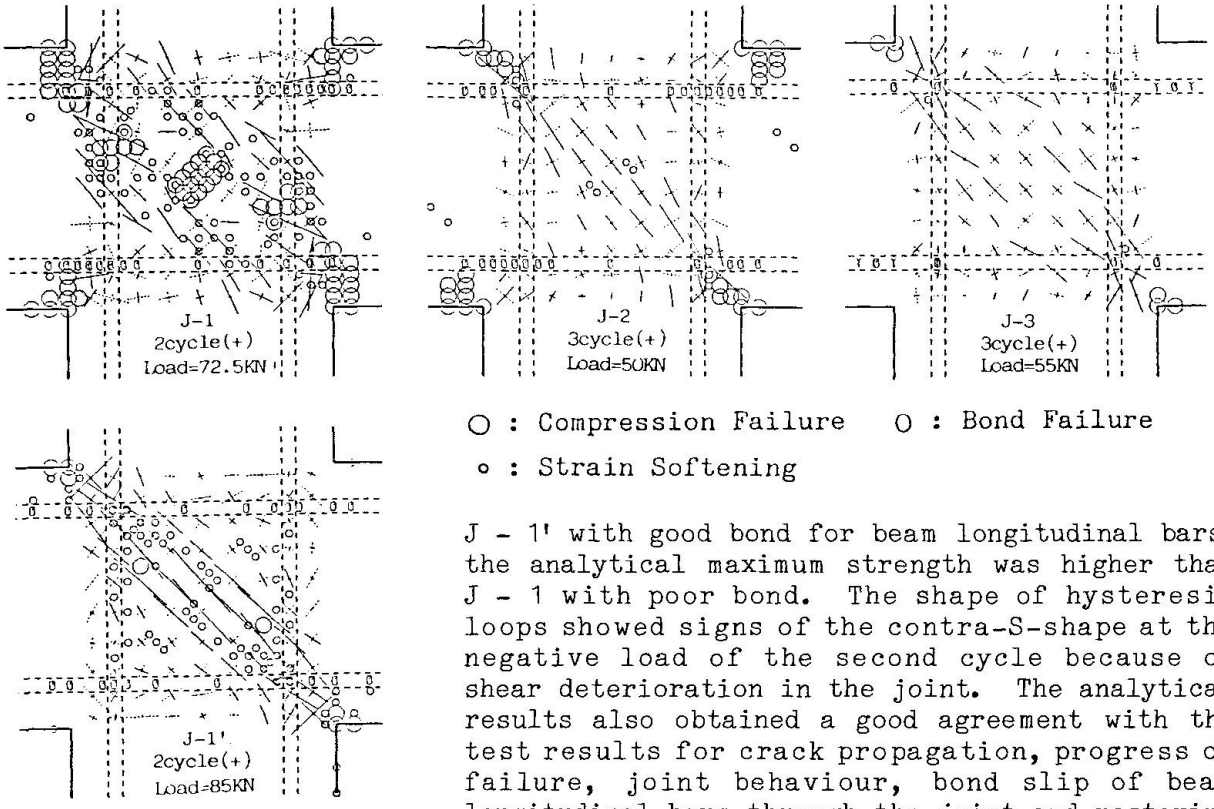

Fig. 5 Principal Stresses

J - 1' with good bond for beam longitudinal bars, the analytical maximum strength was higher than J - 1 with poor bond. The shape of hysteresis loops showed signs of the contra-S-shape at the negative load of the second cycle because of shear deterioration in the joint. The analytical results also obtained a good agreement with the test results for crack propagation, progress of failure, joint behaviour, bond slip of beam longitudinal bars through the joint and restoring force characteristics. The comparisons were discussed in Refs. [8] in detail. From those comparisons, the accuracy of the analytical results were considered to be sufficient for observing the internal stresses to investigate the shear resistance mechanisms in the joint.

5. PRINCIPAL STRESS DISTRIBUTION

Principal stress distribution in the joint concrete was shown in Fig. 5. It is one of the most distinctive points that internal stress flow is visible in FEM analysis. The compressive strut was formed along the diagonal line of the joint under near the peak load of each loading cycle. Strain-softening and compressive failure of concrete were remarkable both on the beam compression zone and along the diagonal line on the joint for J - 1. The width of compressive strut for good bond specimen, J - 3, was wider than bond deterioration type specimen, J - 2. The clear compressive strut was formed along the diagonal line for J - 1'. Strain-softening was remarkable along the diagonal line on the joint, but the compressive failure was not so remarkable as compared with J - 1.

6. SHEAR STRESSES CONTRIBUTED BY JOINT CONCRETE

The concrete shear stresses obtained by the shear distribution model were shown in Fig. 6. In the shear stress distribution model shown in Fig. 7, shear forces were obtained by subtracting the reaction forces in concrete, which were made by the truss action of shear reinforcing bars in the joint, from the integration value of the concrete shear stress over the central horizontal section in the joint. The concrete shear stresses were higher for J - 1, J - 1', joint shear failure type than J - 2, J - 3, beam flexural yielding type. The maximum

shear stresses reached about 0.47 - 0.56 F_c for J - 1, J - 1'. (F_c = compressive strength of concrete) These values were corresponding to the upper bound shear stresses observed in the previous experimental studies [16]. For J - 1, the shear stress at the positive load was higher than that at the negative load for the first and second cycle. It seemed to be caused by the local compressive failure of concrete under relatively lower load. For J - 1', this tendency was not observed, because the compressive failure of concrete was not so remarkable until near the maximum strength in the second cycle. For J - 2, J - 3, the peak shear stresses kept constant values of about 0.15 F_c, and the compressive failure was not observed even after the beam flexural yielding.

The comparisons of shear stresses by joint concrete for J - 2 between the three models were shown in Fig. 7. The compressive strut mechanism model was proposed by Paulay and Park for the shear resistant component by joint concrete [15]. The concept of the beam shear model was adopted in the ACI Code. The three models obtained good agreements with the test results.

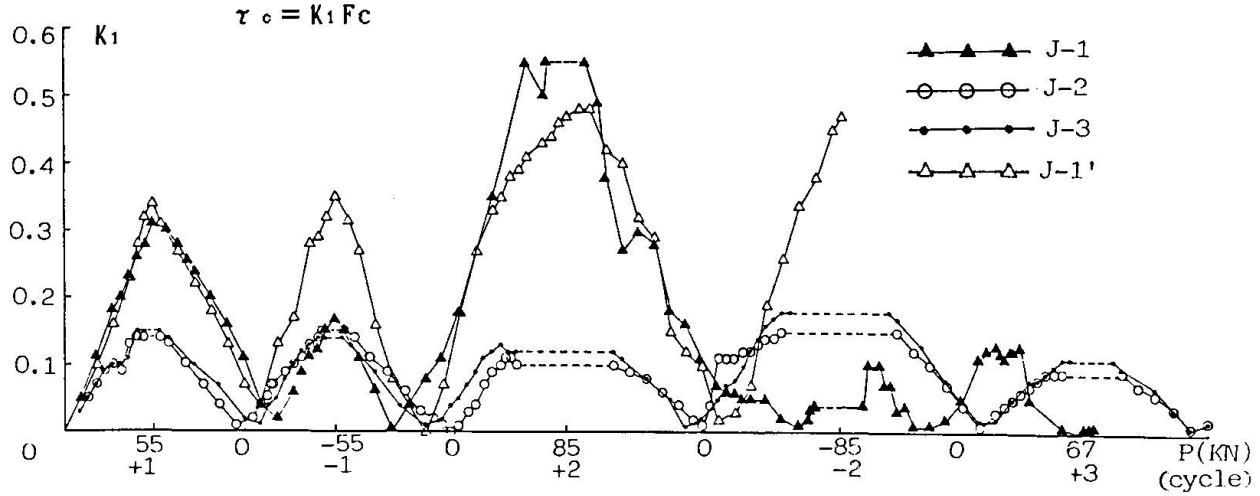

Fig. 6 Concrete Shear Stresses Calculated by Shear Distribution Model

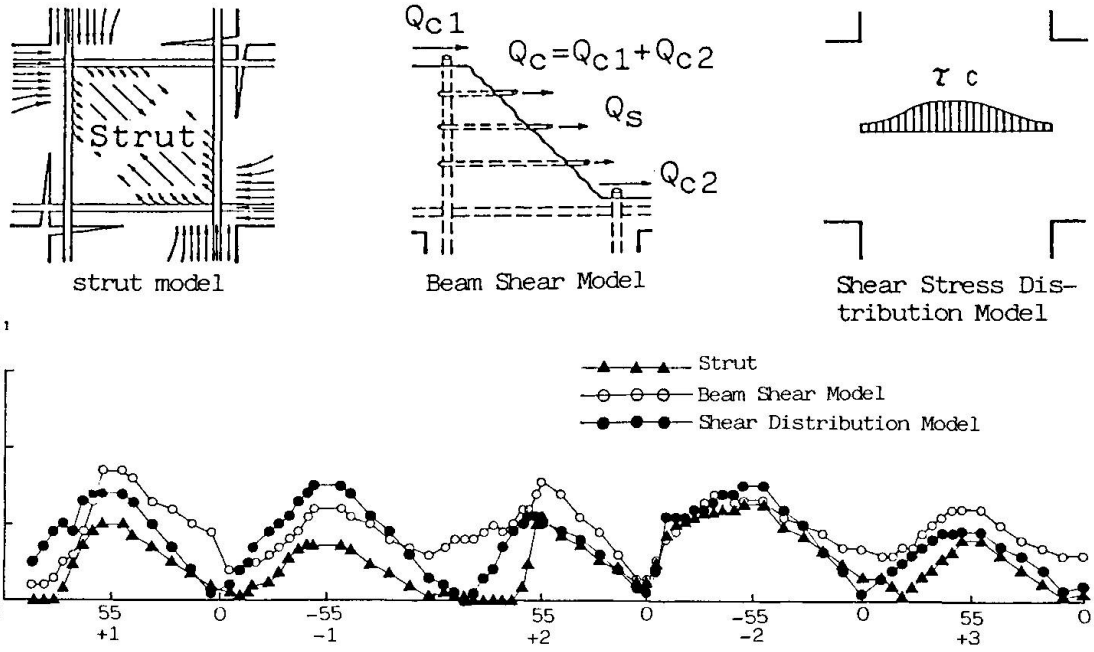

Fig. 7 Concrete Shear Stresses Calculated by Three Models

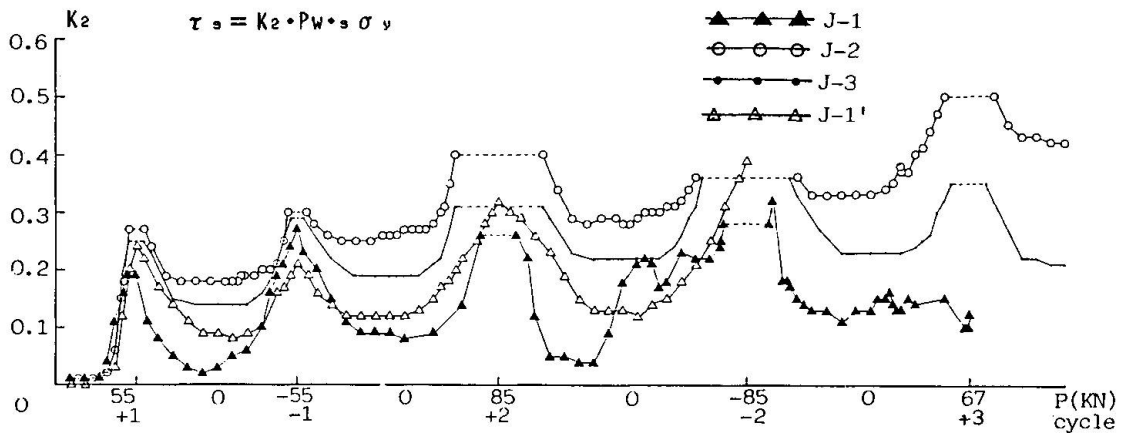

Fig. 8 Shear Stresses Contributed by Joint Reinforcing Bars

7. SHEAR STRESSES CONTRIBUTED BY JOINT REINFORCING BARS

The shear stresses, τ_s, contributed by the joint reinforcing bars were obtained from the strain in the reinforcing bars and shown as the coefficient of $p_{ws}\sigma_y$ in Fig. 8, in which p_w = the ratio of reinforcing bars and ${}_s\sigma_y$ = yielding strength of reinforcing bars. The residual stresses under lower load seemed to be caused by the local contact effect of a crack. The maximum shear forces, τ_{smax} were 0.33 - 0.39 $p_{ws}\sigma_y$ in the joint failure type, J - 1, J - 1', and 0.37 - 0.5$p_{ws}\sigma_y$ in the beam flexural yielding type, J - 2, J - 3. From Fig. 6 and Fig. 8, τ_c was larger for J - 3 than that for J - 2, and τ_s was larger for J - 2 than that for J - 3. Considering that p_w was the same for both specimens, it was considered that the shear forces flew into the joint mainly through the bond of beam reinforcing bars, and consequently the concrete shear stress got larger in J - 3. There was little difference between J - 1 and J - 1', but the peak shear stress increased gradually even at the second cycle for J - 1'.

8. SHEAR STRESSES CONTRIBUTED BY COMPRESSIVE STRUT MECHANISM

The macro model for the shear resistance mechanisms proposed by Park and Paulay [15] were shown in Fig. 9. In the proposed macro model, the contribution of the concrete and joint reinforcing bars to the joint shear resistance were represented by the compressive strut mechanism, and the truss mechanism, respectively. The horizontal joint shear force, V_{ch}, contributed by the compressive strut mechanism was calculated from the corresponding FEM analytical data as follows,

$$V_{ch} = {}_BC_c + \Delta {}_BT_c - V_{col} \qquad (1)$$

in which ${}_BC_c$ = horizontal concrete compression force from the beam, $\Delta {}_BT_c$ =force transferred from the beam bars to the concrete strut and V_{col} = horizontal shear force across a column (See Fig. 9). ${}_BC_c$ was obtained indirectly from the difference between the resultant forces of beam compressive and

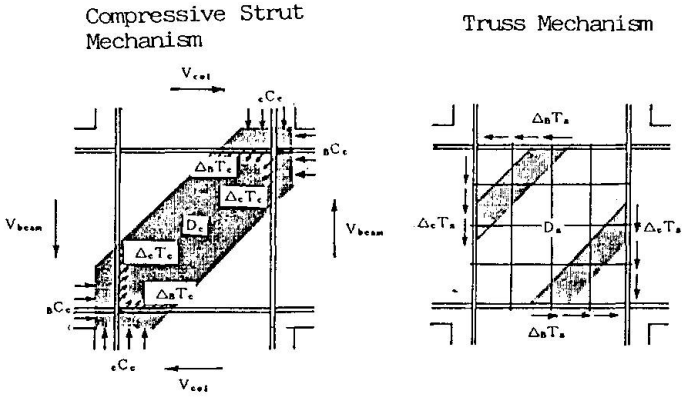

Fig. 9 Macro Model for Shear Resistance Mechanisms Proposed by Park and Paulay

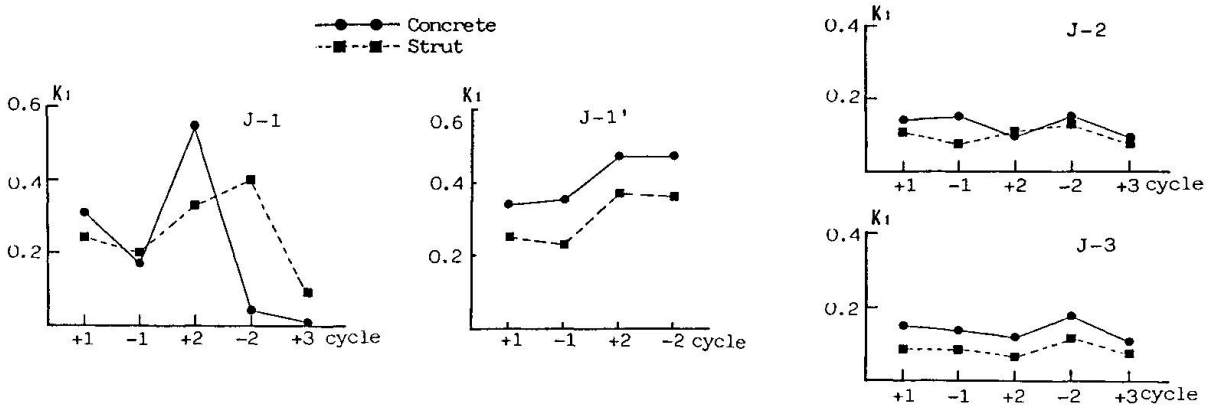

Fig.10 Concrete Shear Stresses Calculated by Strut Mechanism and Shear Stress Distribution Models

tensile longitudinal bars. The shear forces, V_{ch}, calculated by Eq. 1 were compared for the peak load in each cycle with the shear forces obtained by the shear stress distribution model in Chapter 6 in Fig. 10. The strut mechanism model gave a good agreement with the shear stress distribution model for all four specimens. It was shown that the shear stress contributed by concrete could be estimated by the compressive strut mechanism from Fig. 10 and Fig. 7.

9. SHEAR STRESSES CONTRIBUTED BY TRUSS MECHANISM

The horizontal shear forces, V_{sh}, contributed by the truss mechanism was calculated from the FEM analytical data as follows,

$$V_{sh} = \Delta_B T_s \qquad (2)$$

in which $\Delta_B T_s$ = force transferred from the beam bars to the outer concrete of the strut (See Fig.9).

The shear forces, V_{sh}, calculated by Eq. 2 were compared for the peak load in each cycle with the shear forces obtained by the strain in the joint reinforcing bars in Chapter 7 in Fig. 11. The truss model was not in agreement with

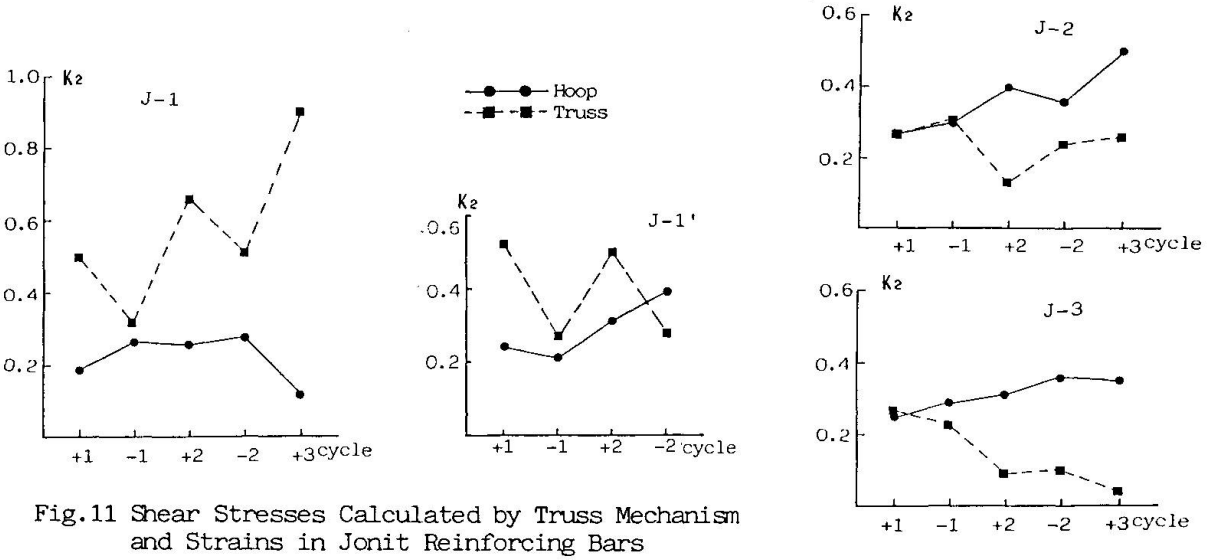

Fig.11 Shear Stresses Calculated by Truss Mechanism and Strains in Jonit Reinforcing Bars

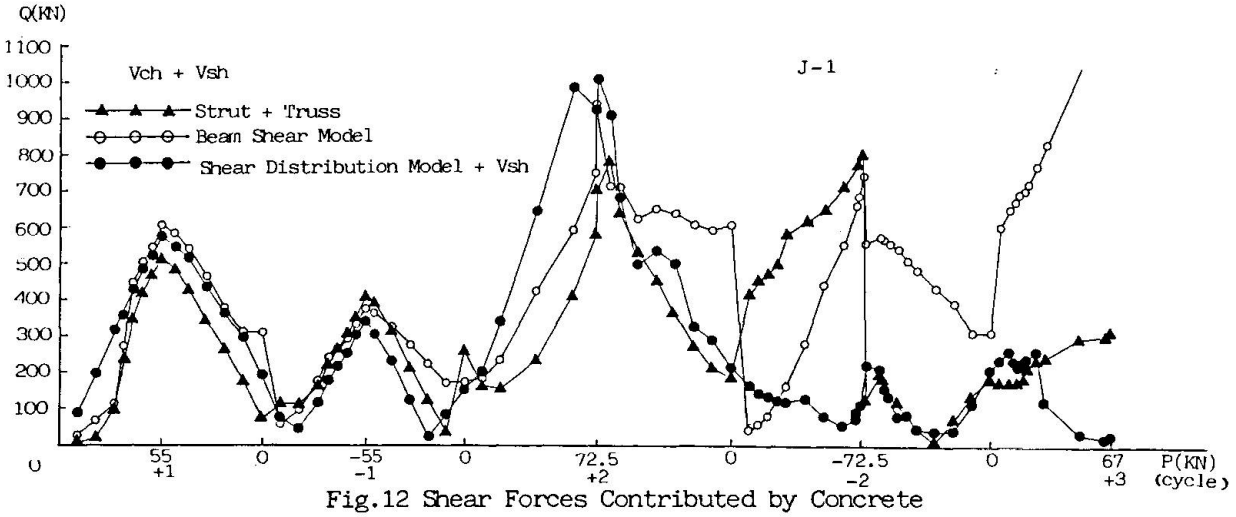

Fig.12 Shear Forces Contributed by Concrete and Joint Reinforcing Bars

the contribution of joint reinforcing bars for J - 1, J - 2, J - 3. It was considered that this was because these three specimens had no middle longitudinal bars in the column. The middle longitudinal bars in the column are considered to be necessary for forming the truss action in the proposed macro model. For J - 1' with the middle longitudinal bars in the column, the truss model gave a better agreement with the contribution of the joint reinforcing bars. For the truss model, it is considered that the further investigation is needed for the role of the middle longitudinal bars in the column and the bond forces of the beam and column longitudinal bars in the shear resistance.

10. TOTAL SHEAR FORCES CONTRIBUTED BY CONCRETE AND SHEAR REINFORCING BARS

The total of shear forces contributed by concrete and joint reinforcing bars was calculated by the three method (Figs. 6, 7) as shown in Fig. 12 for J - 1. The two mechanisms (strut and truss) model gave a good agreement with the shear stress distribution model and the beam shear model for the specimen J - 1, joint failure and bond deterioration type to the positive peak load in the second cycle. But one should note that the errors in the strut and truss mechanism were compensated each other in the two mechanism model. After the positive peak load in the second cycle, the good correspondence with the other two models could not be observed because of the local compressive failure of joint concrete.

11. INTERNAL STRESS RESULTANTS AROUND A JOINT

The vertical shear forces contributed by the strut and truss mechanisms were calculated as follows,

$$V_{cv} = {}_{C}C_{c} + \Delta_{C}T_{c} - V_{beam} \qquad (3)$$

$$V_{sv} = \Delta_{C}T_{s} \qquad (4)$$

in which V_{cv} = vertical joint shear force provided by compressive strut mechanism, V_{sv} = vertical joint shear force provided by the vertical shear reinforcing bars, ${}_{C}C_{c}$ = vertical concrete compression force from the column, $\Delta_{C}T_{c}$ = force transferred from the column bars to the concrete strut, V_{beam} = vertical shear force across a beam and $\Delta_{C}T_{s}$ = force transferred from the column bars to the outer concrete of the strut (See Fig. 9).

The internal stress resultants around a joint combined in an equilibrium vector polygon were calculated from the FEM analytical data as shown in Fig. 13. It was shown that the concrete compression force from the beam, ${}_{B}C_{c}$, was distinguished in J - 1 and J - 2, bond deterioration type. The force transferred from the beam bars to the concrete strut, $\Delta_{B}T_{c}$, was distinguished in J - 1' and J - 3 with good bond for beam bars.

Though the internal stress resultants around a joint were discussed qualitatively by Paulay and Park [15], it is possible to discuss quantitatively the internal stress resultants using the FEM analytical data.

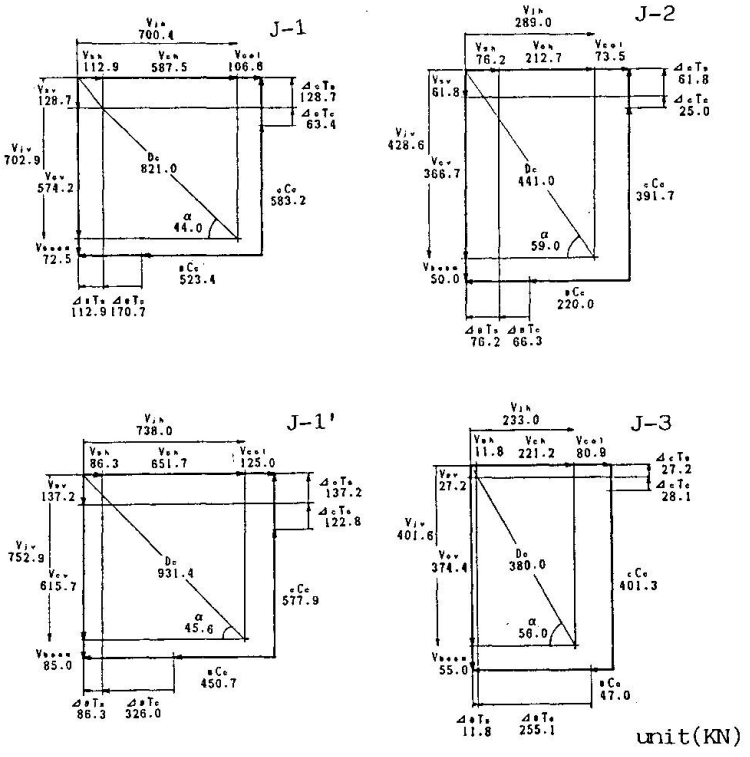

Fig.13 Internal Stress Resultants around a Joint

12. CONCLUSIONS

The nonlinear behaviour of reinforced concrete beam-column joints under reversed cyclic loading was analyzed by the FEM with the emphasis on the shear resistance mechanisms of a joint.

The maximum shear forces contributed by the joint concrete, τ_{c}, were 0.47 - 0.56 F_{c} in the joint failure type and about 0.15 F_{c} in the beam flexural yielding type. The shear forces contributed by joint concrete could be estimated by the compressive strut mechanism model considerably well.

The maximum shear forces contributed by the joint reinforcing bars, τ_{s}, were 0.33 - 0.39 $p_{ws}\sigma_{y}$ in the joint failure type, and 0.37 - 0.5 $p_{ws}\sigma_{y}$ in the beam flexural yielding type. The truss model was not in agreement with the contribution of joint reinforcing bars for the specimens without the middle longitudinal bars in the column. It was pointed out that the further investigation is needed for the role of each component of the truss model.

The investigating approach of the internal stress conditions by FEM analytical data will be one of the useful tool for the verification and development of macro model and design equations, if the systematic analysis is carried out in the further work.

REFERENCES

1. ARCHITECTURAL INSTITUTE OF JAPAN, AIJ Standard for Structural Calculation of Reinforced Concrete Structures, Sept. 1982.

2. AOYAMA, H., Problems Associated with "Weak-Beam" Design of Reinforced

Concrete Frames, ATC-15, Comparison of Building Seismic Design Practices in the United States and Japan, 1984, pp. 117-158.

3. AMERICAN CONCRETE INSTITUTE, Building Code Requirements for Reinforced Concrete Structures (ACI318-83), Detroit, 1983.

4. STANDARDS ASSOCIATION OF NEW ZEALAND, Code of Practice for the Design of Concrete Structures, NZS 3101, 1982.

5. INOUE, N. AND NOGUCHI, H., Finite Element Analysis of Reinforced Concrete in Japan, Finite Element Analysis of Reinforced Concrete Structures, Proc. of the Japan - U. S. Seminar in Tokyo, May 1985, ASCE, 1986, pp. 25-47.

6. NOGUCHI, H., Nonlinear Finite Element Analysis of Beam-Column Joints, Final Report, IABSE Colloquium on Advanced Mechanics of Reinforced Concrete, Delft, 1981, pp. 639-654.

7. NOGUCHI, H., Analytical Models for cyclic Loading of Reinforced Concrete Members, Finite Element Analysis of Reinforced Concrete Structures, Proc. of the Japan - U.S. Seminar in Tokyo, May 1985, ASCE, 1986, pp. 486-506.

8. NOGUCHI, H. and NAGANUMA, K., Nonlinear Finite Element Analysis of Restoring Force Characteristics of Reinforced Concrete Beam-Column Joints, Proc. of Eighth World Conf. on Earthquake Engrg., San Francisco, July 1984, pp. 543-550.

9. AOYAMA, H. and NOGUCHI, H., Future Prospects for Finite Element Analysis of Reinforced Concrete Structures, Finite Element Analysis of Reinforced Concrete Structures, Proc. of the Japan - U. S. Seminar in Tokyo, May 1985, ASCE, 1986, pp. 667- 681.

10. DARWIN, D. and PECKNOLD, D. A., Nonlinear Biaxial Stress-Strain Law for Concrete, Jour. Engr. Mech. Div., ASCE, Vol. 103, No.EM2, April 1977, pp. 229-241.

11. KUPFER, H. B. and GERSTLE, K. H., Behaviour of Concrete under Biaxial Stresses, Jour. Engr. Mech. Div., ASCE, Vol. 99, No.EM4, August 1973, pp. 853-866.

12. MORITA, S. and KAKU, T., Local Bond Stress-Slip Relationship under Repeated Loading, Proc. IABSE Symp., Lisbon, Portugal, Sept. 1973.

13. Kamimura, T. and Hamada, T., et al., Experimental Study on Reinforced Concrete Beam-Column Joints, Part 1-3, Proc. Annual Conv., AIJ, Sept. 1978, pp. 1673-1674, Sept. 1979, pp. 1303-1306 (in Japanese).

14. Tada, T., Takeda, T. and Takemoto, Y., Experimental Study on the Reinforcing Method of RC Beam-Column Joints, Proc. Kanto District Symp., AIJ, July 1976, pp. 225-236 (in Japanese).

15. PAULAY, T. and PARK, R., Joints in Reinforced Concrete Frames Designed for Earthquake Resistance, A Report Prepared for the U.S. - New Zealand - Japan Seminar, Monterey, California, August 1984, pp. 16-18.

16. OGURA, K. and SEKINE, M., The State of the Art of the Studies on the Reinforced Concrete Beam to Column Joint, Concrete Journal, Vol. 19, No. 9, Sept. 1981, pp. 2-15 (in Japanese).

Dynamic Response of Softening Concrete Frames

Réponse dynamique de portiques en béton armé ramollissants

Dynamisches Verhalten von Betonrahmentragwerken mit Entfestigung

G. SANJAYAN
Civil Eng.
Monash Univ.
Clayton, Vic., Australia

G. Sanjayan, graduated as B.Sc. Eng. with first class honours from the University of Peradeniya, in 1982. He is a research student in the Dept. of Civil Engineering at Monash University.

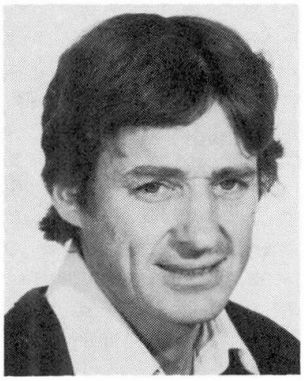

Peter Darvall obtained his Ph.D. from Princeton in 1969. He is Reader in Civil Engineering at Monash University. His research is in the field of reinforced and prestressed concrete structures.

Peter DARVALL
Reader in Civil Eng.
Monash Univ.
Clayton, Vic., Australia

SUMMARY

A method is presented to include flexural softening in the analysis of multi degree-of-freedom unbraced plane frame structures. The element model has finite length hinges which follow a degrading stiffness and softening hysteresis model. An example of a two storey frame is subjected to the factored El Centro 1940 SOOE earthquake ground motion. The maximum load factor for a given ductility and the ductility requirement for a given load factor are both sensitive to the softening slope.

RÉSUMÉ

La méthode proposée permet d'inclure le ramollisement dû à la flexion dans l'analyse des portiques plans non-contreventés à plusieurs degrés de liberté. Le modèle de l'élément a des articulations d'une longueur limitée que se conforment à un modèle d'hystérésis de rigidité décroissante et de ramollissement. On soumet le spécimen d'un portique à deux étages aux tremblements de terre semblable à ceux d'El Centro 1940 SOOE intensifié. Le facteur de charge maximum pour une ductilité donnée et la ductilité requise pour un facteur de charge donné sont tous deux sensibles à l'inclinaison de la courbe de ramollissement.

ZUSAMMENFASSUNG

Eine Methode zur Erfassung von Biegeentfestigung in knotensteifen Rahmentragwerken mit vielen Freiheitsgraden wird vorgestellt. Das Elementenmodell hat Gelenke endlicher Länge mit abnehmender Steifigkeit und Entfestigungshysterese. Ein zweistöckiger Rahmen wird als Beispiel den El Centro 1940 SOOE-Bodenbewegung ausgesetzt. Es zeigt sich, dass Lastfaktor und Duktilität empfindlich auf die Entfestigungsbeziehung reagieren.

1. INTRODUCTION

Softening is the name used herein for the loss of moment capacity of a reinforced or prestressed section at advanced curvature. Softening is less likely to occur where critical sections have been carefully detailed for extended plasticity. On the other hand, tests show that softening often occurs earlier, and is more pronounced, at joints, when the shear/moment ratio is high, or when substantial axial load is also present, as for prestressed members. Softening may become a factor of considerable significance when very high strength concretes are used with high proportions of high yield strength steel.

The unidirectional moment-curvature (M-ϕ) curve has been approximated by an elastic-plastic-softening trilinear model. Softening was considered to take place over a finite hinge length and the implications for static collapse and shakedown loads were examined [3].

The response of a single degree-of-freedom softening frame to simple unidirectional dynamic loads has also been studied [7]. It was found that a critical softening parameter or slope at which collapse will occur may be identified for each type of loading and depends on the severity of the applied load as represented by the ratio of maximum applied force to maximum resistance (or by energy of impulse to maximum elastic strain energy), on the plastic plateau length (ductility), on any limit to the softening region, and on duration of load.

Computation of the full response of concrete frame structures to severe reversible, repeated and dynamic loads, such as induced by the ground motions of a strong earthquake, requires consideration of the plasticity, softening and hysteresis characteristics of the most severely stressed locations. This is a formidable task, both analytically and in collecting sufficient data on which to predict behaviour over a reasonable range of variables.

An economical method is presented herein for the dynamic analysis of multi degree-of-freedom plane frame structures with softening hinges.

2. TECHNIQUE OF ANALYSIS

2.1 Member model

A flexural element of length L, shown in Fig. 1, is assumed to have discontinuity or hinge lengths at each end as shown. The reference flexural rigidity of this element is EI. The hinge lengths AB and CD have flexural rigidities aEI and bEI respectively, where a and b are negative in the softening region.

These hinges (AB and CD) are the only portions to undergo softening deformations. Points A and D are the only points which may be plastic hinges. The central portion BC has only reversible elastic deformations. In adopting this model it is assumed that bending moment maxima occur at the ends of elements. This normally corresponds to reality, but will always be true if node positions are chosen appropriately.

2.2 Model for hysteresis

The hinge lengths ℓ_{p_1} and ℓ_{p_2} have the idealised hysteretic M-ϕ behaviour shown in Fig. 2, where M is the maximum moment in the hinge length. This is a modification to include softening of the model suggested by Clough [1] for elastic-plastic behaviour.

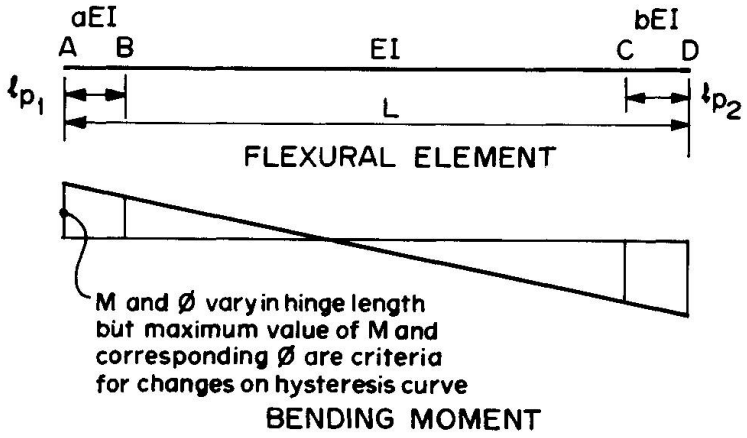

Fig. 1. Plastic-softening hinges at end of flexural element.

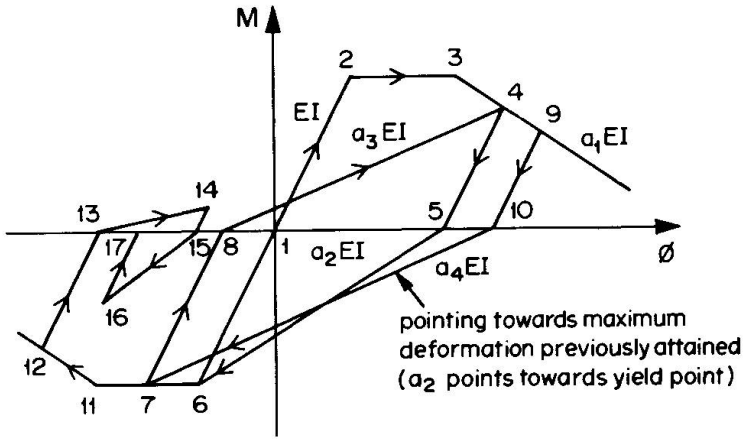

Fig. 2. Hysteresis model for plastic-softening hinges.

The M-ϕ path may be defined as follows: 12-elastic, gradient EI; 23-plastic till specified rotation capacity reached; 34-softening till deformation reversal, gradient a_1EI; 45-unloading with elastic slope to zero moment; 56-reduced elastic slope to yield point in reverse bending; 67-plastic till deformation reversal before specified rotation capacity reached; 78-unloading with elastic slope to zero moment; 84-reduced elastic slope to previous highest deformation point reached with this sign of bending; 49-further softening till deformation reversal; 910-elastic unloading; 107- as 84; 711- as 23; etc.

After reaching 17 the two possible paths could be 17,14 and 17,9. In this case the path with the higher slope is followed, i.e. 17,14 is chosen [6] and then 14,9 is followed.

The parameters a and b (Fig. 1) follow the hysteresis shown in Fig. 2. At each stage of the (separate) deformations of the end hinges, the stiffness matrix can be formed for each straight line segment of the M-ϕ curve by using the corresponding 'a' values (Fig. 2) for a and b. For example, if hinge AB is softening and following the path 3,4 then $a = a_1$; at the same time hinge CD can be following the path 10,7 which gives $b = a_4$.

2.3 Stiffness Matrix

The stiffness matrix for a prismatic flexural element with a finite softening hinge length has previously been developed [2]. The following technique allows the generalisation of this formulation to non-prismatic members.

Six relevant degrees-of-freedom of element AD are shown in Fig. 3. The element is considered as an assembly of AB, BC and CD. Actions and displacements are related in AB by

$$\begin{Bmatrix} A1 \\ A3 \end{Bmatrix} = \frac{a\ EI}{\ell_{AB}} \begin{bmatrix} k_{ii}' & k_{ij}' \\ k_{ij}' & k_{jj}' \end{bmatrix} \begin{Bmatrix} D1 \\ D3 \end{Bmatrix} \qquad (1)$$

where the stiffness coefficients k_{ii}', k_{ij}' and k_{jj}' depend on the shape of the member. For prismatic members $k_{ii}' = k_{jj}' = 4$ and $k_{ij}' = 2$. a is negative when the hinge is softening.

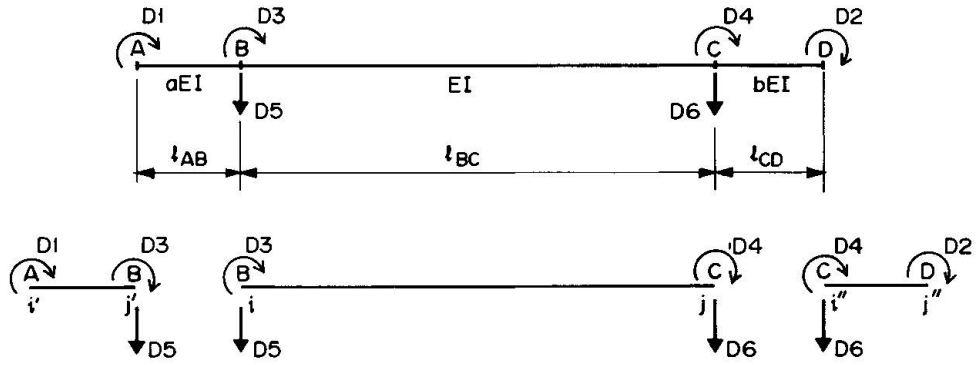

Fig. 3. Assembly of flexural element.

The stiffness Eq. (1) is modified to include the displacement D5 and then assembled with similar equations for BC and CD. Noting that actions A3 = A4 = A5 = A6, the assembled stiffness equation is

$$\begin{Bmatrix} A1 \\ A2 \\ 0 \\ 0 \\ 0 \\ 0 \end{Bmatrix} = \frac{EI}{\ell} \begin{bmatrix} & | & & \\ S_{ee} & | & \cdots & S_{ce}^T \\ & | & & \\ \hline & | & & \\ S_{ce} & | & & S_{cc} \\ & | & & \end{bmatrix} \begin{Bmatrix} D1 \\ D2 \\ D3 \\ D4 \\ D5 \\ D6 \end{Bmatrix} \tag{2}$$

Using the method of condensation the matrix equation can be reduced to a 2 × 2 form

$$\begin{Bmatrix} A1 \\ A2 \end{Bmatrix} = \frac{EI}{\ell} [S_e] \begin{Bmatrix} D1 \\ D2 \end{Bmatrix} \tag{3}$$

where $$S_e = S_{ee} - S_{ce}^T S_{cc}^{-1} S_{ce} \tag{4}$$

The stiffness matrix to include displacement degrees-of-freedom at A and D is related to the flexural stiffness matrix in the normal way.

The structure stiffness matrix is then assembled from the element stiffness matrices S_e and is modified each time a different stage is reached on the hysteresis curve for any hinge.

3 COMPUTER PROGRAM

An element subroutine library has been developed for the model described above, and added to the computer program DRAIN-2D to enable softening deformations to be handled. DRAIN-2D is a general purpose computer program for the dynamic analysis of inelastic plane structures [4]. The program requires the following information for all possible hinge locations in addition to the usual data input:

- Plastic rotation capacity.
- Softening slope and the maximum allowable reduction of moments through softening.
- Hinge length ratio.

4. EXAMPLE

The same two storey frame example used previously to highlight the effects on static collapse loads of plastic hinges [5]and of softening hinges [3] is used in this paper. Dimensions and loads are shown in Fig. 4. Member stiffness, strength and hinge data are given in Table I. The vertical loads are assumed to be dead loads, hence the floor masses are obtained by dividing the vertical loads shown by $g = 9.81\ ms^{-2}$.

A damping factor $\beta_o = 6.366 \times 10^{-3}$, proportional to the original elastic stiffnes, was assumed. This is approximately 5% critical damping, with a natural period of 0.4 sec.

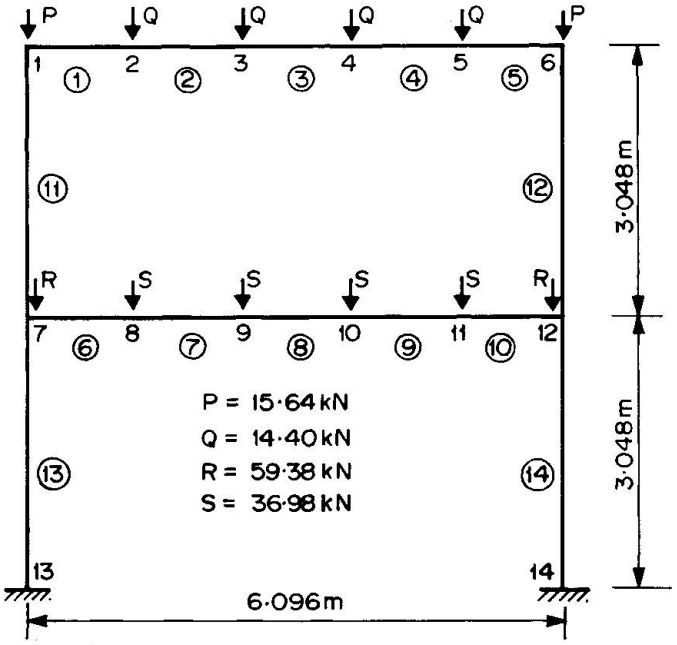

Fig. 4. Dimensions and loads for two-storey example.

The El Centro 1940 S00E ground motion, multiplied by a factor λ, was applied to the two-storey frame. The factor λ can be compared to the load factor for static loading conditions.

The structure with hinge properties shown in Fig. 5 was subjected to the ground motion with $\lambda = 1.39$.

The yield status of the structure at various times is shown in Fig. 6. The moment-curvature path followed by the hinge at node 12, member 10 is shown in Fig. 7 with the corresponding event numbers marked.

TABLE I
DATA FOR EXAMPLE FRAME

Member No.	I $(m^4)\times10^{-4}$	M_p^+ (kN m)	M_p^- (kN m)	L (m)	$h_i = \ell_p/L$
1,5	5.99	62.1	92.6	1.22	1/6
2-4	5.99	92.6	62.1	1.22	1/6
6,10	41.14	186.3	220.1	1.22	1/6
7-9	41.14	275.4	186.3	1.22	1/6
11,12	15.22	162.6	162.6	3.05	1/12
13,14	15.22	189.7	189.7	3.05	1/12

E = 24,800 MPa.

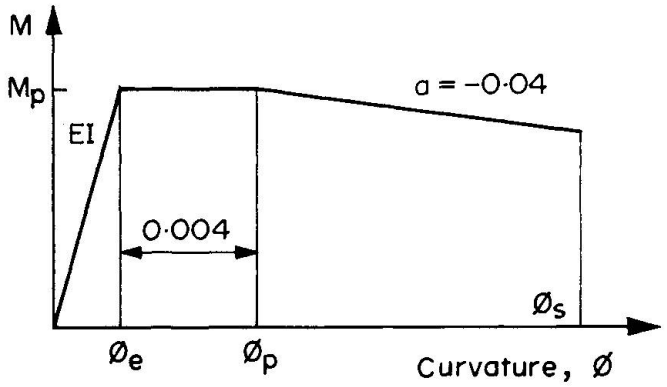

Fig. 5. Hinge properties for example frame.

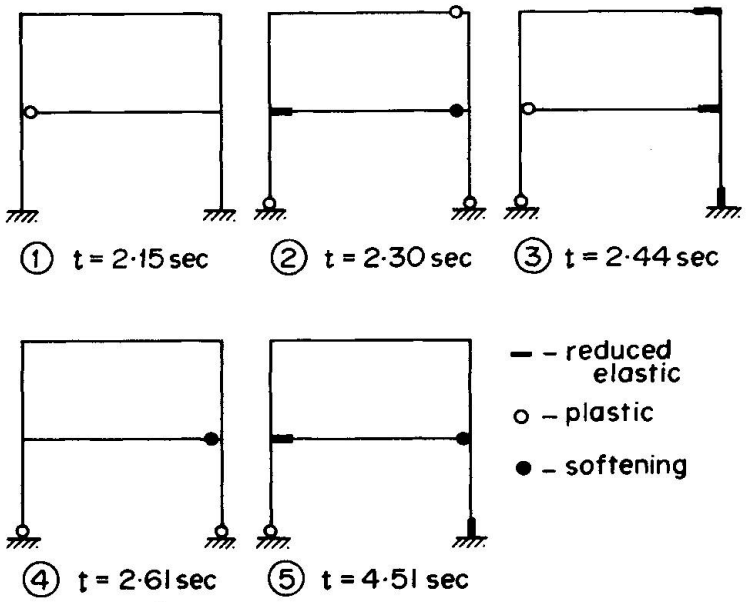

Fig. 6. Yield status of structure.

Similar analyses were performed with different hinge parameters. The various cases are summarised in Table II.

Comparing λ for cases (i) and (ii) shows the importance of including softening deformations in dynamic analysis if the alternative is a stringent limit on plastic curvature. In cases (ii), (iii) and (iv), where the maximum curvatures are limited to the same value, λ is very sensitive to the softening slope. It may also be seen from case (iv) that approximating the softening slope by a continuation of the plastic plateau may lead to significant overestimates of structural capacity.

Two further cases (v) and (vi) demonstrate the effect of softening on the maximum curvature reached. The ground motion is in both cases multiplied by $\lambda = 1.60$ as in case (iv), and the necessary curvature limits are recorded in Table II.

Cases (iv) and (v) show that softening demands significantly more ductility for the same load factor when compared to plastic behaviour. When there is no plastic-plateau, as in elastic-softening case (vi), the demand for ductility is even greater.

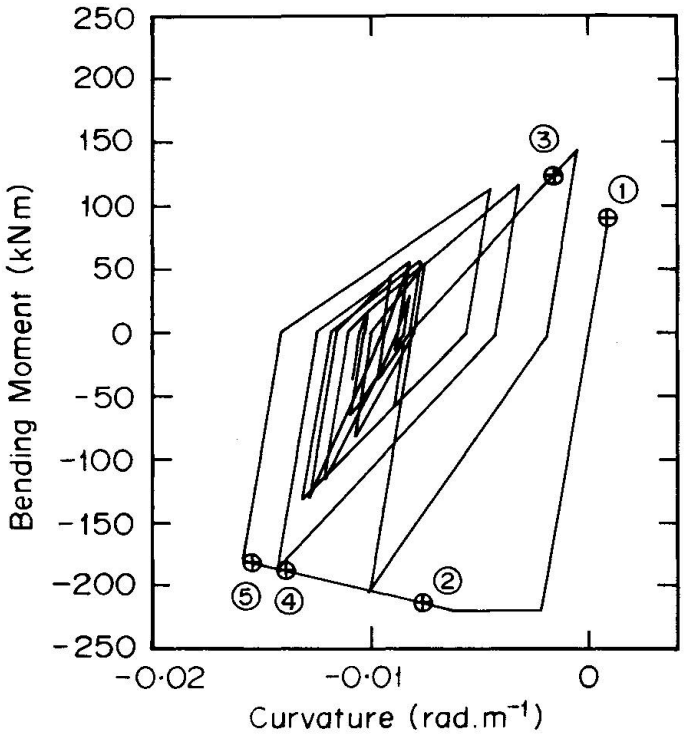

Fig. 7. Bending moment vs. curvature, member no. 10, node no. 12.

TABLE II
SOFTENING HINGE PARAMETERS AND LOAD FACTORS

Case	Type of hinge	$\phi_p - \phi_e$ rad m^{-1}	$\phi_s - \phi_p$ rad m^{-1}	Softening slope a	Maximum λ	Maximum curvature rad m^{-1}
(i)	ep	0.004	-	-	1.00	0.006
(ii)	eps	0.004	0.010	-0.04	1.39	0.016
(iii)	eps	0.004	0.010	-0.06	1.26	0.016
(iv)	ep	0.014	-	-	1.60	0.016
(v)	eps	0.004	0.018	-0.04	1.60	0.024
(vi)	es	0	0.029	-0.04	1.60	0.031

ep = elastic-plastic; ϕ_e = 0.002 rad m^{-1};
eps = elastic-plastic softening; es = elastic-softening.

5. CONCLUSIONS

- Computation of the full response of concrete frame structures to severe dynamic loads requires consideration of softening in addition to plasticity and hysteresis.

- Use of the matrix condensation technique to form the stiffness matrix for flexural elements with finite hinge lengths allows efficient analysis of softening frames with non-prismatic elements.

- The maximum load factor for a given ductility and the ductility requirement for a given load factor are both quite sensitive to the softening slope. Since the softening slope is steeper for members with significant axial load (e.g. prestressed members), this sensitivity would be of particular importance in these cases.

REFERENCES

1. CLOUGH, R.W. Effect of Stiffness Degradation on Earthquake Ductility Requirements. Report 66-16. Structural and Material Research, Structural Engineering Laboratory, University of California, Berkeley, CA., 1966.

2. DARVALL, P. LeP. Stiffness Matrix for Elastic-Softening Beams, Technical Note, Journal of Structural Engineering, ASCE, Vol. 111, No. 2, Feb. 1985, pp. 469-473.

3. DARVALL, P. LeP. and MENDIS, P.A. Elastic-Plastic-Softening Analysis of Plane Frames, Journal of Structural Engineering, ASCE, Vol. 111, No. 4, April 1985, pp. 871-888.

4. KANAAN, A.E. and POWELL, G.H. General Purpose Computer Program for Inelastic Dynamic Response of Plane Structures, Report No. EERC 73-6, Earthquake Engineering Research Center, University of California, Berkeley, CA., 1973.

5. POWELL, G.H., ORR, G. and WHEATON, R. ULARC-Simple Elasto-Plastic Analysis of Plane Frames. NISEE/Computer Applications, University of California, Berkeley, CA., 1972.

6. RIDDELL, R. and NEWMARK, N.M. Force-Deformation Models for Nonlinear Analysis. Journal of the Structural Division, ASCE, Vol. 105, No. ST12, December, 1979, pp. 2773-2778.

7. SANJAYAN, G. and DARVALL, P. LeP. Dynamic Response of a Single Degree-of-Freedom Elastic-Plastic-Softening Structure. Research Report 8/1984, Dept. of Civil Engineering, Monash University, Victoria, Australia.

Discrete Element Method and Beam Dynamics, an Application of TILLY

Méthode des éléments discrets et dynamique des poutres, une application de TILLY

Methode der diskreten Elementen und dynamische Analyse von Trägern, eine Anwendung von TILLY

J. BLAAUWENDRAAD
Delft Univ. of Techn.,
Delft
The Netherlands

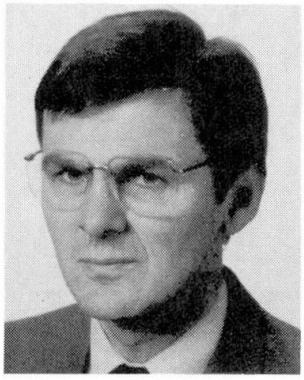

Graduated from Delft University in 1962. Joined TNO in 1964 and Rijkswaterstaat in 1971. Professor in Civil Engineering since 1979.

A.G.T.J. HEINSBROEK
Delft Univ. of Techn.,
Delft
The Netherlands

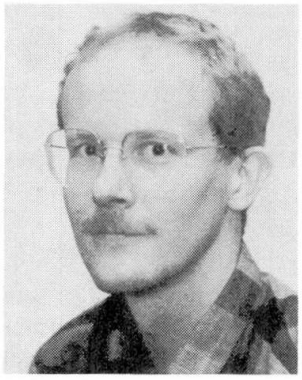

Graduated from Delft University in 1984. Research member of Faculty of Civil Engineering.

L.J. SLUYS
Delft Univ. of Techn.,
Delft
The Netherlands

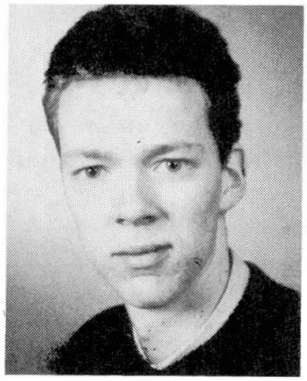

Graduate student of Faculty of Civil Engineering of Delft University.

SUMMARY

A discrete element method (DEM) is applied for the dynamic response of a reinforced beam. The motives to do so are explained and an example is discussed. A comparison with the results of a test and a finite element analysis shows the possibilities and limitations.

RÉSUMÉ

Une méthode des éléments discrets est appliquée pour déterminer le comportement dynamique d'une poutre en béton armé. On explique les motifs pour cette application et on présente un exemple. Une comparaison entre les résultats d'un essai et d'un calcul à l'aide de la méthode des éléments finis montre les possibilités et les limites.

ZUSAMMENFASSUNG

Eine Methode mit diskreten Elementen wird auf das dynamische Verhalten eines Trägers aus Stahlbeton angewandt. Der Anlass wird erklärt und ein Beispiel wird besprochen. Ein Vergleich zwischen den Ergebnissen eines Versuchs und einer Berechnung zeigt die Möglichkeiten und Grenzen dieser speziellen Methode der Finiten Elemente.

1. WHY AND WHEN A SIMPLE MODEL

In this paper the name "discrete element method", in short DEM, is used for a mechanical model, which is a composition of undeformable rigid finite elements, which are connected by deformable lumped springs and dampers. Lumped masses can be applied which correspond with the degrees of freedom of the model. The spring behaviour can be defined in a free way, such that nonlinearities and time dependency is involved. Simular options are included for the dampers. The name of the program is TILLY, which is composed of the first characters of the following list of specifications:

- ★ Transient and static analysis: Both dynamic and rheologic transient processes have to be simulated by the model
- ★ Incremental loading and initial strains: The load and initial strains are always applied step–wise in time; even for static calculations one has to introduce one or more time steps.
- ★ Linear and nonlinear behaviour: In due time both material nonlinearity and geometrical nonlinearity will be covered. Material nonlinearity may be plasticity and fracturing, hardening and softening.
- ★ Lumped masses, springs and dampers: In due time to be extended to elements of two and more generalized deformations.
- ★ Young and aging materials: Material properties can be constant in time, but also dependency of time must be included. Material stiffness and damping data may increase in time (for instance: young concrete) or may deteriorate (for instance: damaging by cyclic loading).

Reference is made to [1] and [2] for more details. The reasons to develop and apply such a program are manifold. An important consideration has been the immense computing time which is involved in the use of finite element programs for dynamic analysis in combination with nonlinear behaviour. A complete run on a high speed computer demands many man weeks and cpu hours. The state of the art makes clear, that major changes are needed to place these tools at the disposal of the profession. One way to achieve that, is to use supercomputers and specially designed finite element machines. A remarkable improvement is expected from these new facilities, but it is to be doubted, that practizing engineers will apply them. Research engineers are more likely to profit from these new tools.
Another way to serve the profession is to simplify the model. The engineer does not require exact data. He will be satisfied with approximating engineering models. For him the only requirement is, that researchers have proved by the use of their advanced models, that the course model is sufficiently appropriate.
We conclude, that two parallel activities are needed: continuing research on advanced finite element models (FEM) and the development of approximating course models. The discrete element model (DEM) is an attempt for such a simplified engineering tool. Another reason to start the development of TILLY has been the wish to involve as much graduate students as possible in the development and use of numerical models. Large and powerful finite element packages restrict the number of students, which can participate. Computing time is limited and also the number of specialistic supervisors. A more simple model can run on the PC's of the students themselves and other supervisors can be involved as well.

2. THE FALLING BEAM PROBLEM

To demonstrate the use of TILLY, the falling beam has been calculated which was analyzed earlier using the Dutch finite element package DIANA [3]. The reinforced beam is one of a series which has been tested in Switzerland [4]. In this example the bending and shear behaviour is modelled, so rotational and shear springs are the obvious discrete elements. The reader should keep in mind, that only a specific application of TILLY is discussed. Other spring types and compositions of discrete elements can be used in other cases.

The beam of reinforced concrete has the following dimensions: the total length is 8.15 m, the depth of the beam is 0.3 m and the width 0.4 m. The span l between the two supports is 7.85 m. The support at the right hand end is a hinge. The beam was elevated at the left hand end over the height h = 3.75 m and

then was dropped. The left hand support is a shock absorbing one and has a progressive spring stiffness. For TILLY the average stiffness k = 6800 N/m has been chosen. The reinforcement percentage is constant over the beam span. Both the top reinforcement and the bottom reinforcement are 0.56 %. For the rest, the following strength and other data apply: specific density $\rho = 2500$ kg/m³, $f_s = 650$ N/mm² (steel), $f_{ct} = 4.8$ N/mm² (concrete), $E_s = 210000$ N/mm².

From the test result it is known, that the shock absorber is compressed over about 6 cm at the very start, when the falling beam gets in contact with the shock absorber (t = 0), but ignorable compression occurs at later time. The maximum displacement at midspan is 0.69 m at time t = 0.164 s. This displacement is mainly due to plastic bending deformation. The final state is the result of a complex history. The beam cross– section starts to become a plastic hinge near to the shock absorber and this plastic region then moves in midspan direction. So, at maximum deflection the deformation state is more or less to be compared with the failure mechanism for static loading, but it takes some time and it requires some other intermediate limit states to achieve the final state.

For the rest, we do not need a computer at all to explain the ultimate deflection. A simple calculation by hand already provides a fair estimate of the maximum displacement $\hat{w}$ at midspan and the time $\hat{t}$ at which it occurs. If one neglects the early limit states, one can assume a rigid plastic behaviour of the beam with a plastic hinge at midspan. The triangular speed distribution with $v_0 = \sqrt{3gh}$ at the shock absorber immediately transforms in another triangular distribution with the maximum speed $\hat{v} = 3/4\ v_0$ at midspan. This yields a rigid plastic model with one degree of freedom. In this model a mass M with initial momentum P is decelerated by a plastic force F_p and accelerated by a gravity force F_g. The equivalent mass is M = 1/3 ml in which m is the mass per unit length, the equivalent momentum P at t = 0 is $P = M\hat{v}$, the equivalent force from dead weight is $F_g = 1/2$ mgl in which g is the acceleration due to gravity and the equivalent yield force $F_p = 4M_p/l$, in which M_p is the full plastic moment of the cross– section. The resulting force on the mass M is $F = F_g - F_p$. The time $\hat{t}$ at maximum deflection is calculated from $\hat{t} = P/F$, the acceleration of the mass from $\hat{a} = -\hat{v}/\hat{t}$ and the maximum displacement $\hat{w} = \hat{v}\hat{t} - 1/2\ \hat{a}\hat{t}^2$. Applying all available data, it is found that $\hat{t} = 0.16$ s and $\hat{w} = 0.62$ m, which is close to the test results $\hat{t} = 0.164$ s and $\hat{w} = 0.69$ m.

3. THE DISCRETE ELEMENT MODEL

The beam has been divided in 21 elements. The length of the end elements is 0.275 m and all other elements are 0.4 m in length. Four different models have been used. One difference between the 4 models is the number of springs (model A and model B) and another difference regards the nonlinear characteristics of the spring (type I and type II). Model A contains rotational springs only. Fig. 1 shows this model and makes clear, that 1 degree of freedom occurs between the rigid elements at the position of

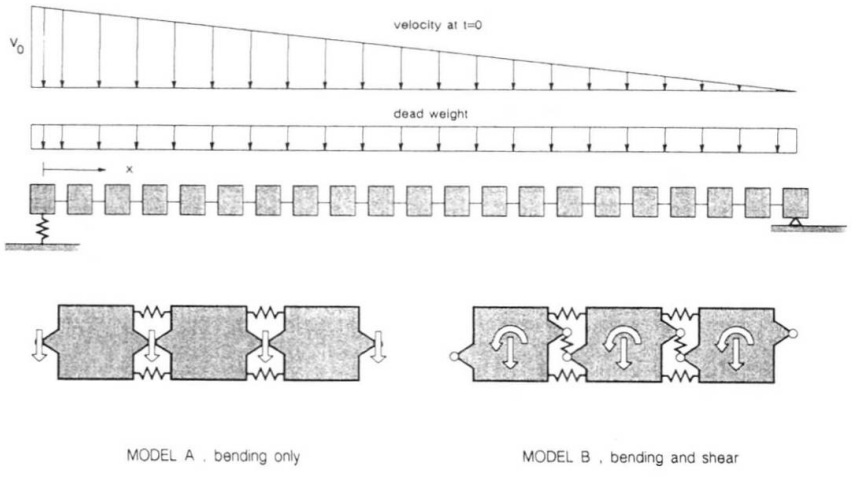

Fig. 1 Two different discrete element models

each rotational spring. The degrees of freedom are vertical displacements. The mass is lumped at the same position. This model takes into account the inertia of translation, but neglects the inertia of rotation. Also shear deformation is ignored. This model predicts moments and displacements but does not provide any information on shear forces. Model B uses both rotational springs and shear springs (fig.1). Now the degrees of freedom are defined in the mid of the rigid elements and 2 ones occur per element, a vertical displacement and a rotation. This model can account for bending deformation, shear deformation, inertia of translation and inertia of rotation. The results are displacements, bending moments and shear forces. The extra information for the shear forces is got at the cost of more computing time. The number of degrees of freedom is doubled, which makes the computing time increase by a factor 1.5 to 2.

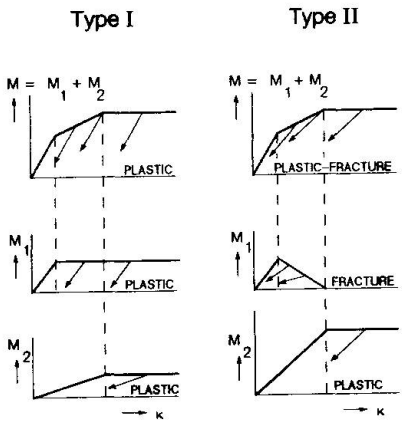

Fig. 2 Decomposition of constitutive model in two components. Left: two elastic-plastic springs representing the plastic model. Right: one elastic-fracture spring representing the plastic-fracture model.

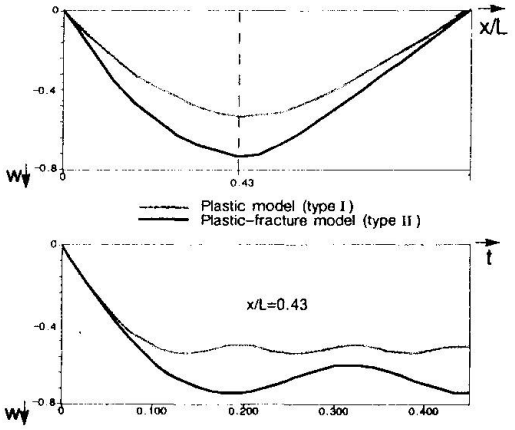

Fig. 3 Results for model I (rotational springs only). Spring type I is far more stiff than spring type II which models fracturing.

Fig. 2 is helpful to explain the similarity and the difference between the two rotational spring types I and II. They have in common, that a moment-curvature relation is used which consists of three branches, one for the uncracked state, one for the cracked state and one for the limit state at yield of the reinforcement. In both models the tri-linear behaviour is simulated by a fraction model of two parallel springs, which have different stiffnesses and fail at different stress levels. In both models an ultimate value can be specified for the plastic curvature (deformation capacity). Type I is a fraction model of two elastic-plastic springs. This means, that unloading always takes place with the stiffness of the branch for the uncracked state. In type II one elastic-plastic spring is used and one elastic-fracture element. This last one represents the softening at the first loading cycle due to cracking in the tensile zone. In concrete research this contribution sometimes is mentioned tension stiffening. It is not present any more after full loading has been applied. This type II is closer to reality than the approximation of type I. Also the unloading stiffness is better. For the shear spring in model B only one stiffness type is applied. Both rotational type I and rotational type II have been combined with an elastic shear spring.
To be honest, at the time the runs were made, the softening spring did not exist yet. At that time this spring was built from five separate parallel elastic springs which fail in a brittle way at different ultimate strengths. The result is practically the same, but the needed CPU time is higher.

4. RESULTS

The difference between the models A and B is not noticeable. Almost the same displacements and bending moments are found. The most important extra of model B proves to be that also shear forces can be calculated. The difference between the spring types I and II, however, is notable. Fig. 3 shows the results for model A (only rotational springs). Spring type I is far more stiff. The maximum displacement is smaller and the natural frequency after unloading is roughly two times higher. The result of type II is closer to the test results than type I. From here we only show data for type II.

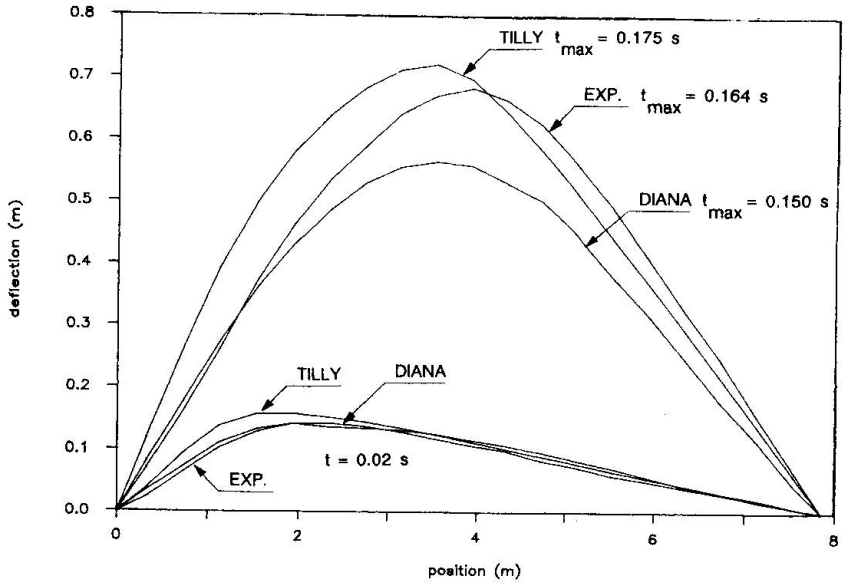

Fig. 4 Deflection lines for two times (t=0.02 s and t_{max}). Comparison of test, DIANA and TILLY (model B, type II)

In fig. 4 deflection lines are shown at two different times, viz. t = 0.02 s and t_{max} max at which the maximum value is reached. In both cases 3 lines are presented, namely the test result, the result of the finite element package DIANA and the TILLY result. At t = 0.02 s the largest curvature occurs between 1 and 2 meters distance from the left hand end. The DIANA result is closer to the test than the TILLY result, but TILLY does pretty well taking in account that the number of degrees of freedom is 8 times smaller (DIANA 344, TILLY 41). At the time of the maximum deflection, both TILLY and DIANA differ from the test. Near the shock absorber DIANA fits better than TILLY, but in a global sense the result of TILLY is sufficiently accurate. Fig. 5 shows a plot of the maximum displacement at x = 3.35 m versus time. TILLY and DIANA produce comparable results. The natural period of the beam after the maximum deflection is reached seems to be longer in the test than in the analysis. However, for later cycles the period in the test becomes smaller and is closer to the analysis result.

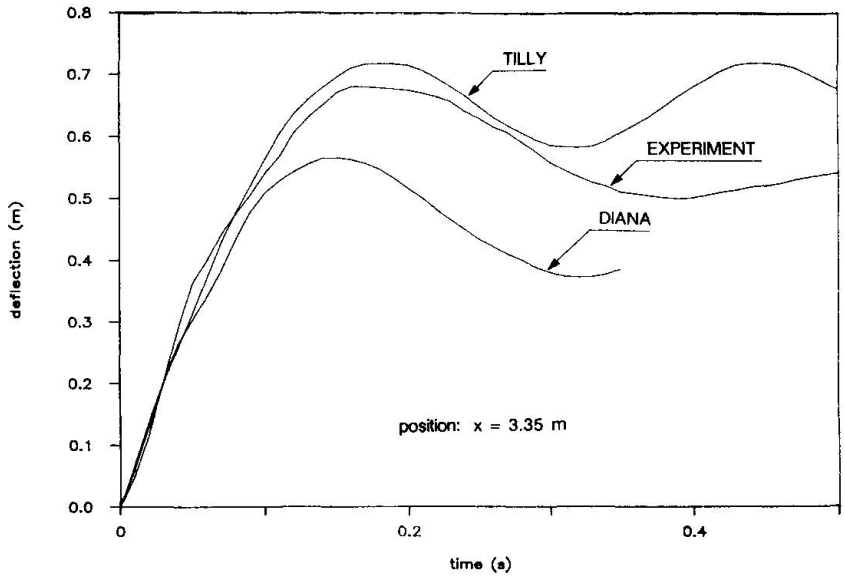

Fig. 5 Displacement close to midspan as function of time. Comparison of test, DIANA and TILLY (model B, type II)

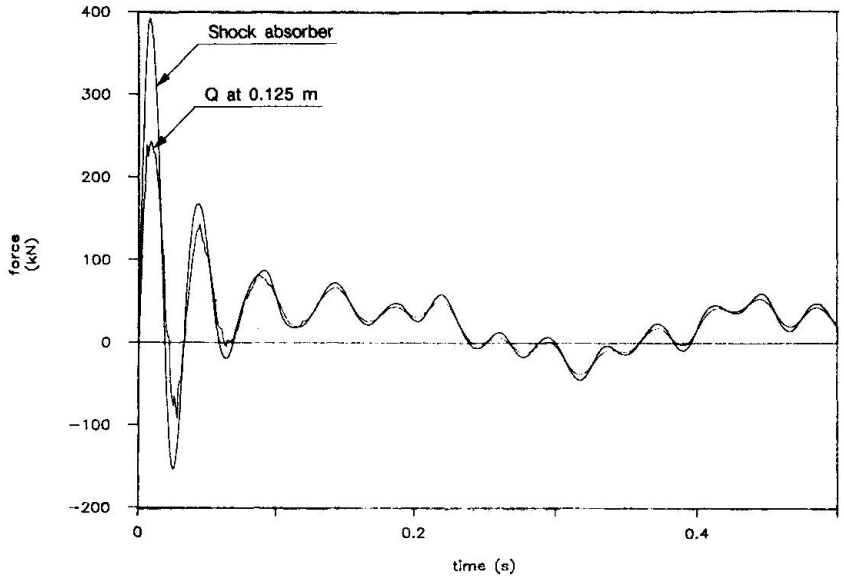

Fig. 6 Support reaction in shock absorber and shear force close to shock absorber for model B and type II.

Fig. 6 is a time–plot for the support reaction in the shock absorber and the shear force in the beam at x = 0.125 m close to the absorber. The shear force is strongly influenced by the high frequencies of the discrete model, so dampers have been used parallel with the springs to moderate the high–frequent signals.

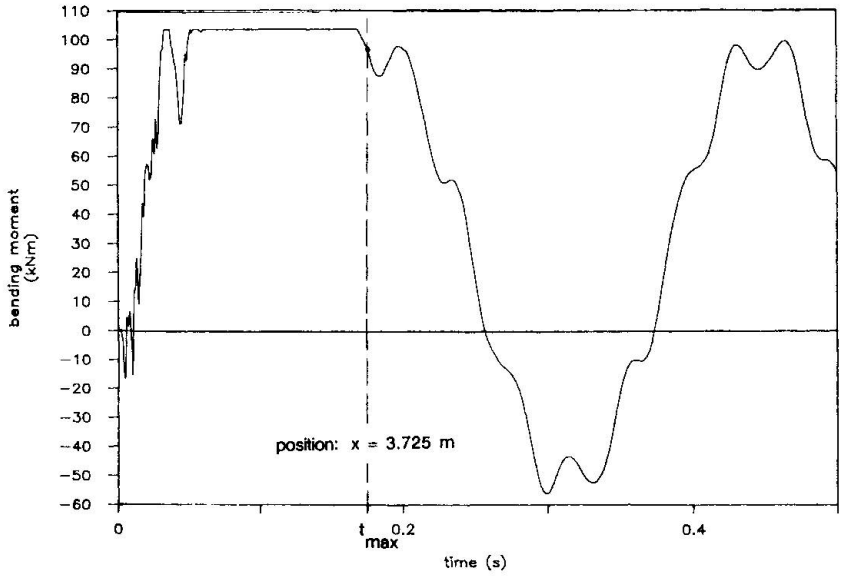

Fig. 7 Moment close to midspan as a function of time. During a long period a full plastic moment occurs.

Fig. 7 is a typical plot for the bending moment versus time for a cross–section close to the mid of the span. It can be seen, that a constant plastic moment occurs during a long time untill the maximum displacement is reached. This plot is more or less a confirmation of the assumptions for the course calculation by hand.

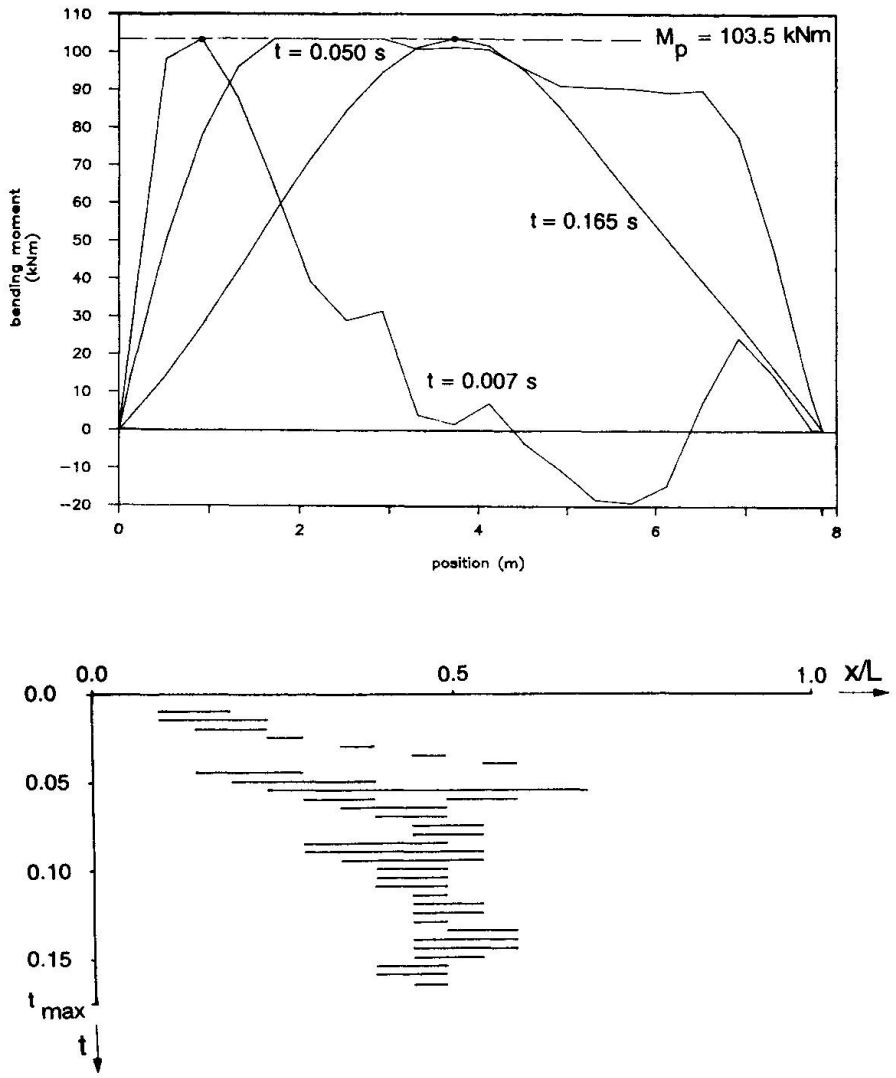

Fig. 8 Bending moment diagrams at different times and location of the plastic bending zones.

Fig. 8 shows some moment diagrams at different times. It also makes clear which part of the beam is in a plastic bending state at different times. This figure once more verifies the assumption, that the plastic zone in the mid of the span comes into being already at an early time. The shown result holds for the model in which dampers have been applied. In the TILLY run no correct model has been used for the shock absorber. It is believed that this does not influence the final results worth mentioning. However the reaction force in the shock absorber will not be too correct. In the test the time is shorter to reach the first zero value of the reaction force. At that time the beam looses contact with the absorber for a very short time. In the TILLY run a tensile force comes into being during this short time. So a more refined absorber behaviour should be modelled in order to attach much value to detailed data at early times of the calculation. This may even be an explanation why TILLY does not produce a very correct deflection line at early times. The results for later times are highly credible, even for the non– correct modelling of the absorber. After t_{max} the beam is vibrating in its natural mode around a permanent plastic deflection line, which has a displacement of about 0.65 m at midspan. Moments and shear forces oscillate then around the low values which occur statically for dead weight.

5. FINAL REMARKS AND CONCLUSIONS

The TILLY computations were done on an Olivetti M24 personal computer and require computing times of the order of 1 hour CPU. Runs for the same beam by the advanced finite element package DIANA demand in the order of 20 hours CPU on a far more powerful SEL GOULD computer. A TILLY–run is prepared and executed in a time which is expressed in a number of days. It requires weeks to complete an intensive DIANA–run. One can conclude, that the use of the course TILLY model has big advantages in all cases for which it has been proved that such a model provides sufficiently accurate results.

The program TILLY is still being developed. Other element features will be implemented in due time, for instance gap elements or contact elements. Such options are helpful to model slip of reinforcement and related phenomena. The authors are fully aware, that the applicability of models like TILLY has its own limitations. However, the engineering problems for which TILLY does apply, are sufficiently numerous to proceed. The category of simple models is another mechanism to transfer high–tech knowledge on reinforced concrete structures to the engineering profession and construction industry.

6. REFERENCES

1a. Willems, P.: TILLY, the theoretical background of a Discrete Element Program (in Dutch). Delft University of Technology, Dept. of Civil Engineering, 1985.
b. Willems, P.: User guide of TILLY.
c. Willems, P.: Programmers guide of TILLY.

2. Blaauwendraad, J., Kok, A.W.M.: Handicraft in Finite Elements. Proceedings of Numeta 1987, Swansea, U.K.

3. HERON: Examples of Nonlinear Analysis of Reinforced Concrete Structures with DIANA. Vol. 32, 1987, no. 3.

4. Amman, W.: Reinforced and Prestressed Concrete Structures Subjected to Shock Loading (in German), ETH Zurich, June 1983.

Bond Deterioration in Reinforced Concrete Members Subjected to Seismic Loading

Diminution de l'adhérence dans des éléments en béton armé soumis à des séismes

Das Zerrüttungsprozess des Verbundes in Stahlbetongliedern bei seismischer Belastung

Toshimasa TADA
Structural Engineer
Techn. Res. Inst.
Ohbayashi Corporation
Tokyo, Japan

Toshimasa Tada, born 1948, got his Master's degree at the Kyoto University. For fifteen years he has been engaged in research of RC and PC structures in the laboratory of the Ohbayashi Corporation. He is now doctoral candidate for Kyoto University.

SUMMARY

A theoretical investigation was made of bond deterioration in reinforcement to concrete in RC members subjected to seismic loading. A computer program assessing bond was developed and slippage of reinforcing bars in beam-column joints was examined.

RÉSUMÉ

L'étude concerne le processus de détérioration de l'adhérence entre béton et armatures dans des éléments en béton armé sous l'effet de charges sismiques. Un logiciel a été développé et permet d'évaluer la valeur de l'adhérence et le glissement des armatures dans un assemblage poutre-colonne.

ZUSAMMENFASSUNG

Eine theoretische Untersuchung über den Zerrüttungsprozess des Verbundes der Bewehrung von Stahlbetongliedern, die seismischer Belastung ausgesetzt sind, wird vorgestellt. Ein Computerprogramm wird entwickelt, das die Verbundeigenschaften auswertet und darüber hinaus das Ausweichen von Bewehrungsgliedern in Knoten zwischen Stützen und Balken untersucht.

1. INTRODUCTION

In Japan and in other countries, there are many test results available concerning reinforced concrete beam-column joint sub-assemblages subjected to repeated reversible loading representing earthquake excitations. The conspicuous features observed in many such test results are the degradations in strength or stiffness in load-deformation curves. These hysteresis curves are usually referred to as "pinched" and the cause of such degradation may be deterioration in bond of reinforcement to concrete in joint mainly.

A theoretical investigation was made into the deterioration process of bond of reinforcement to concrete, and a computer program assessing bond was developed. Then phenomenon of slippage of reinforcing bars in beam-column joint under seismic loading was clarified.

2. ANALYTICAL MODEL OF BEAM-COLUMN JOINT REGION AND ANALYTICAL METHOD ADOPTED

2.1 Idealization of Beam Column Joint Region under Seismic Force

Regarding a beam-column sub-assemblage as a portion of a highrise structure under seismic horizontal force, a typical moment diagram of the frame is shown in Fig. 1. The situation of bond of beam or column reinforcement continuous through the joint is considered to be as shown in Fig. 2.

Hypothesizeing the upper and lower reinformcements of beam are equal, an analytical model of a beam-column joint region is made as shown in Fig. 3. Beam-column joint region is represented by steel elements, concrete fiber elements and bond links.

2.2 Hysteresis rules for each element

Hysteresis rules for each constituent element are shown in Fig. 4 and these relationships are described as follows.

- Concrete $c\sigma = C(c\varepsilon)$ ..... (1)
- Steel $s\sigma = f(s\varepsilon)$ ..... (2)
- Bond link $\tau = B(S)$ ..... (3)

2.3 Bond equation in Bond region and moment of hinge

In the bond region, the following bond equations are solved in succession:

Si : given ..... (4)

$\tau i = B(Si)$ ..... (5)

$s\sigma i = (s\sigma i_{-1} \cdot sAi_{-1} - \tau i \phi i \Delta x)/sAi$ ..... (6)

$s\varepsilon i = f^{-1}(s\sigma i)$ ..... (7)

$Si_{+1} = Si - s\varepsilon i \cdot \Delta x$ ..... (8)

where Si : slip of i-th bond link.
sAi : area of i-th steel element.
Δx : bond length between each link.

Strain of concrete in a hinge is decided by the deformation of the boundary to the beam side concrete face, and linear distribution is assumed.

$$c\varepsilon u = -S_1/DHL \quad \text{..... (9)}$$

$$c\varepsilon L = Sn_{+1}/DHL \quad \text{..... (10)}$$

$$c\varepsilon i = -\frac{c\varepsilon u - c\varepsilon_L}{d} \times cLi + \frac{c\varepsilon u + c\varepsilon L}{2} \quad \text{..... (11)}$$

where, $c\varepsilon_u$, $c\varepsilon_L$: concrete strains at level of upper steel and lower steel, respectively
DHL : hinge length
d : distance between upper and lower reinforcing bars
cLi : distance of i-th concrete fiber from center of beam section
$c\varepsilon_i$: strain of i-th concrete fiber

From equation (1) and (11)

$$c\sigma_i = C(c\varepsilon_i) \quad \text{..... (12)}$$

the equilibrium equation at the hinge is

$$\Sigma c\sigma_i \cdot cA_i + s\sigma_1 \cdot sA_1 + s\sigma_n \cdot sA_N = 0 \quad \text{..... (13)}$$

If the equilibrium equation (13) is satisfied, then the moment and rotation of end hinge are calculated by the following equation

$$M = \Sigma\, c\sigma_i \cdot cA_i \cdot cL_i + s\sigma_1 \cdot sA_1 \cdot \frac{d}{2} + s\sigma_N \cdot sA_N \cdot \frac{d}{2} \quad \text{..... (14)}$$

$$\theta = (S_1+S_N)/d \quad \text{..... (15)}$$

2.4 Computational flow and transitions of deviated forces

The flow diagram of the computer program is shown in Fig. 5. Bar-slip at column face in tension side is hypothesized, then bond equation in joint is solved. And then equilibrium of section in hinge is examined. Further convergence is attempted by varying bar-slip at column-face.
In Fig. 6, transitions of deviated force in an actual calculation case are shown.

3. ANALYSIS OF BEAM-COLUMN JOINT REGION

3.1 Specimen analyzed

Bond deterioration processes of beam-column joint region of two experimental specimens were analyzed.(A and O-specimens)[1]
A-specimen has 30 cm column width and O-specimen has 60 cm column width and beam reinforcements are equal. Postulated hinges and bond properties in joints are shown in Fig. 7. Bond strength of pullout side is weak and push-in side is strong. This general tendency of bond is obtained from bond test conducted in our laboratory.[2]

3.2 Analytical results

Analytical results of moment-rotation curves of end hinge are shown in Fig. 8. A-specimen, pinched shape hysteresis was gained, while O-specimen showed spindle type of hysteresis curve.

Pullout and push-in of beam reinforcemnet at column face are shown in Fig. 9. In A-specimen pullout and push-in were each large amount, while in O-specimen, push-in didn't occur.

Bond-stress-slip history of A-specimen is shown in Fig. 10.

From this analysis the pullout behavior of beam reinforcement from joint under seismic force was clarified.

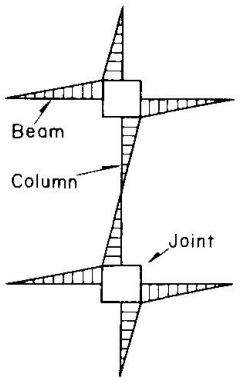

Fig. 1 Moment diagram of frame under seismic force

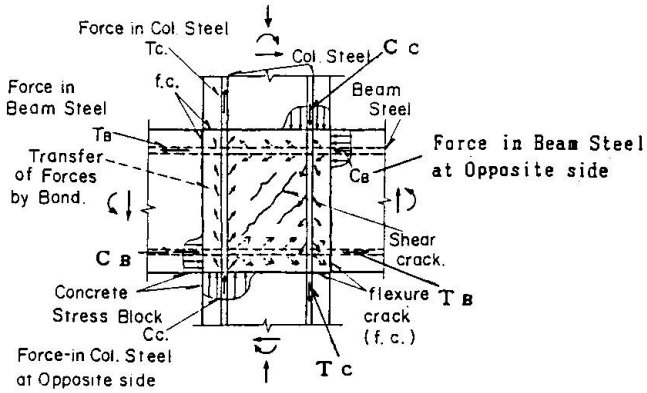

Fig. 2 Forces in joint

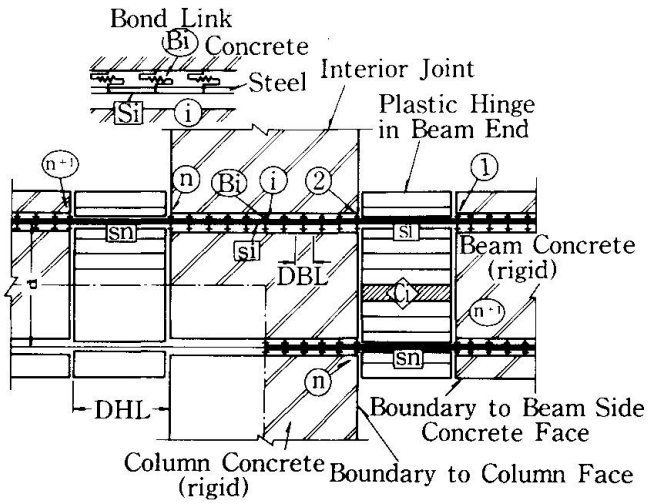

i ; Nodal Point on Straight Bar
Si ; Steel Element
Bi ; Bond Link in Interior Joint
Ci ; Concrete Fiber Element in Hinge
DHL ; Hinge Length
DBL ; Bond Length of Each Link

Fig. 3 Analytical model

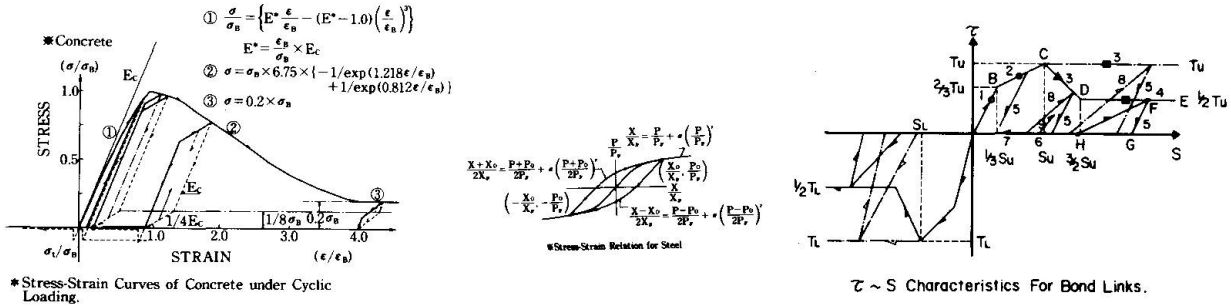

a) Concrete b) Steel c) Bond link

Fig. 4 Hysteresis rules for each element

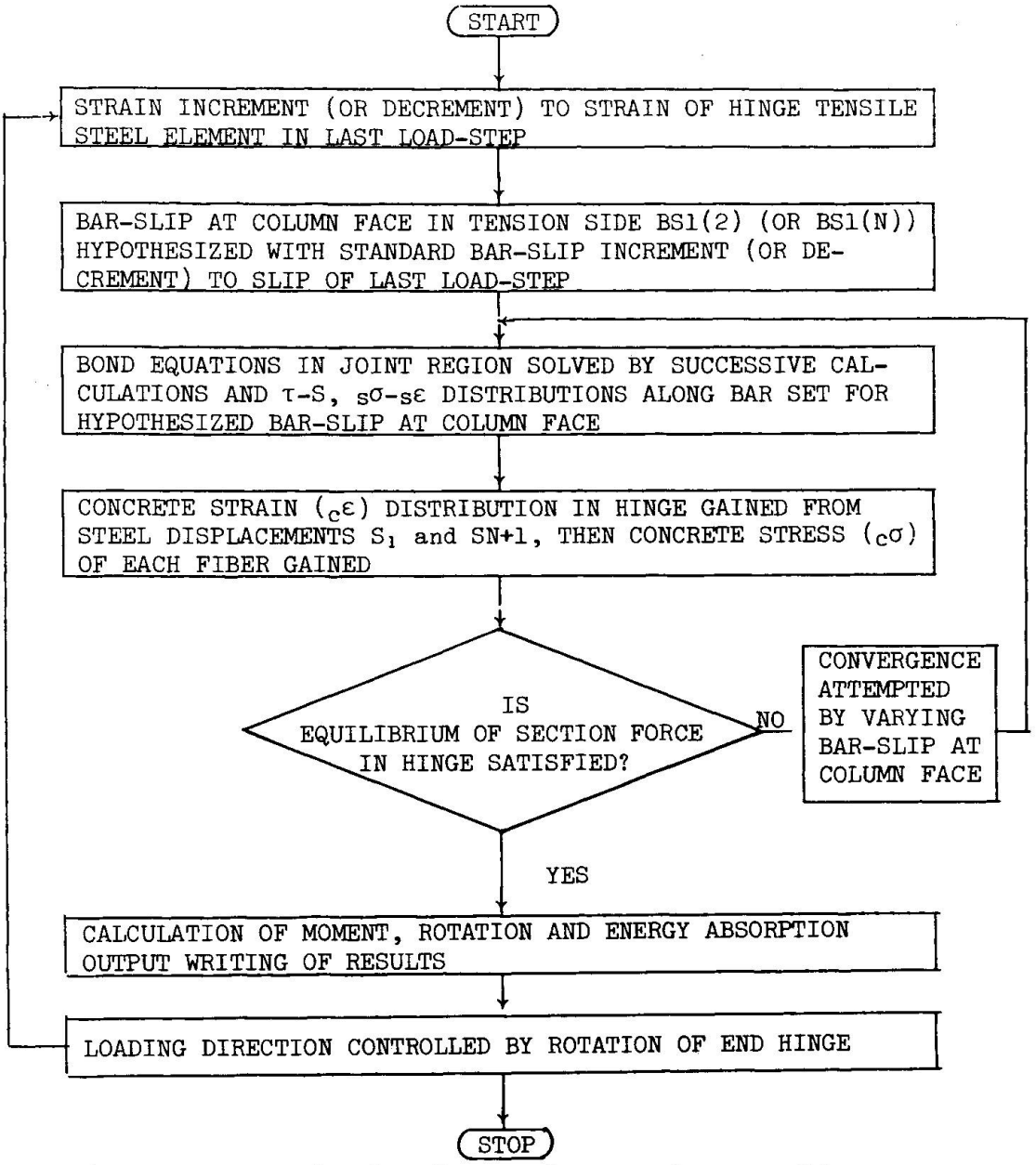

Fig. 5 Flow diagram for computer program

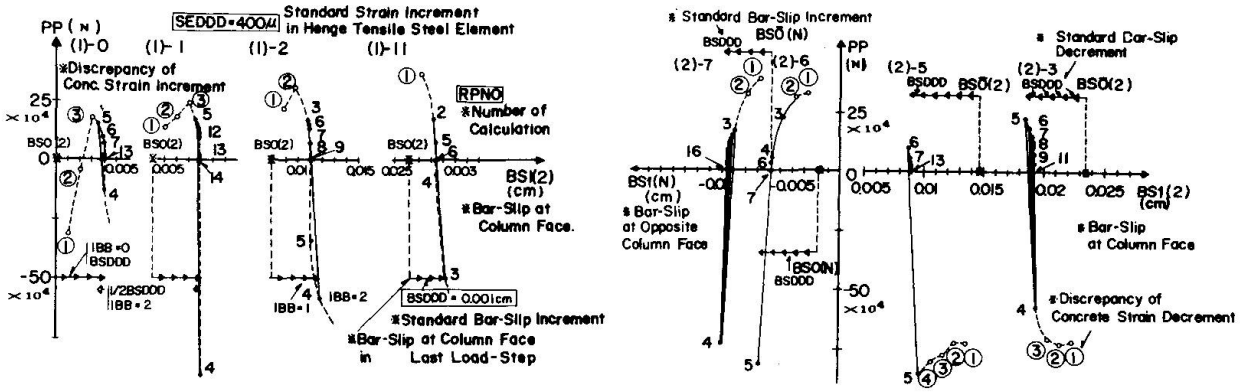

Fig. 6 Transitions of deviated forces in an actual calculation

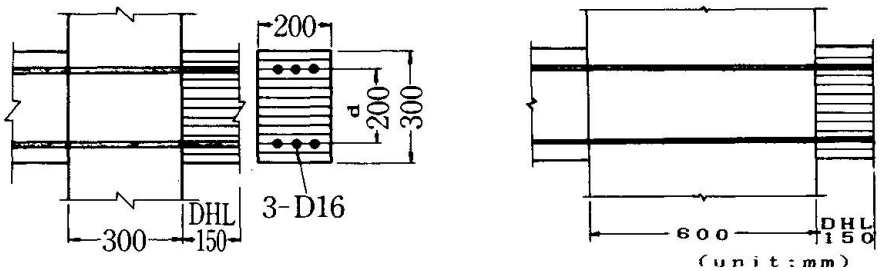

A-specimen O-specimen

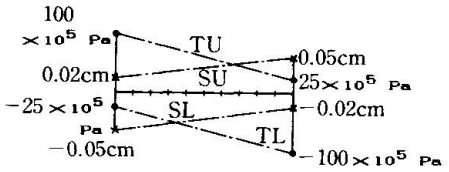

TU-SU, TL-SL, Distribution in Joint

Bond properties in joint

Fig. 7 Postulated hinges and bond properties in joint

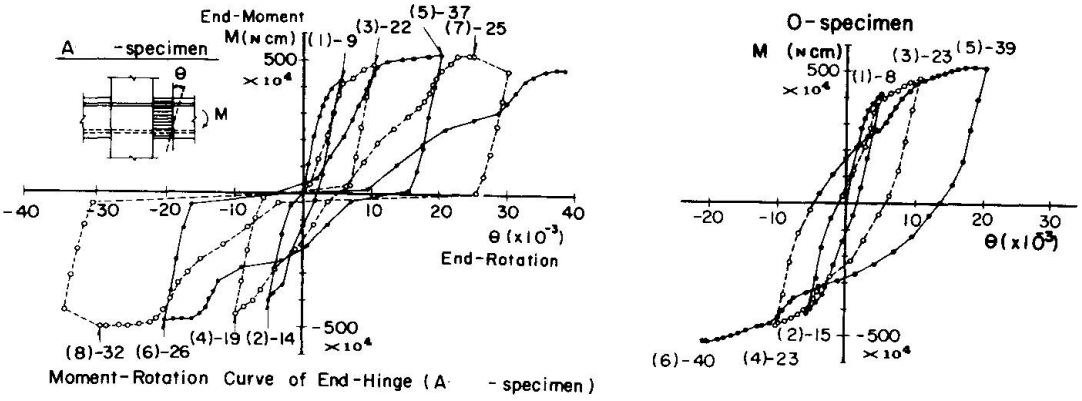

Fig. 8 Analytical moment-rotation curve of end hinge

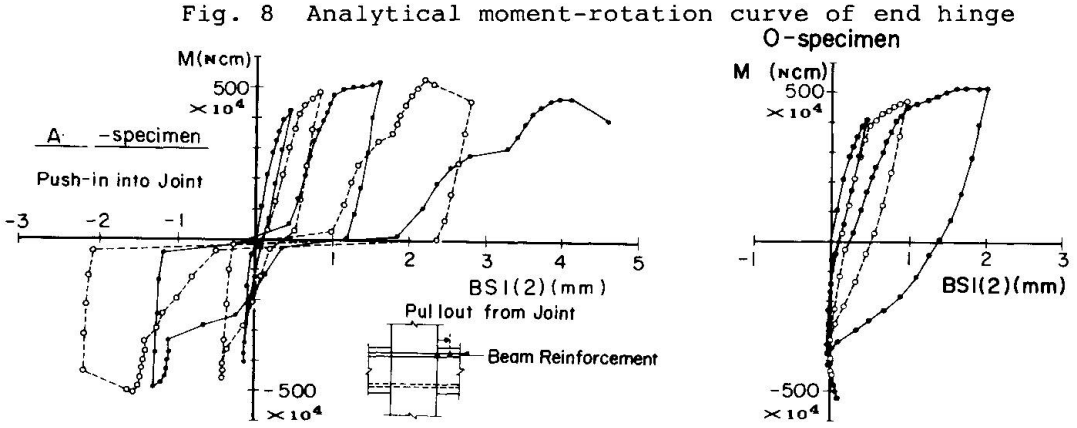

Fig. 9 Pullout and push-in of beam reinforcement at column face

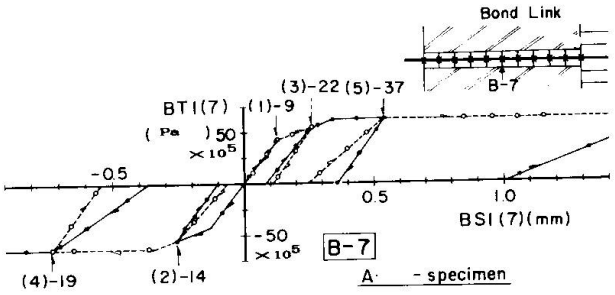

Fig. 10 Bond stress-slip histories in A-specimen

4. ACKNOWLEDGEMENT

The author wish to thank Dr. Toshikazu Takeda, vice director of Technical Research Institute of Ohbayashi Corporation Tokyo Japan, for guidance and valuable comments.

5. REFERENCES

1. T.Tada, T.Takeda, Research on Reinforcement of Beam-Column Joint Panel for Seismic Resistant Reinforced Concrete Frame (part-1) Pullout of beam reinforcement from joint and deformation characteristics of beam end plastic hinge.
Journal of Structural and Construction Engineering (Transactions of AIJ) June, 1985

2. T.Tada, T.Takeda, Research on Reinforcement of Beam-Column Joint Panel for Seismic Resistant Reinforced Concrete Frame (part-2) Bond test of deformed bar and it's analysis. ibid. May, 1986

3. T.Tada, T.Takeda, Analytical Research on the Deformation characteristics of End Plastic Hinge and Bond Deterioration Process of Adjacent Region in Reinforced Concrete Member (part-1) Analytical Model and Method for Solution. Proceeding of Annual Kanto Chapter Symposium of the AIJ, 1980

Leere Seite
Blank page
Page vide

Tension Stiffness Model Under Reversed Loading Including Post Yield Range

Modèle de rigidité sous charges cycliques au-delà du domaine d'écoulement

Zugsteifigkeit von Stahlbeton unter Wechsellast im Fliessbereich

Hiroshi SHIMA
Assist. Lecturer
Univ. of Tokushima
Tokushima, Japan

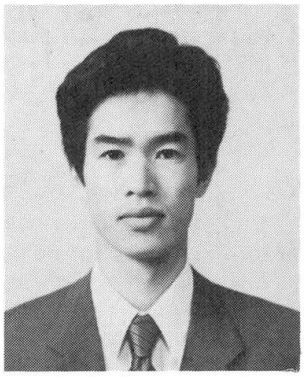

Hiroshi Shima, born 1958, received his Dr. Eng. degree from the University of Tokyo in 1987. He is now engaged in teaching and research in the analysis of reinforced concrete.

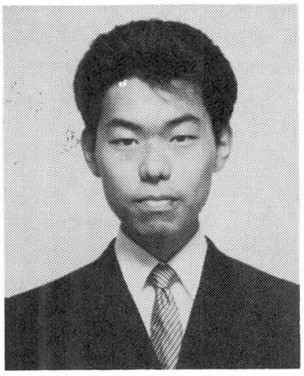

Sinichi Tamai, born 1961, received his B.Eng. in 1985 and M. Eng in 1987 from the University of Tokyo. He now works on the design of reinforced concrete structures.

Sinichi TAMAI
Civil Engineer
Tokyo Constr. Co
Tokyo, Japan

SUMMARY

A method for calculating tensile stiffness of a reinforced concrete element is proposed by referring to the test results. This method is applicable for reversed cyclic loading, including the post yield range of steel bars. In the post yield range, the average stress of a steel bar is obtained from the average strain by modeling the stress distribution along the bar.

RÉSUMÉ

Une méthode est proposée pour le calcul de la rigidité à la tension d'un élément en béton armé sur la base de résultats d'essais. Cette méthode peut être appliquée pour des charges cycliques inversées, et va au-delà du domaine d'écoulement des barres d'armature. Au-delà du domaine d'écoulement, la contrainte moyenne d'une barre d'armature est obtenue à partir de la déformation moyenne, par modélisation de la distribution des contraintes le long de la barre.

ZUSAMMENFASSUNG

Eine Methode zur Berechnung der Zugsteifigkeit von Stahlbeton wird vorgeschlagen und an Versuchsresultaten überprüft. Die Methode ist für Wechselbelastung anwendbar, einschliesslich des Nachfliessverhaltens der Bewehrung. In diesem Bereich erhält man die mittlere Stahlspannung aus der mittleren Dehnung durch die Betrachtung der Stahlspannungsverteilung entlang des Stabes.

1. INTRODUCTION

In the smeared crack model, the tension stiffness of a reinforced concrete element is usually obtained by superimposing the average stiffness of concrete and that of reinforcing bars, and the stiffness of the bars in concrete is usually modeled as same as that in the air. However, this modeling is not applicable for the post yield range of steel as indicated in this paper. The first object of this research is to obtain the average stress strain relationship in the post yield range of a bar in concrete.

Many models have already been proposed for the average tension stiffness of cracked concrete under monotonic loading [1,2]. However, any tension stiffness models of concrete under reversed cyclic loading have not yet proposed. Formulation of the tension stiffness under reversed cyclic loading is the second object of this research.

Uniaxial tension-compression tests were carried out using prismatic reinforced concrete specimens. When the bar starts to yield at a crack in reinforced concrete element, the yielding does not extend into concrete so quickly due to the existence of bond. Generally, both yielded and non-yielded portions exist along the bar. This makes difficult to determine the average steel stress directly from the average steel strain in the post-yield range. Therefore, the appropriate method to determine the average steel stress from the average steel strain has to be established.

The stress distribution of a bar along its axis was measured to obtain the average steel stress. The relationship between the average stress and average strain of a bar was predicted by modeling the stress distribution curve of the bar. The average stress strain relationship of concrete under reversed cyclic loading was also formulated referring this test results.

2. TESTS

The important parameters for the tension stiffness of a reinforced concrete element are concrete strength, reinforcement ratio, yield strength of steel and curing conditions. Combining these factors, six specimens were tested under tensile cyclic loading and one specimen was tested under reversed cyclic loading as shown in Table 1.

Table 1 Outline of test specimens

Specimen No.	f'c (MPa)	p (%)	Steel Bar	Curing condition
1	45	1.0	SD50	in Water
2				in Air
3	25			
4		0.6		
5			SD70	
6			SD30	
7 *	29	1.0		

f'c : Compressive strength of concrete
p : Reinforcement ratio
* : Reversed cyclic loading test

The dimensions of the specimens are shown in Fig.1. The strains of a bar were

measured and converted to the stresses by using the stress strain relationship. In order to measure the strain distribution along the bar, foil resistance strain gauges having length of 5mm were attached on the opposite faces at an interval of 10 ribs.

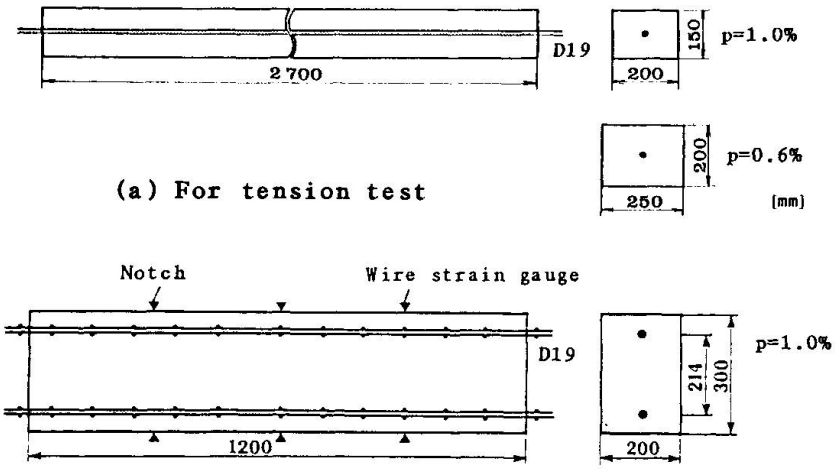

(a) For tension test

(b) For reversed cyclic loading test

Fig.1 Specimens

Table 2 gives the properties of steel bars. The measured stress strain curves of steel bars are plotted in Fig.2. The solid curves in the figure were used in the analysis. These curves are obtained from the following equations.

$$\sigma = Es\,\varepsilon \qquad \text{for } \varepsilon < \varepsilon_y \qquad (1)$$

$$\sigma = f_y \qquad \text{for } \varepsilon_y < \varepsilon < \varepsilon_{sh} \qquad (2)$$

$$\sigma = f_y + (1-e^{(\varepsilon_{sh}-\varepsilon)/k})(1.01f_u-f_y) \qquad \text{for } \varepsilon > \varepsilon_{sh} \qquad (3)$$

where

$k = 0.032(400\text{MPa}/f_y)^{1/3}$

σ : stress (MPa)

ε : strain.

Table 2 Properties of steel bars

Steel bar	SD30	SD50	SD70
Diameter of bar D, mm	19.5	19.5	19.5
Young's modulus Es, GPa	190	190	190
Yield strength fy, MPa	350	610	820
Tensile strength fu, MPa	540	800	910
Initial strain of strain hardening εsh, %	1.65	1.40	0.60

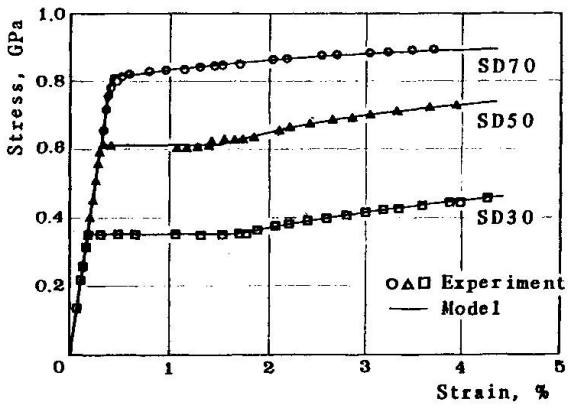

Fig.2 Stress-strain relationships of steel bars

The testing apparatus for tension loading is shown in Fig.3. The friction between the specimen and the floor was prevented by setting rollers under the specimen. The testing apparatus for the reversed loading is shown in Fig.4. Tensile force was applied to the bar and compressive force was applied to both the bar and concrete using loading plates as shown in the figure.

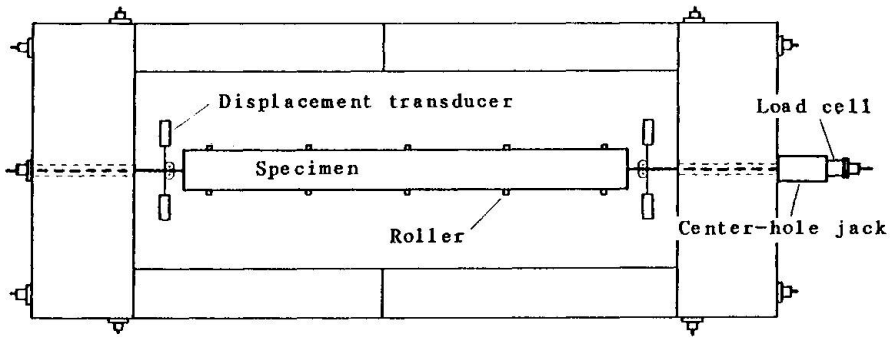

Fig.3 Testing apparatus for tension

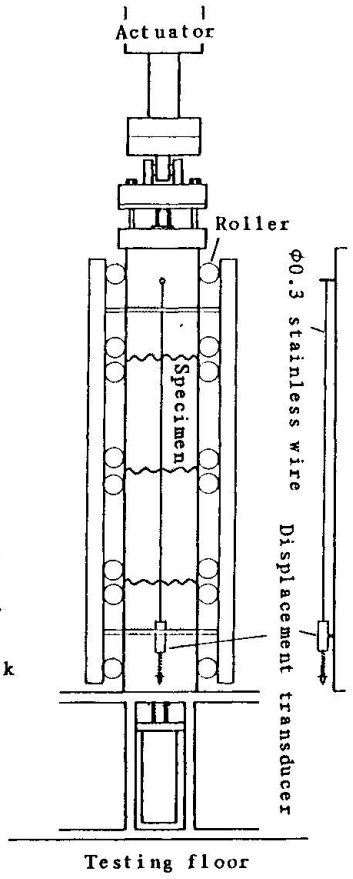

Fig.4 Testing apparatus for reversed loading

In addition to strains, the applied force and the total elongation were measured. The total elongation was obtained from the relative displacement of the both end of the specimen. In the tension loading test, the stainless wires had been adhired to the opposite surfaces of the bar at the end faces of the concrete. The wires were pulled out of the specimen and connected to electrical displacement meters. In the reversed cyclic loading test, the stainless wires were extended from the central point on the opposite faces of concrete block to displacement meters fixed at those points at the other end as shown in Fig.4.

3. AVERAGE STRESS-STRAIN RELATIONSHIP IN POST YIELD RANGE

3.1 Test results

The typical strain distributions along the bar as well as the stress in post yield range are shown in Fig.5. The stresses at the measured points were obtained from the strain measurement and the stress strain relationship shown in Fig.2. The stress distribution was drawn by using the 2nd order polynomial curve fitting the three neighboring points. The average stress was calculated by integrating the stress along the specimen.

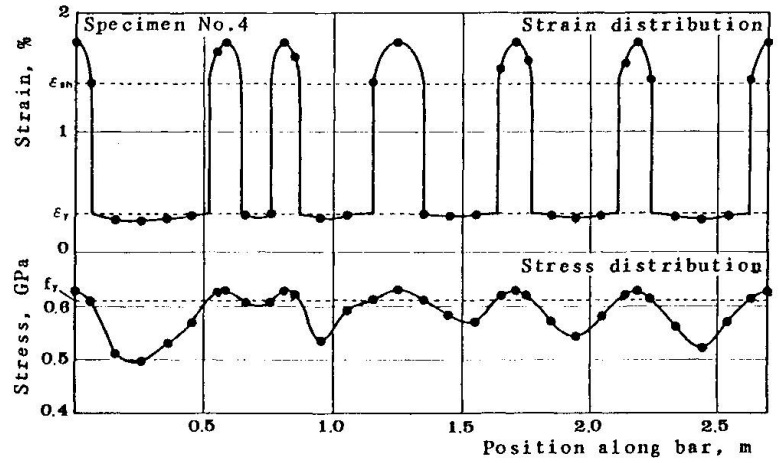

Fig.5
Distributions of strain and stress of steel bar in post yield range of Specimen No.4

The strain is in the elastic range or in the post yield range according to whether the stress is smaller or larger than the yield strength. The steel strain should jump up to the strain hardening range when the stress becomes to yield. This is because the stresses at both sides of an infinitesimal length at yielding location of the bar in concrete should be different due to the existence of bond.

The measured load and the average strains are plotted in Fig.6. The load carried by the bar is calculated from the average stress of the bar. The load carried by concrete is obtained by subtracting the load carried by the bar from the total load. In Fig.6, the average stress strain curve thus obtained is also shown for the steel bar and concrete respectively.

The concrete carries the tensile load even after the bar has yielded and there is hardly any tendency of sudden reduction of tension stiffness. The concrete resists the load roughly 10% of its tensile strength when the average strain was exceeded 2%. This means that the stiffness of bars in concrete shows higher stiffness than in the air for even post yield range. The other specimens also showed the similar tendency.

The average stress strain curve of a bar in a reinforced concrete element has the following distinction from that in the air.

1) The yield point is lower.
2) No yield plateau exists.

When a bar at cracked sections starts to

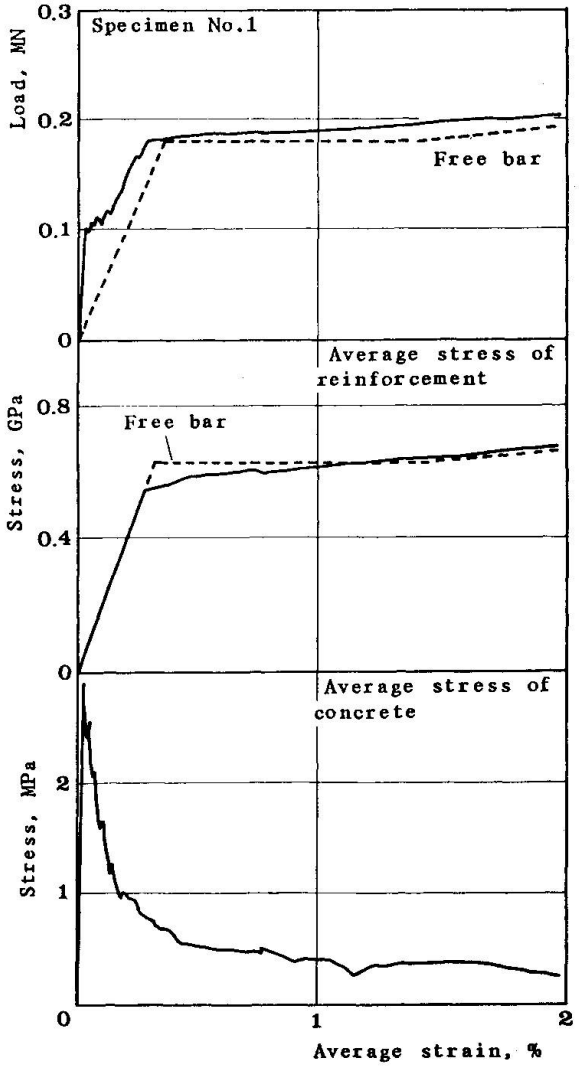

Fig.6 Load vs average strain and average stress-strain relationships of steel bar and concrete

yield, the steel stress between the cracks should be less than the yield strength. This causes the average stress strain relationship of steel to have lower yielding point than that of the bar in the air. Immediately after the bar yields at cracks, the strain jumps up to the strain hardening range as shown in Fig.5. This causes no yield plateau in the average stress strain curve of steel in reinforced concrete element. After the strain at cracked sections has entered the strain hardening range, the strain of the bar between cracks gradually enters the strain hardening range as long as the applied load increases. This phenomenon brings the gradual increase of the average stress in post yield range. When the strain becomes large, the average stress strain curve approaches that of the bar in the air. This is because the larger the steel strain, the lower the bond stress and the smaller the tension stiffness of concrete.

3.2 Modeling

The average stress of a bar in concrete can be obtained from the stress distribution along the bar and the average strain can also be obtained from the strain distribution. The stress and the strain of a bar can be converted each other by using the stress strain relationship so that the determination of the stress distribution or the strain distribution is enough for predicting the average stress strain relationship of the bar in concrete.

The bond stresses at a cracked section and at the center of a segment are zero and the bond stress is the differential of the stress distribution curve. Therefore, the stress distribution curve should have a form such that the slopes of the tangent at the cracks and the center of segment are zero. The cosine is one of the functions which agree with the above conditions. Experimental results indicated that the stress distribution could be shown by cosine curve independent on the strength of the bar or concrete and on crack spacings which were varied with drying shrinkage or reinforcement ratio.

The calculate procedure to obtain the average stress strain relationship of a bar in concrete after yielding is given in Fig.7. The accuracy of the cosine curve model for stress distribution can be verified by the comparison of the analytical and the experimental results as shown in Fig.8. In this calculation, the average stress strain relationship of concrete in tension obtained from the experiments was used.

In the analysis of reinforced concrete, the average stress strain relationship of concrete shall be given. The following equation is one of the tension stiffness model of concrete [3].

$$\sigma c = f_t \left(\frac{\varepsilon_{tu}}{\varepsilon}\right)^c \qquad (4)$$

where

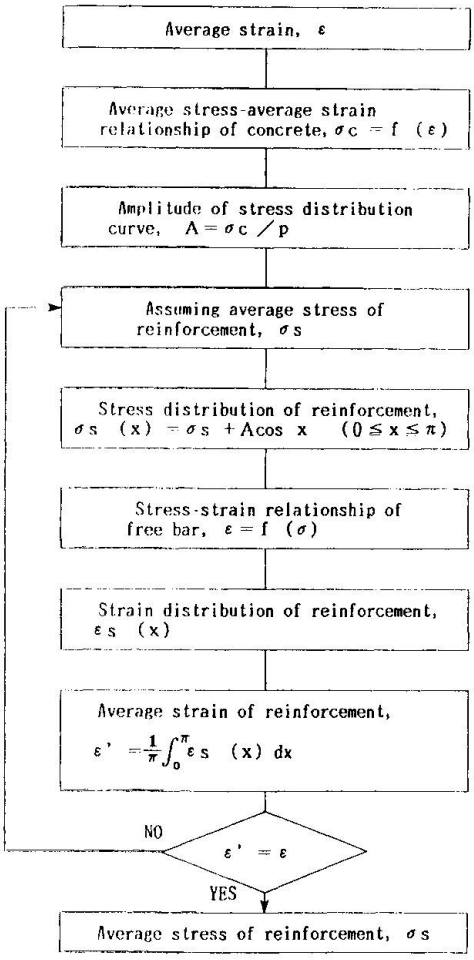

Fig.7 Calculate procedure to obtain average stress-strain relationship of steel bar in post yield range

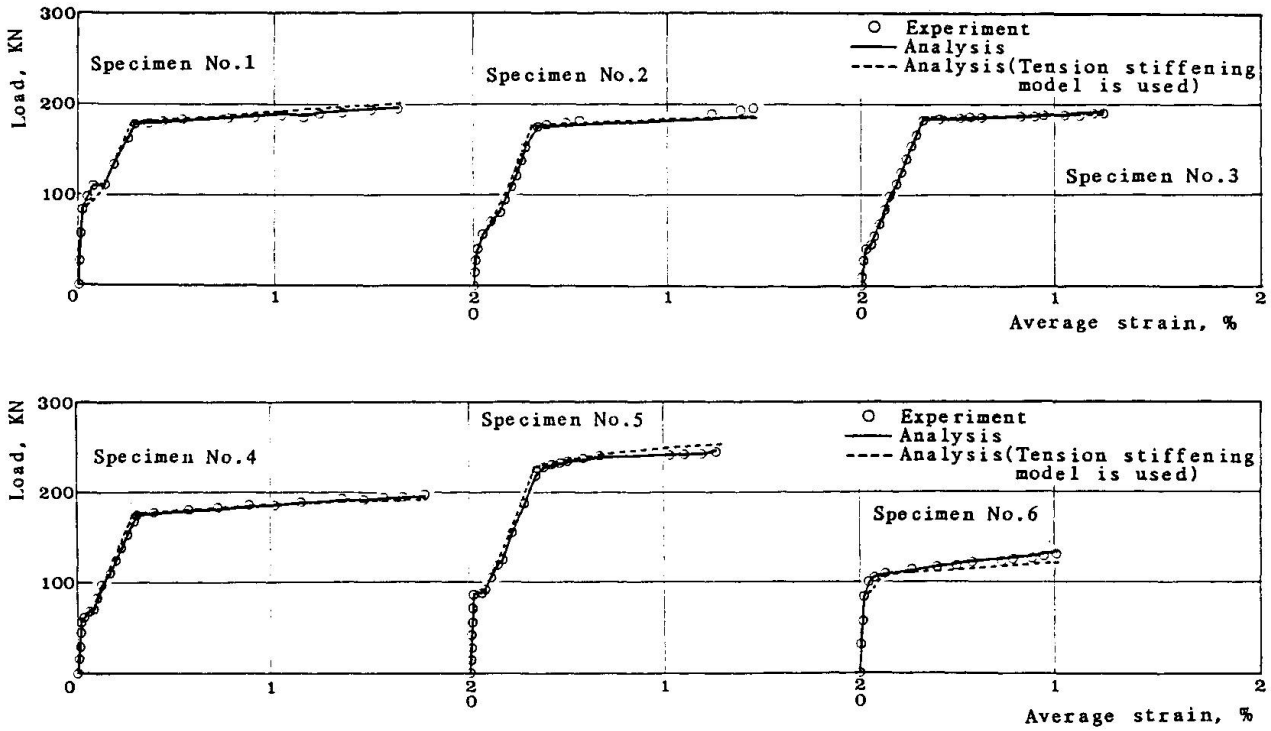

Fig.8 Comparison of analytical and experimental results of load-average strain curve

f_t : tensile strength of concrete
ε_{tu} : cracking strain equal to 0.02%
c : coefficient depending on bond characteristic, 0.4 for deformed bar.

For simplicity this equation is assumed to be applied to post yield range. The analytical results of load average strain relationship using eq.(4) are illustrated by the broken curves in Fig.8. The analytical results agree fairly well with the experimental results.

4. TENSION STIFFNESS UNDER REVERSED CYCLIC LOADING

4.1 Average stress average strain relationship of concrete

The stress in concrete under reversed cyclic loading is produced by the bond action and the contact of the crack. Therefore, the average stress of concrete shall be divided as follows.

$$\sigma c = \sigma cc + \sigma cb \tag{5}$$

where
σc : average stress of concrete
σcc : average stress of concrete produced by contact of the crack
σcb : average stress of concrete produced by the bond action.

The average stresses of concrete produced by bond and contact of the crack can be determined by the following equations.

$$\sigma cb = p\ (\ \sigma s,cr - \sigma s\ ) \tag{6}$$

$$\sigma cc = \frac{P - As\ \sigma s}{Ac} - \sigma cb \tag{7}$$

where
p : reinforcement ratio
σs,cr : stress of steel bar at crack
σs : average stress of steel bar
P : external load.

The relationship between the stress produced by contact of the crack and the average strain is shown in Fig.9. This relationship for the unloading path is formulated as

$$\sigma cc = Ecc(\varepsilon - \varepsilon cs) \geq 0 \qquad \text{for } \varepsilon cp < \varepsilon \qquad (8)$$

$$\sigma cc = Kc(\varepsilon) \qquad \text{for } \varepsilon \leq \varepsilon cp \qquad (9)$$

where
Ecc : stiffness of concrete at contacting state
εcs : strain when the crack starts to contact
Kc : stress-strain relationship of plain concrete
εcp : strain when the crack contacts perfectly
and that for reloading path is assumed to be according to Kc. What the crack starts to contact at the strain larger than zero results from looseness or local plastic deformation of concrete at crack surface. The strain when the crack starts to contact and the stiffness of concrete at contacting state were 0.015% and Ec/3 respectively.

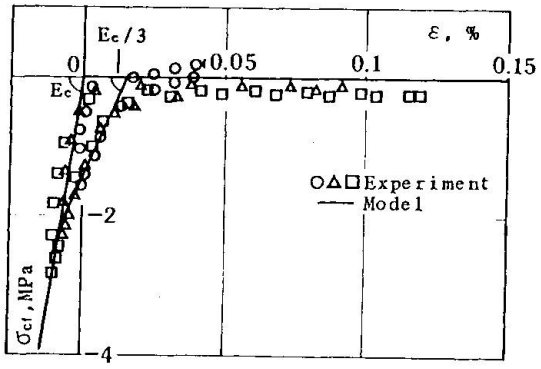

Fig.9 Relationship between σcc and average strain

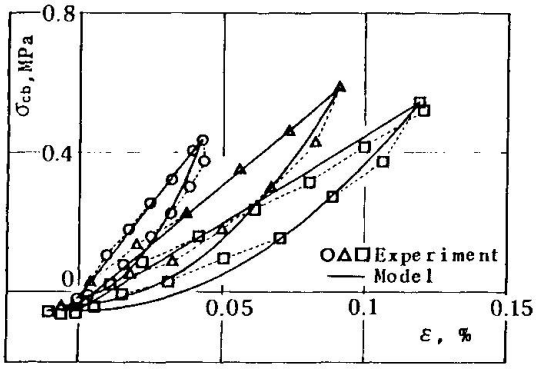

Fig.10 Relationship between σcb and average strain

The relationships between the stress produced by bond and the average strain are shown in Fig.10. The stress produced by bond is assumed to be constant when the external stress is carried by contact of the crack. This constant stress starts at a certain strain between the strain when the crack starts to contact and that when the crack contacts perfectly. This strain was assumed to be zero and the stress produced by bond at this strain was found from experimental results to be given by

$$\sigma cbo = -0.0016\ Ec\ \varepsilon max \qquad (10)$$

where
σcbo : stress produced by bond at zero of strain
εmax : maximum strain produced before
Ec : young's modulus of concrete.
The relationship between the stress produced by bond and the average strain is

formulated using this stress. The second degree polynomial curve was used for the unloading path and straight line was used for the reloading path as follows.

$$\sigma cb = \frac{\sigma cbun - \sigma cbo}{\varepsilon un^2} \varepsilon^2 + \sigma cbo \qquad \text{for unloading} \qquad (11)$$

$$\sigma cb = \sigma cbre + \frac{\sigma cbun - \sigma cbre}{\varepsilon un - \varepsilon re} (\varepsilon - \varepsilon re) \qquad \text{for reloading} \qquad (12)$$

where

εun : strain at the turning point where unloading starts
$\sigma cbun$: stress produced by bond corresponding to εun
εre : strain at the turning point where reloading starts ($\varepsilon re \geq 0$)
$\sigma cbre$: stress produced by bond corresponding to εre

The relationship between the stress produced by bond and average strain for the envelope curve in tension can be given by the average stress strain relationship of concrete under monotonic tension because the contact of crack does not occur in this state.

4.2 Load-average strain relationship of uniaxial member

Before yielding of steel bar, the average stress strain relationship of the bar is $\sigma s = E s \varepsilon$ independently of the loading history. Fig.11 shows the comparison of analytical and experimental results of the load average strain relationship before yielding. The analytical result agrees with the experimental result.

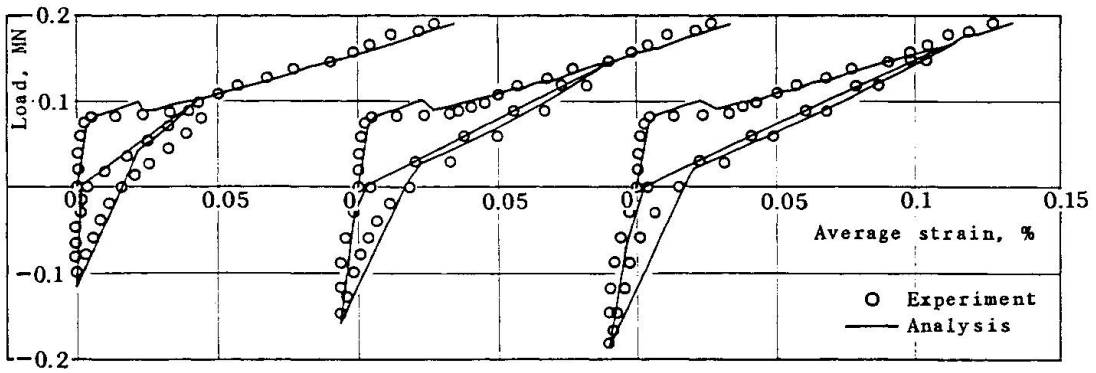

Fig.11 Comparison of analytical and experimental results of load-average strain relationship before yielding

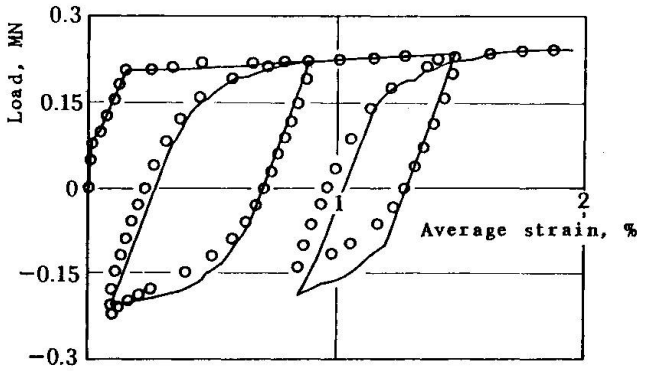

Fig.12 Comparison of analytical and experimental results of load-average strain relationship in post yield range

After yielding of steel bar, the average stress average strain relationship of the bar can be calculated in the same way as under monotonic loading if the

stress distribution curve of steel bar is assumed to be cosine curve independently of the load. From the experiment, it was certified that the stress distribution curve of steel bar could be expressed by cosine curve. The comparison of analytical and experimental results of load average strain relationship in post yield range is shown in Fig.12. The conversion of stress distribution into strain distribution in the analysis was made by tracing the stress strain history by using Kato's model [4] at the points which divide half of crack spacing into 20 equal length portions. The analytical result agrees with the experimental result.

5. CONCLUSIONS

(1) A method for calculating tensile stiffness of a reinforced concrete element is proposed by referring the test results. This method is applicable for reversed cyclic loading, including the post yield range of steel bars.

(2) The average stress strain relationship of concrete under reversed cyclic loading was formulated. The average stress was divided into two components which were produced by the bond action and the contact of crack.

(3) In the post yield range the average stress of a steel bar is obtained from the average strain by modeling the stress distribution along the bar. This approach can be applied to reversed cyclic loading.

(4) The yield point of the average stress strain curve of a steel bar in a reinforced concrete element is lower than that of a bar in the air and no yield plateau exists in the curve.

REFERENCES

1) Morita,S and Kaku,T. :Experimental study on the deformation of axially reinforced concrete prisms subjected to tension and drying, Review of the 18th general meeting, Tokyo, May 1964, The Cement Association of Japan, pp.205-209.
2) Moosecker,W. and Grasser,E. :Evaluation of tension stiffening effects in reinforced concrete linear members, IABSE Colloquium Delft 1981, Report of the Working Commissions, Vol.34, IABSE, pp.615-624.
3) Okamura,H., Maekawa,K. and Sivasubramaniyam,S. :Verification of modeling for reinforced concrete finite element, Proc. of Japan-US seminar on finite element analysis of reinforced concrete structures, Tokyo, May 1985, ASCE, pp.528-543.
4) Kato,B. :Mechanical properties of steel under load cycles idealizing seismic actions, Structural concrete under seismic actions, Vol.1 -State of the art reports-, AICAP-CEB Symposium, Rome, May 1979, Bulletin D'Information No.131, CEB, pp.7-27.